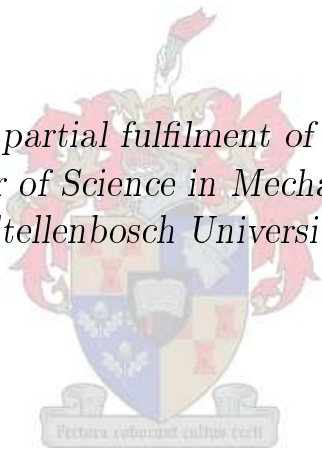


Development of a Hybrid Light Alloy - Carbon Fibre Aerospace Structural Panel

by

Philip J. Roets

*Thesis presented in partial fulfilment of the requirements for
the degree of Master of Science in Mechanical Engineering at
Stellenbosch University*



Department of Mechanical and Mechatronic Engineering,
University of Stellenbosch,
Private Bag X1, Matieland 7602, South Africa.

Supervisor: Mr. K. van der Westhuizen

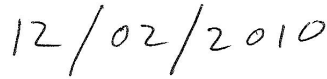
March 2010

Declaration

By submitting this thesis electronically, I declare that the entirety of the work contained therein is my own, original work, that I am the owner of the copyright thereof (unless to the extent explicitly otherwise stated) and that I have not previously in its entirety or in part submitted it for obtaining any qualification.

Signature: 

P.J. Roets

Date: 

Copyright © 2010 Stellenbosch University
All rights reserved.

Abstract

Development of a Hybrid Light Alloy - Carbon Fibre Aerospace Structural Panel

P.J. Roets

*Department of Mechanical and Mechatronic Engineering,
University of Stellenbosch,
Private Bag X1, Matieland 7602, South Africa.*

Thesis: MScEng (Mech)

March 2010

The development of light and stiff aerospace structural panels is very important in the aerospace industry, e.g. a lighter satellite requires less fuel to launch it into space which in turn saves money for the owner of the satellite. This thesis describes the design, optimisation, manufacturing and testing of a ribbed light alloy core - carbon fibre face sheets, sandwich-type, satellite panel operating at launch loading conditions (115 m/s^2 accelerations and requiring a minimum structural natural frequency of 90 Hz) to determine the optimum stiffness per mass ratio of the panel.

The panel layout was based on a satellite panel designed by SunSpace and Information Systems for the Sumbandila satellite. Only the black box mounting positions of the original panel were used in the optimisation of the new panel. The core of the evaluation panel was manufactured from aluminium (6082-T6). The carbon fibre skins were manufactured from unidirectional high modulus carbon fibre (K63712) in a $[0/90/0]$ wet layup with the 0° direction in the longitudinal direction of the panel. A three-dimensional model of the panel consisting of 3D wedge elements and containing all the boundary conditions was modelled with the use of the finite element software MSC Patran. The model was optimised with the use of optimisation software Genesis to locate the rib positions. Genesis removes all the elements containing the least amount of stress; only 30% of the core elements were kept while restricting the elements to form an extruded configuration (for milling machining) throughout the thickness of the panel. The rib elements remaining were replaced in MSC Patran by shell elements and the shell element thicknesses were optimised with the use of Genesis to ensure the lightest and stiffest possible structure. The optimised rib thicknesses were imported into MSC Patran and the numerically optimised model could then be analysed with MSC Nastran.

The numerical model was converted into a manufacturable structure and the core was machined from a solid aluminium sheet. The ribs were machined in the shape of an I-beam to allow for minimum weight and a sufficient bonding area for the two carbon fibre face sheets. Elevated circular surfaces, protruding through the carbon fibre sheets, were machined in the position of the black box mountings to allow for better heat transfer away from the black boxes. The carbon fibre face sheets were bonded to the metal core (3M Scotch-Weld 9323 B/A).

The finished panel was put through various tests to determine whether it is suitable for use in the aviation industry. The tests included modal testing, random vibration testing and temperature testing to determine if the structure is durable enough for use in satellites.

The test results are promising and show that a substantive amount of money can be saved by reducing the mass on the structure. By using optimisation software and ribbed light alloy - carbon fibre face sheets sandwich structures the performance of the structures can be improved without adding mass to the structure.

Uittreksel

Ontwikkeling van 'n Hibriede Ligte Allooi - Koolstofvesel Lugvaartstruktuur Paneel

(“Development of a Hybrid Light Alloy - Carbon Fibre Aerospace Structural Panel”)

P.J. Roets

*Departement Meganiese en Megatroniese Ingenieurswese,
Universiteit van Stellenbosch,
Privaatsak X1, Matieland 7602, Suid-Afrika.*

Tesis: MScIng (Meg)

Maart 2010

Die ontwikkeling van ligter en stywer lugvaartstruktuur panele is baie belangrik in die lugvaart-industrie, bv. 'n ligter satelliet benodig minder brandstof om tot in 'n wentelbaan lanseer te word. Dit bespaar sodoende lanseerkostes vir die eienaar van die satelliet. In die verslag word die ontwerp, optimering, vervaardiging en toets van 'n gewebde, ligte allooi kern - koolstofveselvel, saamgestelde materiaal, satelliet struktuurpaneel wat onderwerp word aan lanseer belastingstoestande van ongeveer 115 m/s^2 versnellings ondersoek. Die tegnieke word gebruik om die optimale styfheid per eenheidsmassa-verhouding te bepaal. Die paneel benodig 'n minimum strukturele eerste natuurlike frekwensie van 90 Hz.

Die basiese paneel uitleg is verkry vanaf 'n satellietpaneel wat deur SunSpace and Information Systems ontwerp is vir die basisplaat van die Sumbandila satelliet. Die enigste geometrie wat van die oorspronklike struktuur behou is om die nuwe struktuur te optimeer is die vashegtingspunt-posisies van die swart-kassies. Die kern van die ge-optimeerde struktuur is vervaardig uit gemasjieneerde aluminium (6082-T6). Die koolstofvesel-velle is vervaardig uit enkelrigting hoë-modulus koolstofvesel-doeke (K63712). Die oplegging is gedoen met 'n nat-opleggingsproses waar die drie lae van elke vel 'n $[0/90/0]$ oriëntasie het met, die 0° lae in die langsrigting van die paneel. 'n Drie-dimensionele eindige element model van die paneel is geskep met behulp van die MSC Patran sagteware pakket met die model hoofsaaklik opgebou uit 3D wig-elemente. Al die lanseertuig vashegtingsrandwaardes is in die eindige element model ingebou. Om die web posisies te bepaal is die Genesis optimeringsagteware pakket gebruik. Verskeie ontwerpvoorwaardes is gespesifiseer waaraan die optimeringsproses moes voldoen. Slegs 30% van die wig-elemente mag behoue bly in die optimeringsproses en al die elemente deur die dikte van die paneel moet of behou of verwyder word. Dit verseker dat die resultaat masjieneerbaar is met 'n freesmasjien. Die oorblywende wig-elemente is in MSC Patran vervang met dop-elemente. Die dop-elemente se diktes is ge-optimeer met Genesis om die ligste en styfste struktuur moontlik te kry. Die ge-optimeerde dop-element diktes is in die MSC Patran model ingetrek. Die numeries ge-optimeerde model is daarna met behulp van MSC Nastran ge-analiseer.

Nadat die numeriese model omgeskakel is in 'n vervaardigbare struktuur is die kern gemasjieneer uit 'n soliede blok aluminium. Die webbe is ontwerp en vervaardig in 'n I-balk vorm. Dit laat toe dat die webbe 'n minimum gewig en genoegsame area het waarop die koolstofvesel velle geheg kan word. Verhewe vlakke is gemasjieneer op die aluminium kern in die posisies van die swart-kassie vashegtingpunte. Hierdie verhewe vlakke steek deur die koolstofvesel-vel aan die kant waar die swart-kassies vasgeheg word. Dit verseker 'n metaal-op-metaal verbinding tussen die kern en die swart-kassies vir beter hittegeleiding. 3M Scotch-Weld 9323 B/A epoksie is gebruik om die koolstofvesel-velle aan die aluminium kern te heg.

Die voltooide struktuur is aan 'n reeks toetse onderwerp om te bepaal of dit geskik is om in die ruimtevaart-industrie gebruik te kan word. Dit sluit modale toetse, lukrake vibrasie toetse en temperatuursverandering toetse in. Die toetsresultate sal bepaal of die struktuur duursaam genoeg is om in satelliete gebruik te word.

Die toetsresultate is belowend en dui daarop dat deur massa te bespaar op die struktuur, 'n aansienlike bedrag op satelliet lanseer-kostes bespaar kan word. Deur optimeringsagteware tesame met gewebde ligte allooi kern - koolstofvesel vel, saamgestelde materiaal strukture te gebruik kan die werksverrigting van die strukture verbeter sonder dat massa bygevoeg word.

Acknowledgements

I would like to thank Jesus Christ for the ability and opportunity to study and for carrying me through life and its challenges. I would like to thank my study leader, Mr. Kobus van der Westhuizen, for all the advice and hours of dedication during the course of this study.

My parents, Johan and Maryna, as well as my brothers and sister for always being there for me and supporting me throughout my studies.

Elizabeth Hooneberg for supporting me throughout the course of this study and always being there for me.

To all my friends for their support.

Mr. Herman Malan from MBV Consulting for managing the AMTS project, that this project is part of, and always making sure the funding was in place.

Mr. Hano Steyn from SunSpace and Information Systems for continuous advice and knowledge about the small satellite industry.

Mr. Albert Verburg from GRP Tubing for supplying the facilities for the manufacturing of the carbon fibre face sheets.

Department of Science and technology and the AMTS program for funding the project.

Mr. Jacques Hugo and Rheinmetall Denel Munition for the use of the vibration test facilities.

Prof. Gerhard Venter for advice on Genesis software.

Daliff Precision Engineering for the manufacturing of the aluminium sandwich structure core.

Dedications

To my family and friends

Contents

Declaration	i
Abstract	ii
Uittreksel	iv
Acknowledgements	vi
Dedications	vii
Contents	viii
List of Figures	xi
List of Tables	xv
Nomenclature	xvi
1 Introduction	1
1.1 Background and motivation of the study	2
1.2 Study objectives	3
1.3 Outline of the work done during the study	3
1.4 Contribution of this study	4
2 Literature Study	5
2.1 Sandwich panel core technologies	5
2.1.1 Carbon fibre reinforced cores	5
2.1.2 Aluminium foam core sandwich structures	6
2.1.3 Hollow integrated sandwich composites with hybrid face sheets	6
2.1.4 Sandwich panels with periodic cellular metal cores	7
2.2 Satellite structure with a sandwich T-joint	8
2.3 Characteristics of joining inserts for composite sandwich panels	9
2.4 Multi-objective optimisation of composite structures	9
2.5 First generation aerospace structural panel design overview	10
3 Applicable Finite Element Theory	12
3.1 Finite element techniques and capabilities	12
3.2 Theory of shell elements	12
3.2.1 In-plane behaviour of shell elements	13
3.2.2 Bending behaviour of shell elements	15
3.2.3 Stresses and strains for shell elements	18

3.2.4	Composite behaviour of shell elements	20
3.3	Solid elements	22
4	Materials	24
4.1	Carbon fibre	24
4.2	Aluminium	26
4.3	Magnesium	27
4.4	Adhesives	28
4.4.1	Ply adhesives	28
4.4.2	Room temperature curing adhesives	28
5	Design and Optimisation	34
5.1	Structural optimisation	34
5.1.1	General Genesis optimisation process	34
5.2	Topology optimisation	35
5.3	First generation panel optimisation	35
5.3.1	First generation panel with magnesium core	38
5.4	Second generation aerospace structure panel	39
5.4.1	FE model prior to topology optimisation	39
5.4.2	Topology optimisation of second generation panel core	42
5.4.3	FE model converting topology results into ribs	45
5.4.4	Sizing optimisation of second generation panel ribs	46
5.4.5	FE model of optimised second generation panel	48
6	Manufacturing	52
6.1	Ribbed reinforced aluminium core manufacturing	52
6.1.1	Waterline machining	52
6.1.2	Conversion of FE results in to a CAD model	53
6.1.3	Manufacturing of the core	54
6.2	Carbon fibre face sheet manufacturing	57
6.3	Carbon fibre face sheet bonding to aluminium core	59
6.3.1	Preparation of aluminium core prior to bonding	59
6.3.2	Adhesive application and bonding	60
6.3.3	Post bonding machining	61
7	Structural Testing and Results	63
7.1	Modal test of the structure	63
7.1.1	Test setup for the structural modal test	63
7.1.2	Test procedure and results of the structural modal test	64
7.2	Random vibration testing of the structure	66
7.2.1	Test setup for the random vibration tests	66
7.2.2	Test procedure and results for the random vibration tests	67
7.2.3	Testing the structure for its natural frequencies	70
7.3	Testing the structural stability with temperature fluctuations	72
8	Discussion and Conclusion	76
	Appendices	80
A	Material Properties	81

- B Design and Optimisation Plots** **93**

- C Manufacturing Techniques** **101**
 - C.1 Chromic acid anodising 101
 - C.2 Aluminium rib preperation before the bonding 102

- D Test Results** **103**
 - D.1 Random vibration test results 104

- Bibliography** **106**

List of Figures

1.1	Fully assembled Sumbandila satellite	1
1.2	Aluminium ribbed and pocketed structure	3
2.1	Sandwich panel with carbon fibre Kagome lattice grid (Fan <i>et al.</i> , 2007)	5
2.2	Hollow integrated sandwich core (Hosur <i>et al.</i> , 2004)	7
2.3	Composite T-joint structure showing the I-shaped side insert (Kim and Lee, 2009)	8
2.4	First generation panel core layout (Roets, 2007)	11
2.5	Deformation plot of first generation panel constrained at the four corners (maximum deformation of 0.768 mm)(Roets, 2007)	11
3.1	Quad4 element with its nodal d.o.f., grid numbers and coordinate systems used in a FE model	13
3.2	Element under pure bending	14
3.3	Quad4 element under bending	14
3.4	Tria3 element with its nodal d.o.f., grid numbers and coordinate systems used in a FE model	15
3.5	Nodal displacements and positive directions for Θ_x and Θ_y viewed normal to the xy plane	16
3.6	Relationship between displacements through the thickness of a plate to mid-plane displacements and curvatures	16
3.7	Membrane element forces in shell elements	18
3.8	Plate element moments in shell elements	20
3.9	Quad4 element defining the grid numbers and coordinate systems associated with composite materials	21
3.10	Wedge element with grid numbers defined	22
3.11	Tetrahedral element with grid numbers defined	23
4.1	Simply supported Bernoulli-Euler beam	25
4.2	HMCF test samples prior to the test	26
4.3	Adhesive material test sample	29
4.4	Adhesive material test setup	30
4.5	Adhesive material test results	31
4.6	Outgassing test samples positioned in the vacuum chamber	31
4.7	Vacuum chamber used for outgassing test	32
5.1	High modulus carbon fibre FE model pinned at the four corners (maximum deformation of 0.388 mm)	36
5.2	First generation ribbed core structure imported into Genesis	36

5.3	Deformation plot of the optimised aluminium core of the first generation panel pinned at the four corners (maximum deformation of 0.413 mm)	37
5.4	Stresses in the ribs of the optimised aluminium core of the first generation panel pinned at the four corners (maximum rib stress of 25.3 MPa)	37
5.5	Deformation plot of the optimised magnesium core of the first generation panel pinned at the four corners (maximum deformation of 0.443 mm)	38
5.6	Stresses in the ribs of the optimised magnesium core of the first generation panel pinned at the four corners (maximum rib stress of 21.1 MPa)	38
5.7	Second generation panel black box positions	39
5.8	CAD model of second generation panel geometrical blackbox layout	40
5.9	FE model of second generation panel containing ribs on the blackbox edges	40
5.10	FE model of second generation panel prior to topology optimisation	41
5.11	Illustration of clamped boundary condition used during the duration of the study	42
5.12	Imported model prior to Genesis topology optimisation	42
5.13	Design region for the Genesis topology optimisation	43
5.14	Genesis results from the topology optimisation displaying the proposed rib structure	44
5.15	Genesis results from the topology optimisation used to position the new ribs	45
5.16	FE model displaying the layout where the Genesis results have been converted into a ribbed structure	46
5.17	FE model displaying the rib layout where ribs have been added to make the larger pockets smaller	46
5.18	Imported ribbed model with carbon fibre face sheets and mass elements visible	47
5.19	Imported Genesis ribbed model without carbon fibre face sheets visible	47
5.20	The final geometry of the structure with the rib thicknesses illustrated	49
5.21	First natural frequency of FE model at 141.76 Hz with clamped boundary conditions	49
5.22	First non-rigid body mode of FE model at 145.24 Hz with free (no) boundary conditions	50
5.23	The normal stress in the fibre direction plot of the inner longitudinal carbon fibre layer (maximum fibre stress of 29.6 MPa)	50
5.24	The Von Mises the stress distribution in the ribs under launch conditions (maximum rib stress of 18.7 MPa)	51
5.25	The plot illustrates the displacement of the structure under launch conditions (maximum deformation of 0.172 mm)	51
6.1	I-beam shaped ribs and bolt hole extrusion from the CAD model	53
6.2	Final CAD model of the aluminium core	54
6.3	Sectional dimentions of the ribs	55
6.4	Image of the undercut in the ribbed structure	55
6.5	Image of the machined aluminium core	56
6.6	Image of the machined aluminium core during the quality control process	56
6.7	The wet carbon fibre cloth after resin application	57
6.8	The complete layup of the carbon fibre before it is sealed in the vacuum bag	58
6.9	The carbon fibre layup with the vacuum drawn on the setup	58
6.10	The cleaning process of the surfaces to which the adhesive will be applied	60
6.11	The adhesive being applied on top of the ribs	60

6.12	The adhesive along the ribs are illustrated after the first face sheet has been bonded	61
6.13	The access adhesive that needs to be removed during the final machining process	62
7.1	Dummy masses used to act as the black boxes during structural tests	64
7.2	Positioning of the accelerometers during the modal test	64
7.3	Positioning of the accelerometers during the modal vibration tests	65
7.4	Frequency response plot sensors 1 to 3 for the modal test done on the structure	65
7.5	Vibration shaker used for the random vibration tests	66
7.6	Structure bolted to the shaker	67
7.7	Measurement equipment of the random vibration tests	67
7.8	Accelerometer connection failure during random vibration test	68
7.9	Frequency response plot of the 4.6 gRMS random vibration test	68
7.10	Frequency response plot of the first 12.6 gRMS random vibration test	69
7.11	Frequency response plot of the second 12.6 gRMS random vibration test	69
7.12	Frequency response plot of the first sine sweep	70
7.13	Frequency response plot of the second sine sweep	70
7.14	Frequency response plot of the third sine sweep	71
7.15	Structure in the oven during the elevated temperature test	72
7.16	Rib stresses due to a 80 °C change in temperature	73
7.17	Deformation of the second generation panel due to a 80 °C change in temperature	75
7.18	Deformation of the aluminium ribbed and pocketed panel due to a 80 °C change in temperature	75
A.1	High modulus carbon fibre manufacturers data sheet	82
A.2	Data sheet comparing high modulus carbon fibres from icomposites.com (iComposites, 2009)	83
A.3	CeTePox 3502 manufacturers data sheet	84
A.4	3M Scotch-Weld 9323 B/A manufacturers data sheet	85
A.5	Quotation for the manufacturing of the aluminium core structure	90
A.6	Quotation for magnesium to be used to manufacture the optimised core structure	91
A.7	Quotation for importing Mitsubishi K63712 high modulus carbon fibre	92
B.1	Second natural frequency of the structure with clamped boundary conditions at 162 Hz	93
B.2	Third natural frequency of the structure with clamped boundary conditions at 242 Hz	94
B.3	Fourth natural frequency of the structure with clamped boundary conditions at 394 Hz	94
B.4	Fifth natural frequency of the structure with clamped boundary conditions at 441 Hz	95
B.5	Sixth natural frequency of the structure with clamped boundary conditions at 471 Hz	95
B.6	Seventh natural frequency of the structure with clamped boundary conditions at 514 Hz	96
B.7	Eighth natural frequency of the structure with clamped boundary conditions at 578 Hz	96
B.8	Nineth natural frequency of the structure with clamped boundary conditions at 614 Hz	97

B.9 Tenth natural frequency of the structure with clamped boundary conditions at 646 Hz 97

B.10 First natural frequency of the structure after Genesis sizing optimisation at 219 Hz 98

B.11 Second natural frequency of the structure after Genesis sizing optimisation at 245 Hz 98

B.12 Third natural frequency of the structure after Genesis sizing optimisation at 322 Hz 99

B.13 Fourth natural frequency of the structure after Genesis sizing optimisation at 468 Hz 99

B.14 Second natural frequency of the structure with free boundary conditions at 199 Hz 100

B.15 Third natural frequency of the structure with free boundary conditions at 236 Hz 100

B.16 Fourth natural frequency of the structure with free boundary conditions at 295 Hz 100

D.1 Side view of the structure to be mounted to the shaker table 103

D.2 Setup for random vibration test 103

D.3 Frequency response plot of the low intensity random vibration test with sensor T3 failing 104

D.4 Frequency response plot of the 1st high intensity random vibration test with sensors T3 and 1 failing 104

D.5 Frequency response plot of the 2nd high intensity random vibration test with sensors T3, 2 and 3 failing 105

List of Tables

4.1	HMCF/epoxy material properties	26
4.2	Comparison between 6082-T6 and 7075-T6 aluminium (MatWeb, 2009) (AZOM, 2009)	27
4.3	Comparison between 6082-T6 aluminium and AZ31B-H24 magnesium (MatWeb, 2009) (AZOM, 2009)	27
4.4	Dimensions of the epoxy compression test samples	30
4.5	Results from epoxy pressure test and theoretical data for Scotch-Weld 2216 B/A Gray	31
4.6	Results from the outgassing test	32
5.1	SMS approximation frequency calculation (Vanderplaats R&D, 2008 <i>a</i>)	44
7.1	Measured natural frequencies versus FE natural frequencies	71
7.2	Average length changes caused by temperature changes	73

Nomenclature

Constants

$\pi =$	3.141 592 654	
$g =$	9.81	Gravitational acceleration [m/s ²]

Variables

A	Area	[m ²]
b	Base	[m]
D	Diameter	[m]
E	Modulus of elasticity	[GPa]
F	Force	[N]
G	Shear modulus	[GPa]
h	Height	[m]
I	Area moment of inertia	[m ⁴]
k	Thermal conductivity	[W/m·°C or W/m·K]
L	Length	[m]
M	Bending moment	[N/m]
m	Mass	[kg]
N	Element force	[N]
P	Force	[N]
T	Temperature	[°C or K]
t	Time	[s]
u	Displacement in x	[m]
V	Volume	[m ³]
v	Velocity	[m/s]
v	Displacement in y	[m]
w	Displacement in z	[m]

Variables-Greek Letters

α	Coefficient of thermal expansion	[10 ⁻⁶ ·°C ⁻¹]
ε	Strain	[]
ρ	Density	[kg/m ³]
κ	Bending curvature	[]
τ	Shear stress	[Pa]

σ	Normal stress	[Pa]
γ	Shear strain	[]
ν	Poisson's ratio	[]

Subscripts

C	Layup combination
C	Compression
FS	Face sheet
f	Fibre
fm	Fibre/Matrix combination
H	Hybrid structure
i	Counting Integer
m	Matrix
oct	Octahedral
T	Transverse
T	Tension
VM	Von Mises
z'	Medians of the respective individual cross-section

Abbreviations

ASTM	American Society for Testing and Materials
CAD	Computer aided design
CNC	Computer numerical control
COG	Center of gravity
CTE	Coefficient of thermal expansion
CST	Constant strain triangle
CVCM	Maximum collected volatile condensable material
d.o.f.	Degrees of freedom
FE	Finite element
HMCF	High modulus carbon fibre
PCM	Periodic cellular metal
Quad4	Quadrilateral four noded element

Quad8	Quadrilateral eight noded element
RMS	Root mean square
Tria3	Tri-angular three noded element
Tet3	Tetrahedral four noded element
TML	Total mass loss

Chapter 1

Introduction

The primary aim of this study is to design, manufacture and test an improved hybrid light alloy - carbon fibre composite satellite structure panel. The goal of this study is to optimise a satellite structure panel with the same layout as a satellite panel designed by SunSpace and Information Systems for the Sumbandila satellite, Figure 1.1. The original structure was manufactured entirely from aluminium and this study focussed on designing a structure that is lighter and stiffer than the original by using Genesis optimisation software and composite materials.



Figure 1.1: Fully assembled Sumbandila satellite

Satellite structures often use advanced composites. These composites have high performance reinforcements of a thin diameter embedded in a matrix material such as epoxy or aluminium. Two main characteristics of advanced composites, high specific modulus and strength and dimensional stability during large changes in temperature, make it a clear choice for spacecraft. The light weight of the advanced composite structure panels rapidly decreases the payload launching cost, even though the composite panel may be

considerably more expensive than the conventional metal panels (Kaw, 1997).

1.1 Background and motivation of the study

In this study a new type of hybrid composite satellite structure is developed. This new structure will combine composite materials along with homogeneous materials in the form of a sandwich panel. The most commonly used sandwich structures in aerospace industries are aluminium honeycomb cores combined with carbon fibre face sheets. The outer sheets bear most of the in-plane loading and any transverse bending stresses. The core separates the outer sheets and resists any deformation perpendicular to the outer sheets; it also provides shear rigidity along the planes that are perpendicular to the outer sheets. These honeycomb sandwich structures are extremely light weight and stiff (Callister Jr, 2003).

There is however difficulties and disadvantages when aluminium honeycomb cores are used in sandwich panels. The thermal conductivity from the centre of the panel to the edges is relatively poor because of the extremely thin aluminium hexagon shaped ribs through which the heat needs to flow towards the edge of the panel. It is also extremely difficult to bolt another subsystem to a honeycomb panel, since the honeycomb structure is not strong enough to endure any normal forces. Because of this plastic or aluminium inserts needs to be inserted into the core during manufacturing. It is however hard to locate these inserts once the non-transparent carbon fibre sheets have been bonded to the core (Roets, 2007).

In 2007 a ribbed aluminium-carbon fibre hybrid panel was designed, modelled, manufactured and tested as a BEng final year project. The design of the structure was aimed at eliminating the disadvantages of honeycomb core sandwich structures. The panel was manufactured from 6082-T6 machined aluminium and T300 carbon fibre sheets. The aluminium core was machined from a sheet of aluminium with straight ribs for better heat transfer than honeycomb cores. The design also solved the problem of bolting black boxes (generic name typically used for satellite equipment integrated in a machined aluminium case) to the structure. This was done by designing the core layout for a specific black box position and manufacturing the core with permanent bolt holes. Results of this trial study displayed that although the concept hybrid structure developed had promising behaviour, more detailed analysis, testing and evaluation was required, including higher standard manufacturing techniques and quality standards (Roets, 2007).

Satellites are sent into orbit on a regular basis and are primarily used to capture important imagery and to help with telecommunications on earth. The payload cost of launching satellites into low-earth orbit is unofficially rated at approximately \$20 000(US) for every kilogram, which is very high. These high costs are the reason for a large number of studies done to reduce the weight of satellite structures. A full scale MScEng research project was proposed to address these issues and manufacture a prototype as physical deliverable. This study was funded by a South African Government initiative called the Advanced Manufacturing Technology Strategy (AMTS). This initiative is aimed at research and development through university students in partnership with industry partners that will gain from the research and technologies developed. The industry partners

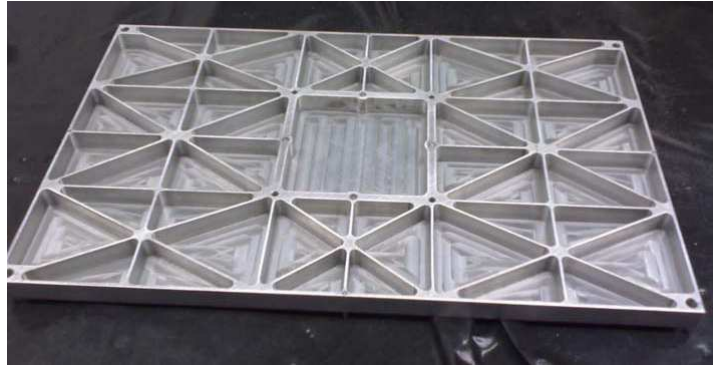


Figure 1.2: Aluminium ribbed and pocketed structure

of this project are MBV Consulting Group (Pty) Ltd, CFRP Composites Africa CC Ltd and SunSpace and Information Systems (Pty).

1.2 Study objectives

The objectives of the study is to fulfil or exceed space structural panel specification standards as set out by the SunSpace structures system engineer. This means the structure will need to have a lower structural volumetric density than 371 kg/m^3 as well as exceed the stiffness to weight properties of current ribbed and pocketed satellite structures illustrated in Figure 1.2. The structural stiffness of the panel will have to be high enough for the structure to be able to go through the launch process without failure. The structure should be able to endure the high launch vibrations to which a satellite will be exposed, without failure. For this to be the case the fundamental free natural frequency have to exceed 90 Hz. The structure should have a yield safety factor of at least 3. The structure should also adhere to the high manufacturing accuracy required for aerospace structures. Due to the constant changes in temperatures to which satellites are exposed it is important for the structure to be stable under the thermal conditions in space at low-earth orbit.

1.3 Outline of the work done during the study

In this section a brief outline of the document and the work done during the study to meet the project objectives is described. In Chapter 2 a literature study is done on the design of different sandwich panel core structures and also covers a brief explanation of the work done during the final year trial study on a ribbed aluminium core. In Chapter 3 the theory behind the optimisation and finite element calculations is covered. All the elements used in the FE model and Genesis optimisation model of this study are covered in Chapter 3.

Chapter 4 will cover the different materials used and the reasoning why the materials were used in this study. This chapter also gives a brief description of the physical properties of magnesium and its place in aerospace structures, as well as the material tests done on carbon fibre and adhesives.

In Chapter 5 the different optimisation techniques used in this study are explained and the capabilities of the Genesis optimiser is tested on the first generation core. A FE analysis is done on this optimised first generation structure and the influence of high modulus carbon fibre as a face sheet material is also evaluated in the FE model. The influence of magnesium as a core material for the optimised first generation structure is inspected with a FE study. This chapter also covers the complete development, FE modelling, Genesis optimisation process and FE analysis of the fully developed second generation structure.

In Chapter 6 the manufacturing process and techniques to produce the different parts of the second generation structure is explained. The assembly of the second generation structure is also explained in this chapter.

Chapter 7 explains the test setup and results of the modal test, to test the stiffness of the structure, as done on the manufactured second generation structure. The random vibration tests, to simulate the launch conditions, and natural frequency test setup and results are explained in detail. The temperature tests done on the structure, to verify the thermal stability of the structure, is also explained in this chapter.

Chapter 8 concludes the study and recommendations for further studies are also given in this section.

1.4 Contribution of this study

To obtain lighter, equally stiff satellite structural panels to lower the mission costs due to lower launching costs or to increase the inclusion of more satellite experimental payloads due to mass saving. The successful completion of this study will add great value to future satellites developed by SunSpace and Information Systems.

Chapter 2

Literature Study

2.1 Sandwich panel core technologies

Different technologies have been developed to act as core materials for sandwich structures. In this section some of these technologies will be discussed. In this study none of these technologies will be used and the reasons for this are briefly discussed in each subsection.

2.1.1 Carbon fibre reinforced cores

At the Tsinghua University in Beijing research has been done on sandwich panels with carbon fibre reinforced cores. There are four typical rib arrangements when working with fibre reinforced cores; these are Bi-grid, Tri-grid, Quadri-grid and the Kagome-Grid (Fan *et al.*, 2007).

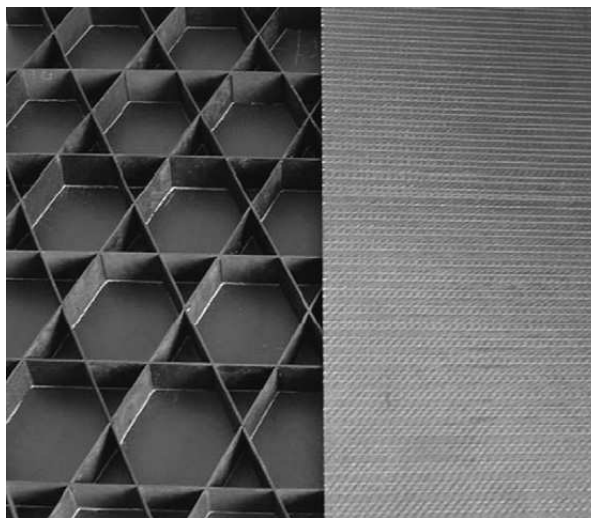


Figure 2.1: Sandwich panel with carbon fibre Kagome lattice grid (Fan *et al.*, 2007)

Due to relatively low density, the carbon fibre reinforced grids are ideal core materials for sandwich panels. The panels were manufactured by using bonded laminate skins. The carbon fibre ribs have a tendency to cut each other at intersection nodes when subjected

to deformations. The problem with using carbon as a core material is its poor thermal regulation (Fan *et al.*, 2007).

A Kagome grid, illustrated in Figure 2.1, was used as a core in various tests. The test results showed that the Kagome lattice grid is much stiffer than foam or honeycomb cores. When using fibre reinforced ribbed cores the most common failure mode is the debonding of the ribs. This is because of the relatively low strength of the matrix in comparison with that of the fibres (Fan *et al.*, 2007).

The heat transfer capability of the carbon fibre ribbed structure will however not be able to sufficiently remove heat from heat generating black boxes bolted to the structure. The carbon fibre ribbed structure is also not suitable for bolt holes and inserts will need to be placed at the mounting points. For these reasons this type of core will not be considered for this study.

2.1.2 Aluminium foam core sandwich structures

In 2006 the Australian National University did research on the effect of core thickness of an aluminium foam core thermoplastic composite facing sandwich structure. These structures were subjected to a deformation mechanism and the effects of the core thickness on four point bending were investigated. Three different core thicknesses were tested, 5 mm, 10 mm and 20 mm and the failure modes, deformation and stresses were investigated (Styles *et al.*, 2007).

Full field strain analysis show that there are a number of failure modes between the different core thicknesses. As expected the areas with high strain concentrations were observed at the region of failure in each core thickness. The thinner samples exhibited core cracking and crushing while the skin wrinkled and fractured. In the thicker samples failure occurred due to indentation of the core. By increasing the skin thickness the core indentation was prevented but, failure occurred due to shear and cracking (Styles *et al.*, 2007).

This core material is not suited for bolt holes and impact resistance is not a particular property that is important for the present study. At the speed at which satellites orbit the earth any impact will destroy the structure, irrespective of the chosen material or structural design.

2.1.3 Hollow integrated sandwich composites with hybrid face sheets

At the Tuskegee University research was done to investigate the damage created by low-velocity impact on hollow integrated sandwich panels. Hollow integrated cores, shown in Figure 2.2, have multi-functionality in terms of fuel storage, routing of electronic wires, fire resistance and it provides a space to mount or store miniature electronic components (Hosur *et al.*, 2004).

These cores are manufactured by using a vacuum assisted resin infusion moulding process. Although these cores have a lot of advantages they have very weak outer faces and cannot sustain any impact, for this reason these faces need to be reinforced by bonding hybrid sheets to the outer faces, that increases the impact resistance dramatically (Hosur *et al.*, 2004).

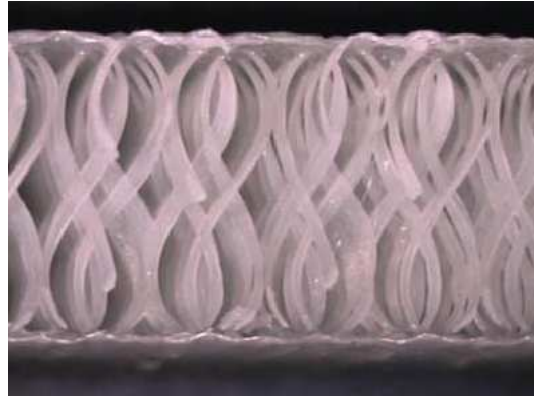


Figure 2.2: Hollow integrated sandwich core (Hosur *et al.*, 2004)

As long as there is no damage to the hybrid face sheets the hollow integrated cores can absorb the impact energy. By using carbon epoxy face sheets the impact load carrying capacity was increased by at least two times, and by using hybrid facings the load carrying capacity increased three times (Hosur *et al.*, 2004). This core structure requires the use of inserts at the bolting points and the low heat transfer ability makes it unsuitable for this study.

2.1.4 Sandwich panels with periodic cellular metal cores

Truss periodic cellular metals (PCMs) have ideal mechanical properties to serve as a core material for sandwich panels subjected to bending. The truss PCMs are as good as honeycomb in terms of strength to weight ratio. There are a few available truss configurations such as the pyramid, octet and Kagome. The octet truss is one of the most ideal configurations because it consists of regular tetrahedrons. The most recent configuration, the Kagome truss has the exact same relative stiffness as the octet truss with the length of each strut in the Kagome truss equal to only half the length of that in the octet truss. The strength against elastic buckling in the Kagome truss can increase by up to four times to that of the octet truss (Lim *et al.*, 2008).

The truss structures will allow for heat transfer through a metal core, it will however not be very effective since the heat transfer path will be relatively long. Inserts will need to be used to join structures together or to bolt black boxes to the structure which makes this structure unsuitable for this study.

2.2 Satellite structure with a sandwich T-joint

At the Korea Advanced Institute of Science and Technology research was done aimed at the overall weight reduction of a small satellite. The main aim was to eliminate the frame of the satellite without compromising the structural rigidity of the satellite. The frame would normally be used as the backbone of the satellite. The panels supporting the black boxes are mechanically fastened to the aluminium frame. In order to eliminate the frame, the researchers have developed a sandwich panel with I-shaped inserts to allow them to bond the carbon fibre-aluminium honeycomb sandwich panels in a T-shape joint. The I-shaped insert was fixed inside the composite sandwich panel edge with a film adhesive. The structure is illustrated in Figure 2.3 (Kim and Lee, 2009).

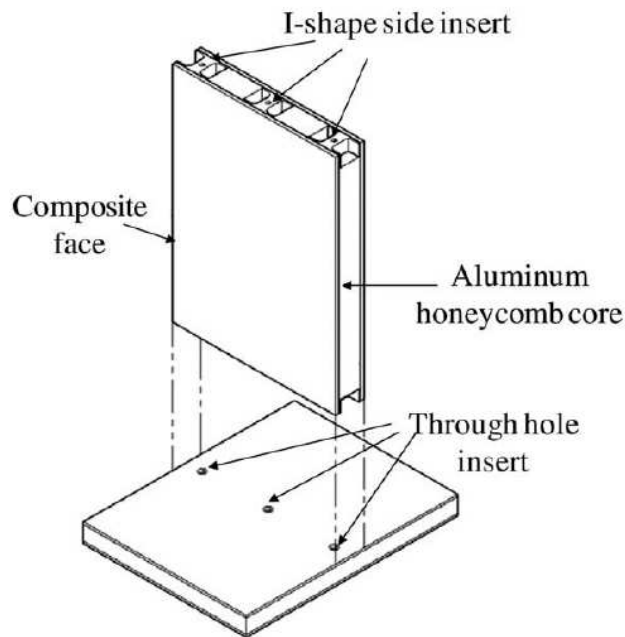


Figure 2.3: Composite T-joint structure showing the I-shaped side insert (Kim and Lee, 2009)

To create a T-shaped joint through the thickness, inserts were used along with the I-shaped inserts. The structure was tested with a quasi-static load case of 11 g and a modal analysis was done on the structure. A finite element model was created to correlate the test results. The launch specifications required a first natural frequency of 35 Hz or more, both the tests and the FE model results satisfied the requirements (Kim and Lee, 2009).

This design shows the capability to effectively bond honeycomb sandwich panels with the use of inserts. A large overall weight saving of 14.6 kg on the entire satellite was made. The first natural frequency is however still not high enough for this study and the bolt holes for the black boxes are still done by inserting threaded inserts that are hidden after the carbon fibre face sheets are bonded to the core. There is still improvements that can be done on this design (Kim and Lee, 2009).

2.3 Characteristics of joining inserts for composite sandwich panels

The light weight and high specific stiffness and strength compared to solid structures, make the use of aluminium honeycomb sandwich structures a common structural material used in aerospace structures. Sandwich structures are not suited to carry localised loads. To overcome this problem inserts are used to join the structure to surrounding structures and transfer the localised loads. The inserts are created by drilling a hole with a tungsten carbide tool (rotating at 3000 rpm), in the sandwich structure in the position where the joint is needed. The insert is placed in position and the hole is then filled up with a high strength adhesive. The adhesive is left to cure the joint is complete (Kim and Lee, 2008).

The insert joints were tested with both static pull tests and dynamic pull tests. The circular I-beam shaped inserts performed the best under the load conditions. Failure occurred due to local fibre breakage of the composite face. The dynamic tests showed that the joints can safely perform under low vibrations between 10 - 20 Hz (Kim and Lee, 2008).

This is not the only technology available to join sandwich structures, but it is a very convenient manner to create sandwich panel joints. However the frequencies these joints, as well as the T-joining method, can operate at is too low to consider this type of joint for this study. In order to have joints working at atleast 90 Hz these joints will not be sufficient.

2.4 Multi-objective optimisation of composite structures

Aerospace industries focused on minimising mass through design optimisation over the past decade. The objectives are to increase payloads, save fuel and to fly faster. However, focus has shifted to minimising cost, time to market and risk. All of these factors can be influenced by the complexity of the design, This implies that the optimisation needs to be done at the conceptual design phase. In the most general case the design decisions come down to a trade-off between weight, cost, risk and time. Risk and time are only included to reduce the complexity of the design (Wang *et al.*, 2002).

Three different approaches of optimising the structure with cost as a design driver were investigated. The first is an approach where an optimal solution is selected in a Pareto sense from a set of designs which meet the performance criteria with minimum weight. Secondly, a penalty function approach is used to find the optimum design that minimises weight and cost. An innovative approach that includes the cost parameter $\Delta\$/\Delta\text{kg}$ directly in the optimisation algorithm to guide a trade-off between cost and weight is applied. The parameter defines the cost increment required to achieve an increment reduction in weight and the process is terminated as soon as the cost penalty exceeds a defined limit. The third approach implements a function that includes both cost and weight, the weight increment is calculated by the same parameter as in the second approach. This method allows more design variables in the optimisation search and

removes the use of a penalty function (Wang *et al.*, 2002).

The researchers used the topology optimisation technique from ANSYS software to identify the significant load paths and the stiffening members. The algorithm maximises stiffness for the best distribution of materials. In previous studies topology optimisation have successfully selected optimal rib or spar dominated structures from a pattern of internal members (Wang *et al.*, 2002).

The cost of manufacturing is dominated by the cost of materials proportional to the weight and the cost of the tooling. This cost estimate does not reflect the complexity of the structure. The Pareto approach is currently the only multi-objective optimisation approach used in engineering applications. The optimal solution by the Pareto approach is defined by: “A feasible solution to a multi-objective optimisation problem is optimal (non-inferior), if there exists no other feasible solution that will yield an improvement in one objective without causing degradation in at least one other objective.” (Wang *et al.*, 2002)

By using cost as a design driver and finding a balanced trade-off between cost and weight composite structures can be successfully optimised. The algorithm proposed works on the principles that if a large cost increment is allowed the design will move to minimum weight and if a small cost increment is allowed the algorithm will drive the designs to minimal cost (Wang *et al.*, 2002).

2.5 First generation aerospace structural panel design overview

The first generation panel was made from a 6082-T6 aluminium core and T300 carbon fibre face sheets. The 400 mm × 250 mm × 16 mm core is stiffened with 1.5 mm thick ribs. The ribs were positioned to give maximum stiffness with a minimum weight, the structure is illustrated in Figure 2.4. Short straight ribs were used to form definite paths for better heat transfer. The design was done without the use of any optimisation software (Roets, 2007).

There were some manufacturing constraints with the manufacturing of the first generation panel. The ribs could only be machined to a minimum thickness of 1.5 mm. The carbon fibre face sheets were manufactured from 3 layers of T300 woven cloth in a wet layup and cured under vacuum. The carbon fibre face sheets were bonded to the aluminium core with a ply adhesive which needed to be cured under vacuum at 120 °C. This caused the aluminium core to expand before the adhesive cured. After the curing was completed and the panel was allowed to cool down the aluminium returned to its original size, which caused the carbon fibre face sheets to buckle and cause indentations in the pockets (Roets, 2007).

The study included stiffness tests and a FE analysis for each stage of production an example where the fully manufactured structure was subdued to pinned boundary conditions is shown in Figure 2.5. The results showed that the panel was too heavy at 0.798 kg and that it was not stiff enough for aerospace applications with a deformation of 0.768



Figure 2.4: First generation panel core layout (Roets, 2007)

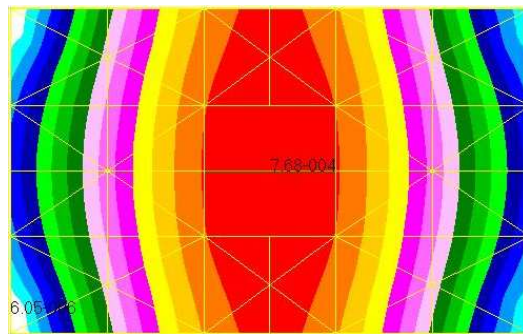


Figure 2.5: Deformation plot of first generation panel constrained at the four corners (maximum deformation of 0.768 mm)(Roets, 2007)

mm at the centre of the panel. The study proposed a look into different core materials, optimisation of the core and finding a bonding technique for the carbon fibre face sheets to eliminate the buckling effect (Roets, 2007).

Chapter 3

Applicable Finite Element Theory

With the use of finite element software there are various techniques and tools that can be used to analyse and optimise structures. In this chapter an overview of the techniques used to set up and analyse the model will be given. The different optimisation tool used and the capability of the optimisation tools will also be explained.

3.1 Finite element techniques and capabilities

The software used in this study is MSC Patran, MSC Nastran and Genesis. The first two programs work as a combination with MSC Patran as the modelling tool and MSC Nastran acts as the solver. In order to create a finite element model of the structure the basic geometric layout of the structure is needed. This can be done by creating points, curves, surfaces and solids according to coordinate systems, in the geometrical tools incorporated in the software.

After the geometrical model has been created the model can be meshed and elements can be created. By creating a mesh seed on the model, the user can define the number of elements desired in a specific region of the model. It can also be used to control the number of elements to allow the computational time of the analysis to be reasonable. There are a wide range of elements to choose from. Each have their advantages so it is important to make sure to choose the correct elements for the type of analysis that will be done.

Genesis was used to optimise the finite element model and find the optimum geometry for the lightest and stiffest structure.

3.2 Theory of shell elements

In this section the basic mathematics to calculate the stresses and strains in the two different types of shell elements used in this study will be explained. Shell element theory is a combination of plane element theory and plate element theory, each of these will be discussed separately. The behaviour of these elements with the use of composite materials will also be explained.

3.2.1 In-plane behaviour of shell elements

A Quad4 plane element is a bilinear quadrilateral element with four nodes. Its displacement field is expressed in terms of generalised coordinates β_i . Each node consists of two displacement degrees of freedom, u_i and v_i , this means that each element consists of eight d.o.f. as shown in Figure 3.1 (Cook, 1994).

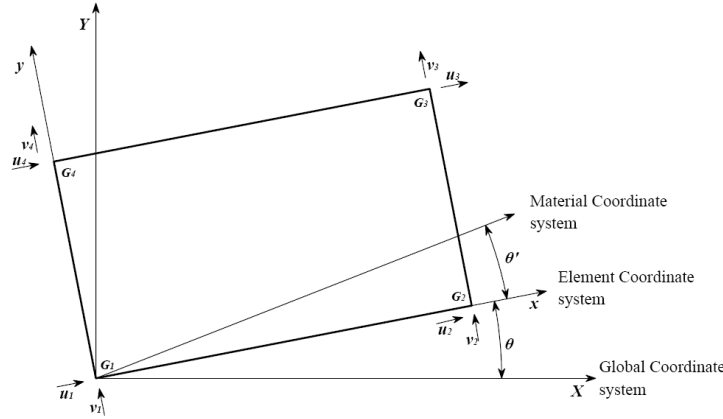


Figure 3.1: Quad4 element with its nodal d.o.f., grid numbers and coordinate systems used in a FE model

$$u = \beta_1 + \beta_2x + \beta_3y + \beta_4xy \quad (3.2.1)$$

$$v = \beta_5 + \beta_6x + \beta_7y + \beta_8xy \quad (3.2.2)$$

The element strain field can be expressed in terms of β_i as:

$$\varepsilon_x = \beta_2 + \beta_4x \quad (3.2.3)$$

$$\varepsilon_y = \beta_7 + \beta_8y \quad (3.2.4)$$

$$\gamma_{xy} = (\beta_3 + \beta_6) + \beta_4x + \beta_4y \quad (3.2.5)$$

The above equations can be used to explain important aspects of plane element behaviour. The strain field shows that ε_x is independent of x , which means that a cantilever beam under a transverse tip force, where axial strain varies linearly with x , cannot be exactly modelled by a Quad4 element. Even though a Quad4 element has the ability to represent an ε_x that varies linearly with y , it cannot exactly model a state of pure bending. From beam theory we know that shear strain γ_{xy} is absent, that top and bottom edges become arcs of practically the same radius curvature and that the plane sections remain plane as shown in Figure 3.2. However with a Quad4 element loaded in pure bending, the sides rotate but the top and bottom edges remain straight as shown in Figure 3.3. Since all sides of Quad4 elements deform as straight lines, the right angles in the element are not preserved under pure moment loading. The consequence of this is that shear strain appears everywhere in the element except along the y -axis. This is also visible when

looking at Equation 3.2.1 and Figure 3.3 which requires β_4 to be nonzero to allow ε_x to vary linearly with y . Since β_4 also appears in Equation 3.2.5, a Quad4 element that bends develops shear strain (Cook, 1994).

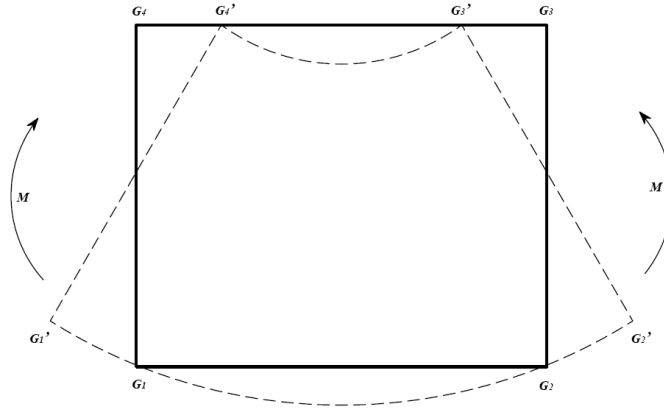


Figure 3.2: Element under pure bending

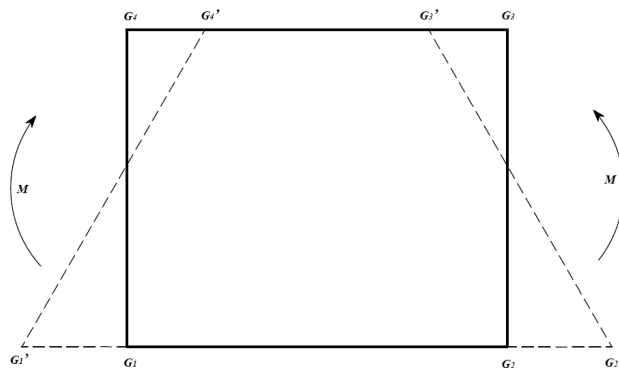


Figure 3.3: Quad4 element under bending

The consequence of this behaviour is that the element is too stiff in bending since an applied bending moment is resisted by spurious shear stress and flexural stresses. This could have an effect on the results obtained (Cook, 1994).

Figure 3.1 defines the ordering of the grid numbers associated with the Quad4 element. The elemental coordinate system is defined by the angle θ measured from the global coordinate system to the side of node 1 to node 2. The local material coordinate system is defined by the angle θ' measured from the elemental coordinate system. The nodal displacements are defined by u_1, u_2, u_3 and u_4 in the elemental x direction and v_1, v_2, v_3 and v_4 in the elemental y direction (Vanderplaats R&D, 2008a).

A Tria3 plane element is also known as a constant strain triangle (CST) element and is perhaps one of the simplest and earliest elements. The strains within the element do not vary and the displacement field of the element is linear in the x and y directions of

the element coordinate frame. The element sides remain straight as the element deforms and the nodes translate in the elemental x and y directions and rotate around the z axis, this rotating motion is also known as drilling, but this will not be discussed in this thesis. The element consists of six d.o.f. as each node consists of two translating d.o.f. (Cook, 1994).

Figure 3.4 defines the ordering of the grid numbers associated with the Tria3 element. The elemental coordinate system is defined by the angle θ measured from the global coordinate system. The local material coordinate system is defined by the angle θ' measured from the elemental coordinate system. The nodal displacements are defined by u_1 , u_2 and u_3 in the elemental x direction and v_1 , v_2 and v_3 in the elemental y direction (Vanderplaats R&D, 2008a).

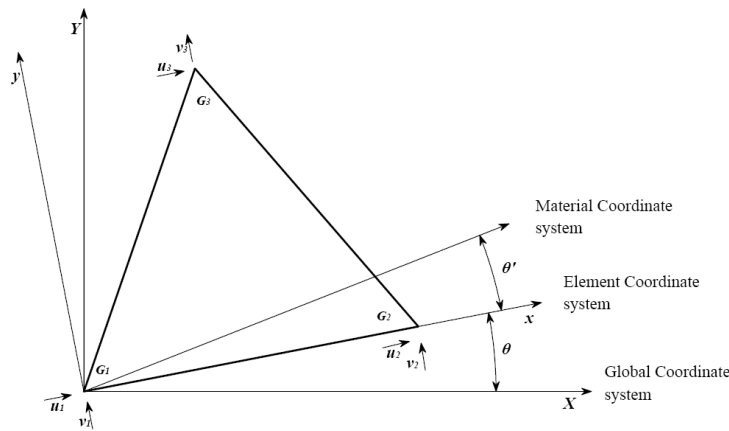


Figure 3.4: Tria3 element with its nodal d.o.f., grid numbers and coordinate systems used in a FE model

The Tria3 plane element gives good results in regions of a FE model where there is a small strain gradient. In cases with a large strain gradient the Tria3 does not work well such as in the case of pure in-plane bending. Correct results are approached as the Tria3 mesh is repeatedly refined. In the case of this study the Tria3 elements are only used for small elements in the carbon fibre face sheets acting as a membrane, this should give credible results (Cook, 1994).

3.2.2 Bending behaviour of shell elements

Bending of shell elements can be explained by plate theory. A plate is a thin solid that may be modeled by 3D elements. A solid element is however a waste of d.o.f. because it computes transverse normal stress and transverse shear stresses. These are all considered negligible in a thin plate. The plate element has only half of the d.o.f. of the comparable solid element. Each node consist of three d.o.f. namely, Θ_x and Θ_y , shown in Figure 3.5, which are both rotational components of a line initially normal to the midsurface and $w = w(x, y)$ which is a lateral displacement in the z direction (Cook, 1994).

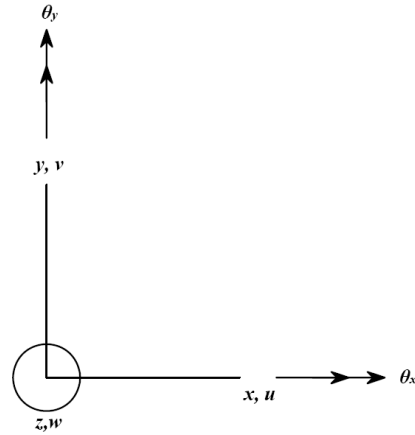


Figure 3.5: Nodal displacements and positive directions for Θ_x and Θ_y viewed normal to the xy plane

Consider a plate of thickness h that straddles the xy plane with the midplane of the plate at $z = 0$ shown in Figure 3.6. Assuming that u_0, v_0 and w_0 are displacements in the x, y and z directions, respectively, positioned at the midplane and that u, v and w are displacements at any point in the x, y and z directions, respectively. The two displacements in the xy plane is dependant on slope of the midplane with the x and y directions and the axial location of that point if it is positioned at any point not located on the midplane (Kaw, 1997).

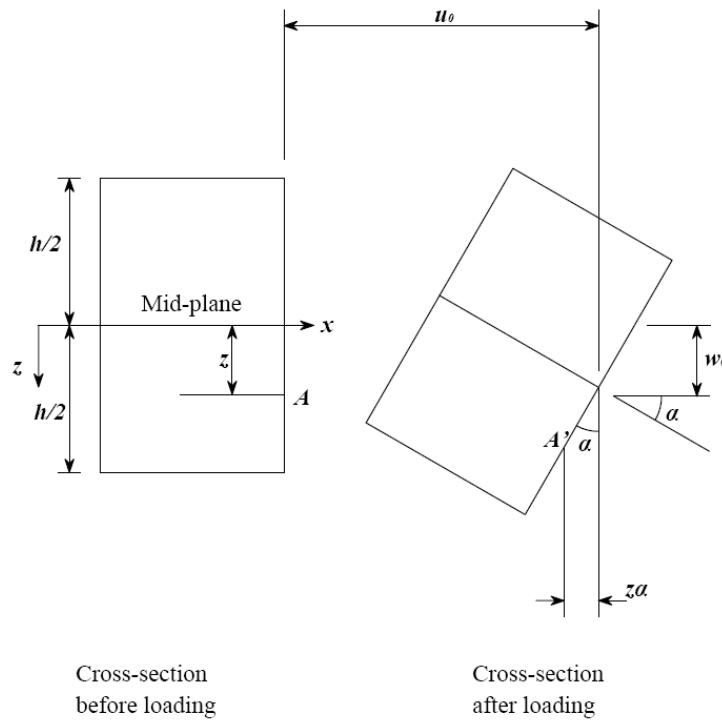


Figure 3.6: Relationship between displacements through the thickness of a plate to mid-plane displacements and curvatures

From Figure 3.6

$$u = u_0 - z\alpha \quad (3.2.6)$$

$$v = v_0 - z\alpha \quad (3.2.7)$$

where

$$\alpha = \frac{\delta w_0}{\delta x} \quad (3.2.8)$$

Thus, the total displacement u in the x direction is

$$u = u_0 - z \frac{\delta w_0}{\delta x} \quad (3.2.9)$$

By taking the cross section in the yz plane the total displacement in the y direction would be

$$v = v_0 - z \frac{\delta w_0}{\delta y} \quad (3.2.10)$$

From Equations 3.2.9 and 3.2.10 and the definition that states that strain is the derivative of displacement in the xy plane.

$$\begin{aligned} \varepsilon_x &= \frac{\delta u}{\delta x} \\ &= \frac{\delta u_0}{\delta x} - z \frac{\delta^2 w_0}{\delta x^2} \end{aligned} \quad (3.2.11)$$

$$\begin{aligned} \varepsilon_x &= \frac{\delta v}{\delta y} \\ &= \frac{\delta v_0}{\delta y} - z \frac{\delta^2 w_0}{\delta y^2} \end{aligned} \quad (3.2.12)$$

and

$$\begin{aligned} \gamma_{xy} &= \frac{\delta u}{\delta x} + \frac{\delta v}{\delta y} \\ &= \frac{\delta u_0}{\delta x} + \frac{\delta v_0}{\delta y} - 2z \frac{\delta^2 w_0}{\delta x \delta y} \end{aligned} \quad (3.2.13)$$

Form plate theory the midplane curvatures have now been derived to be

$$\begin{pmatrix} \kappa_x \\ \kappa_y \\ \kappa_{xy} \end{pmatrix} = \begin{pmatrix} -\frac{\delta^2 w_0}{\delta x^2} \\ -\frac{\delta^2 w_0}{\delta y^2} \\ -\frac{\delta^2 w_0}{\delta x \delta y} \end{pmatrix} \quad (3.2.14)$$

3.2.3 Stresses and strains for shell elements

The 3 midplane element strains: ε_x ε_y and ε_{xy} and 3 bending curvatures: κ_x κ_y and κ_{xy} are used to calculate the element in-plane strains on the lower and upper surface with the following relationships (Vanderplaats R&D, 2008a):

$$\varepsilon_x = \varepsilon_x^0 - z\kappa_x \quad (3.2.15)$$

$$\varepsilon_y = \varepsilon_y^0 - z\kappa_y \quad (3.2.16)$$

$$\gamma_{xy} = \gamma_{xy}^0 - z\kappa_{xy} \quad (3.2.17)$$

Where z is the fibre (the word fibre here refers to a specific out-of-plane distance) distance and the right hand rule is applied to the element grid points in order to determine the positive direction (Vanderplaats R&D, 2008a).

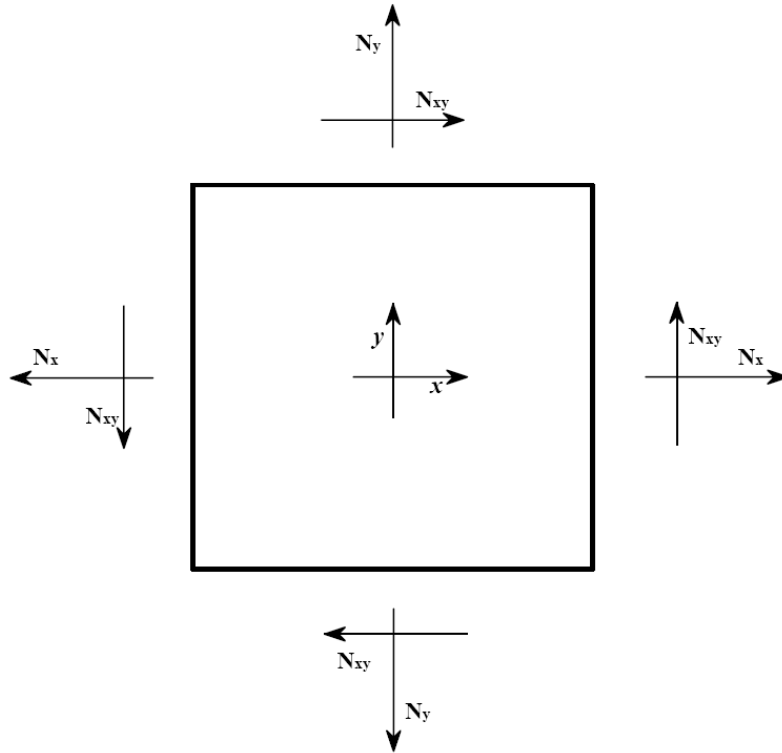


Figure 3.7: Membrane element forces in shell elements

The 3 inplane element forces: N_x N_y and N_{xy} and 3 bending moments: M_x M_y and M_{xy} are used to calculate the element surface stresses on each surface with the following relationships (Vanderplaats R&D, 2008a):

$$\sigma_x = \frac{N_x}{t} - \frac{zM_x}{D} \quad (3.2.18)$$

$$\sigma_y = \frac{N_y}{t} - \frac{zM_y}{D} \quad (3.2.19)$$

$$\sigma_{xy} = \frac{N_{xy}}{t} - \frac{zM_{xy}}{D} \quad (3.2.20)$$

where z is the fibre distance and the positive direction is determined using the right hand rule applied to the element grid points and the plate bending stiffness is represented by D (Vanderplaats R&D, 2008a):

where $D = \frac{t^3}{12}$ for homogeneous isotropic plates (Vanderplaats R&D, 2008a).

In a static analysis the principal, maximum shear and Von Mises strains are calculated on each surface using equations 3.2.21, 3.2.22, 3.2.23 and 3.2.24 (Vanderplaats R&D, 2008a).

$$\varepsilon_1 = \frac{\varepsilon_x + \varepsilon_y}{2} + \sqrt{\frac{(\varepsilon_x - \varepsilon_y)^2}{4} + \frac{\gamma_{xy}^2}{4}} \quad (3.2.21)$$

$$\varepsilon_2 = \frac{\varepsilon_x + \varepsilon_y}{2} - \sqrt{\frac{(\varepsilon_x - \varepsilon_y)^2}{4} + \frac{\gamma_{xy}^2}{4}} \quad (3.2.22)$$

$$\gamma_{max} = \sqrt{(\varepsilon_x - \varepsilon_y)^2 + \gamma_{xy}^2} \quad (3.2.23)$$

$$\gamma_{vm} = \sqrt{\frac{4(\varepsilon_x^2 + \varepsilon_y^2 - \varepsilon_x \varepsilon_y)}{9} + \frac{\gamma_{xy}^2}{3}} \quad (3.2.24)$$

In a static analysis the principal, maximum shear and Von Mises stresses are calculated on each surface using equations 3.2.25, 3.2.26, 3.2.27 and 3.2.28 (Vanderplaats R&D, 2008a).

$$\sigma_1 = \frac{\sigma_x + \sigma_y}{2} + \sqrt{\frac{(\sigma_x - \sigma_y)^2}{4} + \sigma_{xy}^2} \quad (3.2.25)$$

$$\sigma_2 = \frac{\sigma_x + \sigma_y}{2} - \sqrt{\frac{(\sigma_x - \sigma_y)^2}{4} + \sigma_{xy}^2} \quad (3.2.26)$$

$$\tau_{max} = \sqrt{\frac{(\sigma_x - \sigma_y)^2}{4} + \sigma_{xy}^2} \quad (3.2.27)$$

$$\sigma_{vm} = \sqrt{\frac{(\sigma_x - \sigma_y)^2 + (\sigma_x - \sigma_z)^2 + (\sigma_z - \sigma_x)^2}{2} + 3\sigma_{xy}^2} \quad (3.2.28)$$

Where $\sigma_z = \nu(\sigma_x + \sigma_y) - \alpha\Delta T$ for plane strain analysis and $\sigma_z = 0$ for plane stress analysis (Vanderplaats R&D, 2008a).

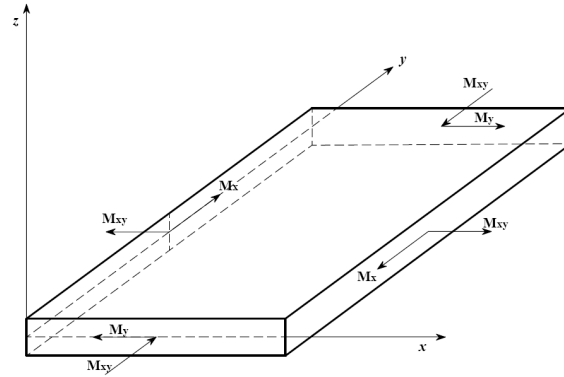


Figure 3.8: Plate element moments in shell elements

The sign convention for moments and forces in shell elements are defined in Figure 3.8 and Figure 3.7. The stresses and strains in shell elements are the same as the sign convention of the element forces (Vanderplaats R&D, 2008*a*).

3.2.4 Composite behaviour of shell elements

The elemental behaviour differs with the use of isotropic and orthotropic materials. This is because orthotropic materials have more complex material properties and a specific material orientation such as carbon fibre used in this study. This material orientation requires a change in the mathematical approach of the element (Vanderplaats R&D, 2008*a*).

With the use of composite materials the mathematical model changes to accommodate the different materials and the orientation of each material. With the use of shell elements more than one layer of materials can be modelled on a single element. Each layer can consist of either an isotropic or an orthotropic material. Composites require a specified material orientation, layer thickness and material. In the case of an isotropic material the material orientation is irrelevant. For orthotropic materials the material orientation for each layer is specified with respect to the material property orientation of the shell element. The element forces are calculated in the element coordinate system. The stresses and strains in each layer are calculated in the layer's material coordinate system (Vanderplaats R&D, 2008*a*).

The grid numbers associated with the Quad4 composite element are shown in Figure 3.9. The local material coordinate system are defined by the angle θ' , while the layer orientation is defined by the angle θ_i (Vanderplaats R&D, 2008*a*).

The composite elements use the same equations as the normal shell elements to calculate the layer stresses and strains, while the normal shell elements calculate the element stresses and strains. Composite elements calculate the failure index for each layer. These failure indexes are used as a response for design optimisation. The following relationships are used to calculate the Tsai-Wu failure criteria (Vanderplaats R&D, 2008*a*). When one of the normal stresses (fibre direction or normal to fibre direction) is significant relative to the failure stress in that direction the maximum stress failure criteria is also an accurate alternative.

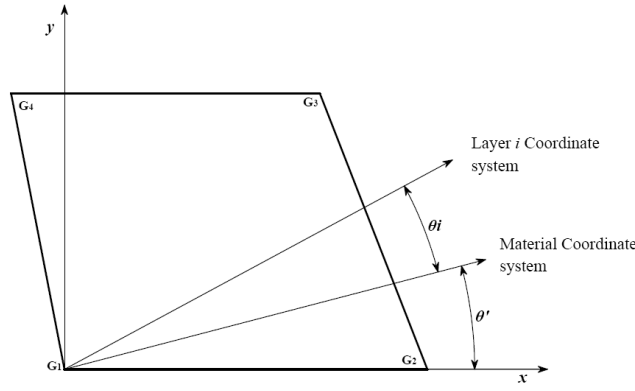


Figure 3.9: Quad4 element defining the grid numbers and coordinate systems associated with composite materials

$$FI = MAX \left(\frac{\varepsilon_1}{X_1}, \frac{\varepsilon_2}{X_2}, \frac{\gamma_{12}}{X_{12}} \right) \quad (3.2.29)$$

Where:

ε_1 = Strain in fibre direction

ε_2 = Strain transverse to fibre direction

γ_{12} = In-plane shear strain

$$X1 = \frac{X_T}{E_1} \quad \text{if } \sigma_1 \geq 0 \quad (3.2.30)$$

or

$$X1 = \frac{X_C}{E_1} \quad \text{if } \sigma_1 < 0 \quad (3.2.31)$$

$$X2 = \frac{Y_T}{E_2} \quad \text{if } \sigma_2 \geq 0 \quad (3.2.32)$$

or

$$X2 = \frac{Y_C}{E_2} \quad \text{if } \sigma_2 < 0 \quad (3.2.33)$$

$E1$ = Modulus of elasticity to fibre direction 1

$E2$ = Modulus of elasticity to fibre direction 2

$G12$ = In-plane shear modulus

$$FI = \sigma_I \left(\frac{1}{X_T} + \frac{1}{X_C} \right) + \sigma_{II} \left(\frac{1}{Y_T} + \frac{1}{Y_C} \right) - \frac{\sigma_I^2}{X_T X_C} - \frac{\sigma_{II}^2}{Y_T Y_C} + \frac{\tau_{III}^2}{S^2} + 2F_{12} \sigma_I \sigma_{II} \quad (3.2.34)$$

Where I represents the fibre direction and II the transverse direction while X_C is the allowable compressive stress in the I direction

X_T is the allowable tensile stress in the I direction

Y_C is the allowable compressive stress in the II direction

Y_T is the allowable tensile stress in the II direction

S is the allowable shear stress in the principal material system

F_{12} is the interaction term in the tensor polynomial theory of Tsai-Wu

σ_I is the stress in the I direction

σ_{II} is the stress in the II direction

3.3 Solid elements

In this study two types of solid elements were used in different parts of the FE model. These element types are the pentahedron element also known as the wedge element, and the tetrahedral element also known as the Tet3 element. Solid elements can be used to model isotropic and anisotropic materials while centrifugal, thermal and gravity loads can be applied to solid elements (Vanderplaats R&D, 2008a).

Solid elements have three displacement d.o.f. at each of the nodes, in the x, y and z directions, respectively. The grid numbers and general shape of the six noded wedge elements are illustrated in the Figure 3.10.

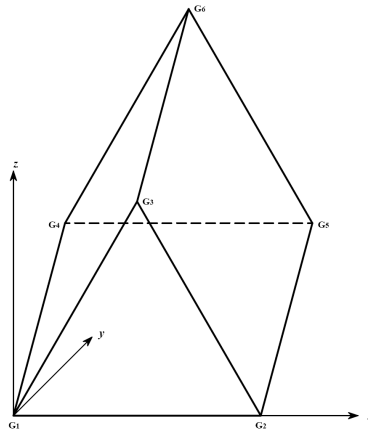


Figure 3.10: Wedge element with grid numbers defined

The grid numbers and general shape of the four noded tetrahedral elements are illustrated in the Figure 3.11.

Stresses and strains in solid elements are calculated at the centroid of each element in the material coordinate system. In a static analysis the three principal stresses or strains are calculated by sorting the results of the 3×3 eigenvalue problem from maximum to minimum. The following relationships are used to calculate the octahedral stress, maximum shear stress, Von Mises shear stress and mean pressure in static analysis (Vanderplaats R&D, 2008a).

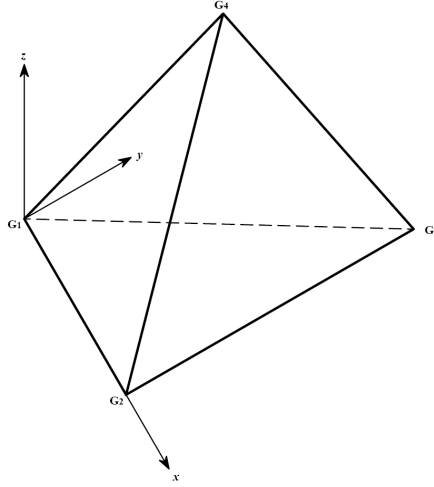


Figure 3.11: Tetrahedral element with grid numbers defined

$$\tau_{oct} = \frac{\sqrt{(\sigma_1 - \sigma_2)^2 + (\sigma_2 - \sigma_3)^2 + (\sigma_3 - \sigma_1)^2}}{3} \quad (3.3.1)$$

$$\tau_{max} = \frac{\sigma_1 - \sigma_3}{2} \quad (3.3.2)$$

$$\sigma_{VM} = \frac{3\tau_{oct}}{\sqrt{2}} \quad (3.3.3)$$

$$P_m = - \left(\frac{\sigma_1 + \sigma_2 + \sigma_3}{3} \right) \quad (3.3.4)$$

In a static analysis the Octahedral shear strain, maximum shear strain, Von Mises shear strain and the delta volume are calculated from the relationships below (Vanderplaats R&D, 2008a).

$$\varepsilon_{oct} = \frac{\sqrt{(\varepsilon_1 - \varepsilon_2)^2 + (\varepsilon_2 - \varepsilon_3)^2 + (\varepsilon_3 - \varepsilon_1)^2}}{3} \quad (3.3.5)$$

$$\varepsilon_{max} = \frac{\varepsilon_1 - \varepsilon_3}{2} \quad (3.3.6)$$

$$\varepsilon_{VM} = \sqrt{2}\varepsilon_{oct} \quad (3.3.7)$$

$$\frac{\Delta V}{V} = \varepsilon_1 + \varepsilon_2 + \varepsilon_3 \quad (3.3.8)$$

Chapter 4

Materials

In this chapter the different materials used in this study and the reasons for selecting the materials will be explained. The material related problems that occurred during the manufacturing and testing of the first generation panel will be explained. The manufacturing and material tests done on adhesives and core materials will also be explained.

4.1 Carbon fibre

In the study done in 2007 the carbon fibre sheets used were manufactured from T300 carbon fibre. This is a standard modulus carbon fibre which is readily available. The sheets were made from woven cloth in a wet layup. The study showed promising results but a FE study revealed that the face sheets should be manufactured from a high modulus carbon fibre to allow the face sheets to act as the primary stiffening agent. This can be explained by the Bernoulli-Euler beam theory which states that if a force P is applied at the mid-point of a simply-supported beam, Figure 4.1, the deflection at the mid-point is described by Equation 4.1.1.

$$\text{Deflection} = \frac{Px}{48EI} (3L^2 - 4x^2) \quad (4.1.1)$$

Where L is the length of the beam, E is the Young's modulus and I is the area moment of inertia of the structure. By looking at the relationship it is clear that an increase in the Young's modulus will decrease the deflection, which means a stiffer structure. This can also be said about the moment of inertia.

The area moment of inertia is calculated by the relationship:

$$I = \frac{bh^3}{12} \quad (4.1.2)$$

By increasing the values of b and h the value of the inertia will increase. This can be done by increasing the overall thickness h of the structure, or the width b of the structure. The overall area moment of inertia is described in Equation 4.1.3

The moment of inertia can also be increased by having as much of the material located at the outer edges of the structure i.e. increase the value of the variable y (the distance between the median z , of the overall cross-sectional area and the medians of the respective

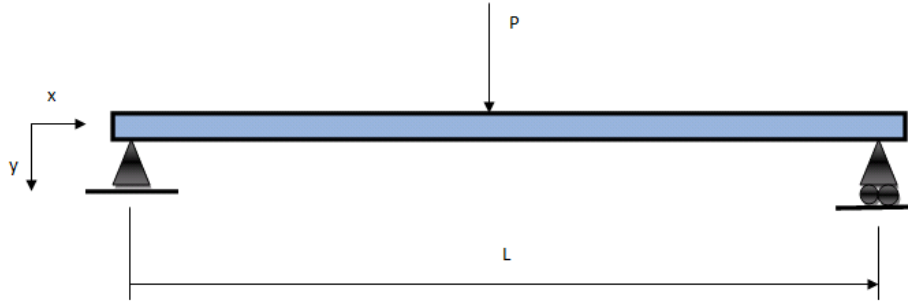


Figure 4.1: Simply supported Bernoulli-Euler beam

individual cross-sections z') in Equation 4.1.3. In Equation 4.1.3 $I_{z'}$ is the area moment of inertia for all the respective individual cross-sections about their respective medians.

$$I_z = \sum (I_{z'} + Ay^2) \quad (4.1.3)$$

By using this logic the choice was made to use a high modulus carbon fibre for the face sheets of the structure. The carbon fibre selected was K63712 manufactured by Mitsubishi Chemical. This is a very high modulus carbon fibre that can be purchased without the possession of a material licence, which is not the case for most high modulus carbon fibres. The carbon fibre was purchased in the form of an unidirectional dry cloth and the manufacturer's data sheet is illustrated in Appendix A. In this study it is very important to know the physical properties of the material since the properties will be used in the FE model of the structure. Some values for the physical properties of the K63712 dry carbon fibre were found in literature. The samples were laid up with the use of CeTePox AM 3502 A/B epoxy resin, which is the resin used throughout the duration of the study. The CeTePox AM 3502 A/B material data sheet from the manufacturer is illustrated in Appendix A. A decision was made to do tensile tests on the material according to ASTM D3039 since no test results were found in literature on this specific fibre-resin configuration.

Four layers of K63712 HMCF were used to construct the test pieces with all the fibres aligned in the longitudinal direction of the samples. All the samples were 400 mm long, 24.5 mm wide and 1.6 mm thick. Gripping tabs, constructed of a glass-fibre weave and matrix, were bonded to the ends of the test pieces. Strain gauges were also bonded to the test samples in a quarter bridge configuration and can be seen in Figure 4.2.

The material properties were calculated according to ASTM D3039. The results from the tests correlate reasonably well with that of literature and are shown in Table 4.1. The high post-curing temperature of 120 °C has no large detrimental effect on the mechanical properties of the carbon fibre skins. This makes the K63712 carbon fibre suitable for the face sheets that were manufactured for this study.



Figure 4.2: HMCf test samples prior to the test

Table 4.1: HMCf/epoxy material properties

Material	K63712
Longitudinal Modulus (GPa)	286.6
Transverse Modulus (GPa)	5.4
Poisson's Ratio	0.267

4.2 Aluminium

The core material used for this study needed to be light weight and machinable. It is also important that the material has a high thermal conductivity to ensure good heat removal away from the black boxes. One of the most commonly used aerospace structural materials is aluminium. The particular aluminium alloy used to manufacture the core of the panel was 6082-T6. This is a relatively low cost and readily available alloy. Aluminium alloy 6082 is the alloy most commonly used for machining in a plate form. This grade of aluminium is the same as used to manufacture the first generation panel in 2007 and the test samples for the manufacturing study done by Wilsenach, (2008). The most significant material properties for this study is tabulated in Table 4.2. The properties of 7075-T6 aluminium alloy are also displayed in the table.

7075-T6 aluminium alloy is the preferred alloy for aerospace applications. This is mainly because of its superior physical properties to that of the 6082-T6 alloy. The machinability of 7075-T6 is also better and a better surface finish can be achieved by using 7075-T6 aluminium. The downside of using 7075-T6 is that it is more expensive than 6082-T6. For this study the properties of 6082-T6 will be sufficient and will lower the material cost of the study and the total cost of the structure.

Table 4.2: Comparison between 6082-T6 and 7075-T6 aluminium (MatWeb, 2009) (AZOM, 2009)

Alloy Grade	6082-T6	7075-T6
Density (kg/m^3)	2700	2800
Modulus of elasticity (GPa)	70	71
Yield strength (MPa)	260	503
Shear modulus (GPa)	-	26.9
Coefficient of thermal expansion α ($10^{-6} \cdot ^\circ\text{C}^{-1}$)	23.6	23.4
Poisson's ratio	0.33	0.33
Thermal conductivity ($\text{W/m}\cdot\text{K}$)	180	130
Price (R/kg)	60-65	± 85

4.3 Magnesium

Magnesium is an alternative light weight metal that can be used to replace aluminium as the core material. Magnesium will however not be used during the course of this study, but further investigations regarding magnesium may improve the optimised structure. The advantage of using magnesium is that the density of magnesium is much lower than that of aluminium. The Young's modulus is lower but the material will still be strong enough to be used as a core material. A trial study needs to be done to ensure that magnesium can be machined with the same precision as aluminium. If this is the case the aluminium core can be replaced by magnesium. With the use of magnesium the ribs in the core structure may have to be thicker to support the loads. This thickening of the ribs may eliminate the usefulness of the much more expensive magnesium. The material properties of magnesium is given in Table 4.3.

Table 4.3: Comparison between 6082-T6 aluminium and AZ31B-H24 magnesium (MatWeb, 2009) (AZOM, 2009)

Alloy Grade	6082-T6	AZ31B-H24
Density (kg/m^3)	2700	1770
Modulus of elasticity (GPa)	70	45
Yield strength (MPa)	260	220
Shear modulus (GPa)	-	17
Coefficient of thermal expansion ($10^{-6} \cdot ^\circ\text{C}^{-1}$)	23.6	-
Poisson's ratio	0.33	0.35
Thermal conductivity ($\text{W/m}\cdot\text{K}$)	180	96
Price (R/kg)	60-65	± 1560

Because magnesium is 24 times more expensive than aluminium the weight saving will have to be sufficient to support the material cost.

4.4 Adhesives

4.4.1 Ply adhesives

During the study a number of different adhesives were used to bond the carbon fibre face sheets to the ribbed aluminium core. The first adhesive used during the manufacturing process was a ply adhesive which is usually used to bond carbon fibre to aluminium honeycomb cores. The ply adhesive is stored in a refrigerator, when the core has been prepared for the bonding process a section of the adhesive is cut to size and placed on top of the carbon fibre face sheet. A vacuum bag is then placed over the setup and once vacuum is applied the setup is placed in an oven at 120 °C for 8 hours.

This adhesive caused a few problems after the curing process was complete. During the manufacturing of the first generation panel the carbon fibre face sheets tended to make indentations over the pockets in the aluminium core. In a manufacturing study done by Mr. R. Wilsenach in 2008 it was determined that the indentations occurred due to the difference in the thermal expansion coefficient of carbon fibre and aluminium. The aluminium expands a greater amount than the carbon fibre during the bonding process at 120 °C. Since the bond cures at 120 °C the aluminium is still in an expanded state. When the structure cools down to room temperature the aluminium shrinks more than the carbon fibre and this change in size of the aluminium structure causes the carbon fibre face sheets to buckle over the pockets. The larger pockets in the core tend to cause larger indentations. This finding during the study of Mr. R. Wilsenach motivated the decision to find an adhesive which cures at room temperature (Wilsenach, 2008).

4.4.2 Room temperature curing adhesives

The study done by Mr. R. Wilsenach researched the use of an epoxy resin which cures at 25 °C. This epoxy is manufactured by 3M and is known as 3M Scotch-weld 2216 B/A Gray. This is a two part epoxy which is mixed in a weight ratio of 7 parts of part A mixed with 5 parts of part B. This epoxy was chosen because it is outgassing classified which makes it suitable for space industry use. Outgassing is the phenomenon where a material loses mass when placed in a vacuum environment. The mass lost in the vacuum environment could collect on optical lenses or it could interfere with electronics of the satellite. This is the reason why outgassing should be limited with regards to satellites. According to the American Society for Testing and Materials (ASTM), ASTM E 595-93, and the European Cooperation for Space Standardization (ECSS), ECSS-Q70-02, in order for a product to be outgassing certified, two criteria need to be met namely: total mass loss (TML) of less than 1.0% and maximum collected volatile condensable material (CVCM) of less than 0.10% (ASTM, 1999) (ECSS, 2002).

All the structures bonded with the use of the Scotch-weld 2216 B/A Gray presented no indentation or buckling problems. A syringe was used to carefully apply the adhesive on the thin aluminium ribs. Only one carbon fibre face sheet could be bonded at a time since the side of the rib with the applied epoxy needed to be turned to face downwards. This ensures the epoxy doesn't flow down the ribs but onto the carbon fibre face sheet positioned below the ribbed core. The structures bonded with the Scotch-weld 2216 B/A Gray did however have some problems regarding the stiffness of the panel when the high

modulus carbon fibre was used as a face sheet material. The shear modulus of the epoxy is not high enough to fully utilise the stiffness of the high modulus carbon fibre. The flexibility of the epoxy allowed a small amount of movement as the structures deformed, which meant that the structures were not as stiff as the FE models predicted it to be. A different adhesive needed to be found which has a higher shear modulus than the Scotch-weld 2216 B/A Gray. The higher shear modulus will allow the high modulus carbon fibre face sheets to act as the main stiffening agents in the structure (Wilsenach, 2008).

In this study, research was done to find a suitable room temperature curing adhesive, which has a high enough shear modulus to successfully transfer the stresses from the core to the high modulus carbon fibre face sheets, with minimal flexibility of the bond. 3M recommended the use of a high strength Scotch-weld 9323 B/A. The two part epoxy is mixed in a weight ratio of 100 parts of part B to 27 parts of part A. The mechanical properties of the adhesive were however not available which meant that some material tests needed to be done on the cured adhesive to determine the shear modulus and Young's modulus. Outgassing tests were also done on the adhesive to verify the suitability of the Scotch-weld for space use. The material data sheet from the manufacturer is illustrated in Appendix A.

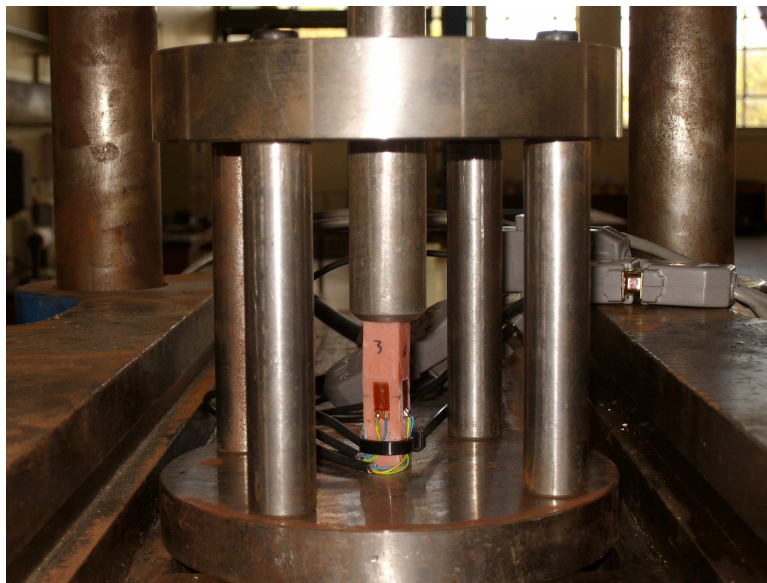


Figure 4.3: Adhesive material test sample

The material test done on the Scotch-weld 9323 B/A was a compression test according to ASTM D695-02a. The test samples were prepared by mixing the two part epoxy and placing the mixed uncured epoxy in a vacuum chamber in order to remove the air bubbles trapped within the epoxy during the mixing process. The mixed epoxy was then potted into moulds to allow the epoxy to cure in a shape close to the shape of the final test sample. The potted uncured epoxy was put back into the vacuum chamber to extract the air bubbles entrapped during the potting process. The samples were left to cure for 7 days at 25 °C. The test was done on two samples. On each of these samples four strain gauges were bonded to accurately measure the strain of the samples under load as shown in Figure 4.3. To measure the force acting on the sample a 10 kN load cell was used. The test setup is shown in Figure 4.4. The test data was gathered with the use of a Spider 8-30

data logger sampling at 50 Hz. The dimensions of the samples are displayed in Table 4.4.

Table 4.4: Dimensions of the epoxy compression test samples

Specimen No.	1	2
Length (mm)	50	50
Thickness: (mm)	12.1	11.88
Width: (mm)	12.14	12.16
Cross-sectional Area (mm ²)	146.89	144.46



Figure 4.4: Adhesive material test setup

After the tests were done the data was analysed to calculate the shear modulus (G) and the Young's modulus of the adhesive. In order to calculate these values the Poisson's ratio needed to be known. Since the material data sheets did not contain the Poisson's ratio literature was used to assume a value to enable the researcher to do the necessary calculations. The value for the Poisson's ratio from O'Brien *et al.*, (2007) of $\nu = 0.4$ was used. The Young's modulus was calculated by calculating the gradient of the linear part on the stress-strain graph (Figure 4.5). The shear modulus was calculated with the following relationship and the results are shown in Table 4.5.

$$G = \frac{E}{2(1 + \nu)} \quad (4.4.1)$$

These tests proved that the Scotch-Weld 9323 B/A should perform better than the Scotch-Weld 2216 B/A Gray during the manufacturing, testing and operation of a hybrid sandwich structure. The finite element results, Chapter 5, showed good agreement with the measured natural frequency results of the structure, Chapter 7.

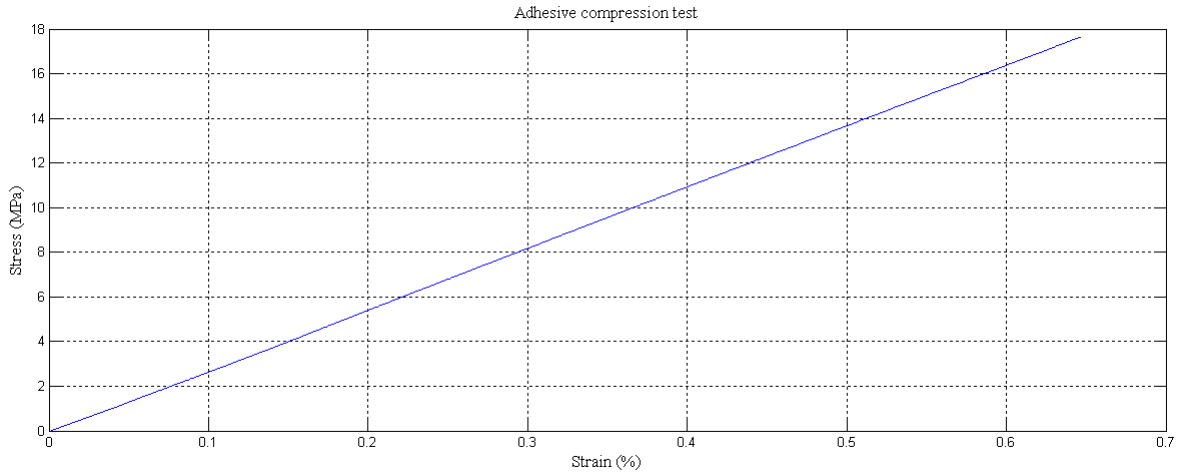


Figure 4.5: Adhesive material test results

Table 4.5: Results from epoxy pressure test and theoretical data for Scotch-Weld 2216 B/A Gray

Specimen No.	1	2	Average	2216 B/A
Modulus of elasticity (GPa)	2.75	2.83	2.79	-
Shear modulus (GPa)	0.983	1.011	0.997	0.342

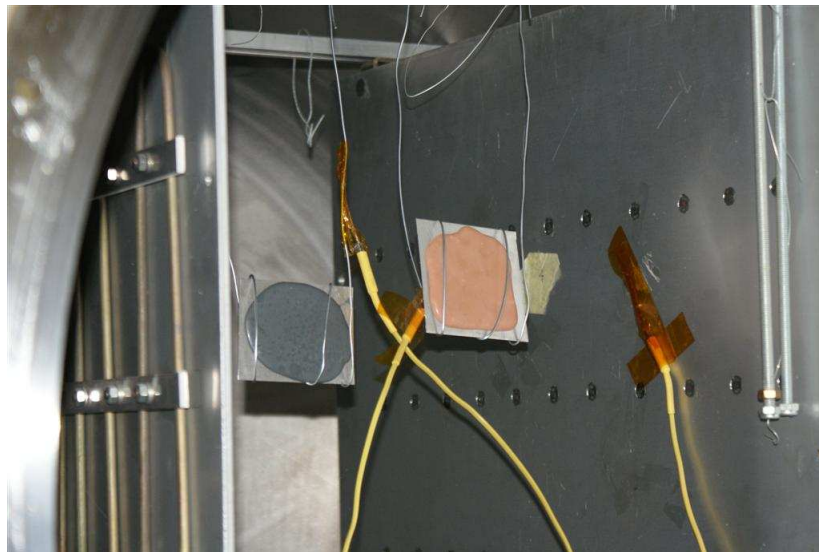


Figure 4.6: Outgassing test samples positioned in the vacuum chamber

Since the Scotch-weld 9323 B/A is not an outgassing certified material, outgassing tests needed to be done on the adhesive to verify that the epoxy is suitable for satellite use. The test samples were prepared by bonding a lump of Scotch-weld 9323 B/A and Scotch-weld 2216 B/A Gray to aluminium plates. These plates are shown in Figure 4.6. The reason why both the adhesives were tested was to compare the results, since Scotch-weld 2216 B/A Gray is an outgassing certified material. A scale that can measure accurately to 0.1 mg was used to measure the adhesives during each stage of the test. The test samples were placed in a vacuum chamber at vacuum pressures between 2 mBAR

and 25 mBAR, Figure 4.7, at 60 °C for a 24 hour period. The results from the tests are displayed in Table 4.6.



Figure 4.7: Vacuum chamber used for outgassing test

To calculate the total mass loss (TML) the test samples were weighed before the test was conducted to find the control mass of the sample. As soon as the 24 hour vacuum test was completed the samples were weighed again. This new mass was used to calculate the TML of the adhesive material with the following relationship:

$$\text{TML} = \left(\frac{m_1 - m_2}{m_1} \right) \times 100\% \quad (4.4.2)$$

Where m_1 is the mass before the samples were placed into the vacuum chamber and m_2 is the mass after the 24 hour vacuum test was completed. The measured TML can be significantly reduced in practice if post curing at an elevated temperature is done on the adhesive (panel) after manufacturing.

Table 4.6: Results from the outgassing test

Scotch-weld No.	9323 B/A	2216 B/A Gray
Aluminium plate (g)	16.6130	14.1294
Uncured epoxy mass (g)	17.4320	15.9908
Cured epoxy mass (g)	17.5249	16.0375
Epoxy mass after 24 hour at 60 °C in vacuum (g)	17.4605	15.9947
Epoxy mass 14 days after vacuum test (g)	17.5076	16.0265
TML after 24 hour vacuum (%)	0.368	0.267
Conservative maximum CVCM (%)	0.099	0.069

The CVCM could not be measured according to ASTM E595-93 where a cold plate is used to collect the collectable volatile condensable materials during the vacuum test.

During this study the CVCM was calculated conservatively by assuming that all volatiles, excluding water vapour, will condense on a cold plate, which is usually not the case since some of the volatiles will not condense on the cold plate and escape with the air through the vacuum pump. By allowing the test samples to re-absorb all the water vapour that evaporated during the heated vacuum test, and comparing the mass of the samples 2 weeks after the test with the sample mass prior to the test, the maximum mass of the volatiles released during the test can be calculated with the following relationship:

$$\text{CVCM} = \left(\frac{m_1 - m_3}{m_1} \right) \times 100\% \quad (4.4.3)$$

Where m_3 is the mass of the sample 14 days after the vacuum test was completed. This allows the cured adhesive to re-absorb the water vapour that evaporated during the vacuum test.

These tests proved that the Scotch-Weld 9323 B/A should perform better than the Scotch-Weld 2216 B/A Gray during the manufacturing, testing and operation of a hybrid sandwich structure.

Chapter 5

Design and Optimisation

5.1 Structural optimisation

Extensive research for automising structural design through numerical optimisation methods has been done and these methods found their way into engineering offices. Much of the research done to optimise structural design has been devoted to creating approximation methods that allow for a high degree of efficiency and maintain the essential features of the design problem. In order to use Genesis for structural optimisation an approximation of the original problem needs to be created. Genesis solves this approximate problem with the advantage of not having to repeatedly call on the finite element analysis during the optimisation process. This reduces design time and cost. The special techniques contained in Genesis used for this study, which makes modern structural optimisation efficient, will be discussed in this section (Vanderplaats R&D, 2008*b*).

5.1.1 General Genesis optimisation process

Genesis uses 10 basic steps during the structural optimisation process. These steps allow Genesis to solve the structural design problem without a large number of full finite element analyses. The process uses approximations which retain the key features of the detailed analysis model in order to find the same design that would have been found when using the FE analysis directly during optimising (Vanderplaats R&D, 2008*b*).

The first step is to pre-process all the input data and to perform all non-repetitive operations. The next step performs a detailed finite element analysis for the initial design the design objectives and constraints are evaluated. Then all constraints are screened and only the critical or near critical constraints are retained for further considerations. Typically only $2n$ or $3n$ constraints are retained, where n represents the number of independent design variables. The next step is to perform a sensitivity analysis for the responses included in the retained constraints and objective function. A high quality approximation to the original problem is created and solved with the use of the DOT or BIGDOT optimisers. If no design improvement is possible due to no change in the design variables the program exits, this is called soft convergence. If the program does not exit, the analysis data is updated and a new detailed finite element analysis is performed for the proposed design. The constraints and the precise objective function are evaluated. If no improvement is made from one design cycle to the next, even if the design variables changes significantly, and all the design constraints are satisfied, hard convergence is achieved. The program

performs a detailed finite element analysis to ensure the quality of the proposed design and exits. If improvements are still being made towards an optimum the design cycle ends and the cycle is repeated from the screening process onwards (Vanderplaats R&D, 2008*b*).

5.2 Topology optimisation

Topology optimisation is used to find the optimal distribution of material in a given space for a specific set of constraints and loading conditions. Topology optimisation does not require an initial design and usually starts of with a block of material formed by a large number of finite elements. The optimisation process will eliminate the elements that do not contribute to the optimal design solution. The normal use of topology optimisation is to perform conceptual design for stiff and light structures.

Genesis associates the design variables with the Young's modulus and density of the elements in a package space in order to perform topology optimisation. The design variables range between 0.0 and 1.0. A value of 1.0 indicates the element has its normal mass and stiffness and 0.0 indicates that the element has no mass or stiffness. Since material properties are not variable the optimised value of the design variable is a indication of which material to keep (design variable value close to 1.0) and which material to discard (design variable value close to 0.0). Genesis allows the user to enforce some manufacturing constraints such as cast ability, extrusion, symmetries and minimum member size (Vanderplaats R&D, 2008*b*). Topology optimisation is used in this study to find the placements of the ribs in the aerospace structure panel.

Genesis does topology optimisation in three steps. First the design regions are defined where topology optimisation needs to be applied. The design constraints and the objective function are then defined. Finally manufacturing constraints are selected for the desired design (Vanderplaats R&D, 2008*b*).

When topology optimisation is finished, sizing optimisation can be done to refine the solution. Sizing optimisation is done by assigning design variables to a design region with a design objective and design constraints (Vanderplaats R&D, 2008*b*). This study uses sizing optimisation to find the optimal rib thickness.

5.3 First generation panel optimisation

The first step in optimising the first generation panel was to replace the T300 carbon fibre with high modulus Mitsubishi K63712 carbon fibre. To calculate the increase in stiffness by using the Mitsubishi K63712 carbon fibre a FE model was created with Mitsubishi K63712 face sheets instead of T300 face sheets. The model showed an increase in stiffness of 97.9% and a reduction in deformation of 0.768 mm to 0.388 mm. Figure 5.1 shows the deformation plot from the FE analysis done with high modulus carbon fibre.

In order to reduce the weight of the core the FE analysis done on the panel with the high modulus carbon fibre was used to identify the ribs that did not contribute to the

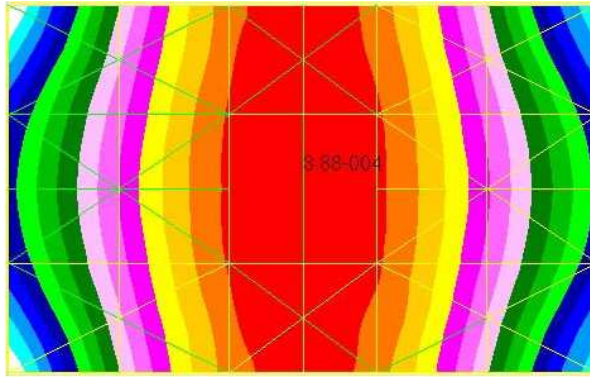


Figure 5.1: High modulus carbon fibre FE model pinned at the four corners (maximum deformation of 0.388 mm)

stiffness of the core. All the ribs with a stress of less than 5 MPa were removed from the model. It is however important for the ribs not to be too far apart since this might lead to problems during the bonding process of the carbon fibre face sheets.

The model where the ribs have been removed was imported into Genesis where the rib thicknesses would be optimised (Figure 5.2). The relatively thick ribs would allow for good heat transfer from the heat source in the centre of the panel. To ensure that the ribs would be easily machinable and to leave sufficient bonding area for the epoxy to bond the face sheets to the ribbed core, the minimum rib thickness was set to 0.5 mm with a maximum rib thickness of 2.5 mm. The ribs below the mounting interface of the black box or electronic box have been limited to a minimum thickness of 2 mm and a maximum thickness of 6 mm. Each rib was assigned an independent design variable to allow Genesis to optimise each rib separately. The maximum rib stress allowed was set to be 50 MPa even though the yield stress of 7075-T6 aluminium is 505 MPa. The design objective for the analysis was to get the panel as light as possible.

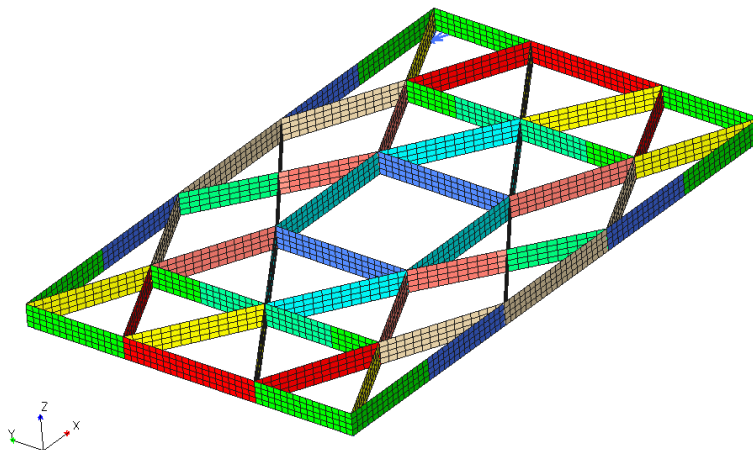


Figure 5.2: First generation ribbed core structure imported into Genesis

The results obtained from the analysis were studied and the MSC Patran FE model was updated and analysed to verify any improvements made on the stiffness and weight of the panel. The Genesis solver thinned all the ribs down to 1.06 mm and the mounting rib for the black box was thinned to the allowed 2 mm. These dimensions were used to update the FE model. The new FE model was analysed and the results showed that the panel was slightly less stiff but a large improvement in the overall weight was obtained.

The maximum panel deformation was 0.388 mm before any ribs were removed; the optimised core had a deformation of 0.413 mm. The optimised panel has a 33% reduction in weight from 0.798 kg to 0.534 kg. The deformation plot of the optimised structure is shown in Figure 5.3.

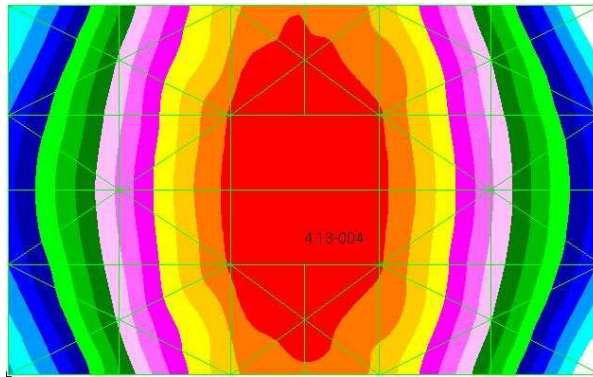


Figure 5.3: Deformation plot of the optimised aluminium core of the first generation panel pinned at the four corners (maximum deformation of 0.413 mm)

The stress values in the ribs reach a maximum of 25.3 MPa; this gives the core a safety factor of about 20. The four ribs that carry most of the load can clearly be seen in Figure 5.4. Most of the other ribs carry a very low amount of the load and thus the stresses in those ribs are low. However to prevent the face sheets to dent into the pockets it is necessary to have more than just the four ribs. The ribs all provide for bonding area for the epoxy that is used to bond the carbon sheets to the metal core.

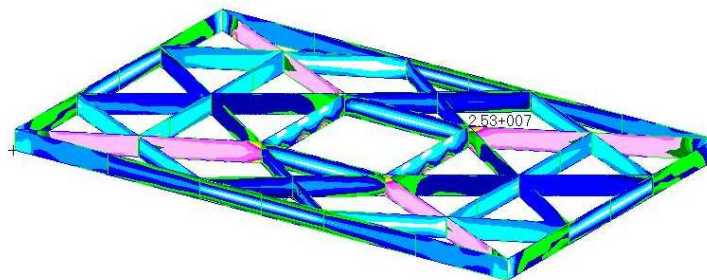


Figure 5.4: Stresses in the ribs of the optimised aluminium core of the first generation panel pinned at the four corners (maximum rib stress of 25.3 MPa)

5.3.1 First generation panel with magnesium core

The FE model used in the first attempt with an aluminium core was modified so that the core material is changed to magnesium. Since magnesium has a density of only 1800 kg/m^3 it will make a big difference in the overall weight of the panel. The FE model was imported into Genesis and the sizing constraints on the rib thicknesses were set to the same values used for the aluminium. The stress constraints were set to a maximum of 30 MPa in the ribs. The low stress constraints keep the ribs thick enough for bonding purposes.

The results from the Genesis analysis was exactly the same as that obtained for the aluminium core. The rib thicknesses of the FE model were changed to the Genesis results and the optimised core was analysed. The analysis showed a slight decrease in stiffness from 0.413 mm deformation to 0.443 mm, shown in Figure 5.5. This is only a minor decrease compared to the 22.1% decrease in weight from 0.534 kg for the aluminium cored panel to 0.416 kg for the magnesium cored panel.

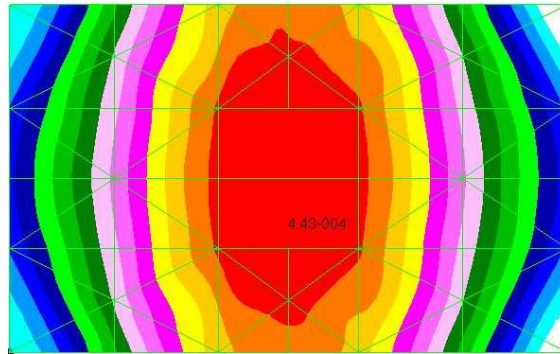


Figure 5.5: Deformation plot of the optimised magnesium core of the first generation panel pinned at the four corners (maximum deformation of 0.443 mm)

The maximum stress in the magnesium core is 21.1 MPa as shown in Figure 5.6 and is slightly less than that of the aluminium core. The weight of the magnesium core is less than that of one of the carbon fibre face sheets. This is one of the aims of the project, namely the core should not add a large amount of weight to the structure.

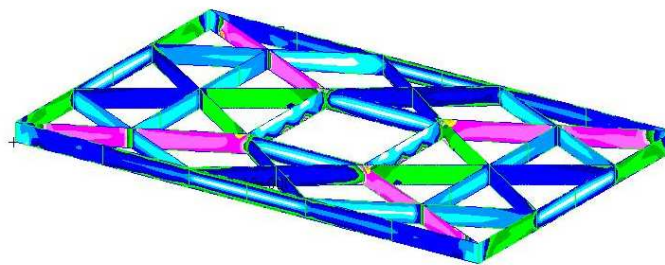


Figure 5.6: Stresses in the ribs of the optimised magnesium core of the first generation panel pinned at the four corners (maximum rib stress of 21.1 MPa)

5.4 Second generation aerospace structure panel

The second generation panel consists of mounting interfaces for five black boxes (packaged electronic units) of different sizes and weights. The panel is a base plate for the satellite and therefore carries nearly all the acceleration mass loading of the complete satellite during launch. The layout of the black boxes is shown in Figure 5.7.

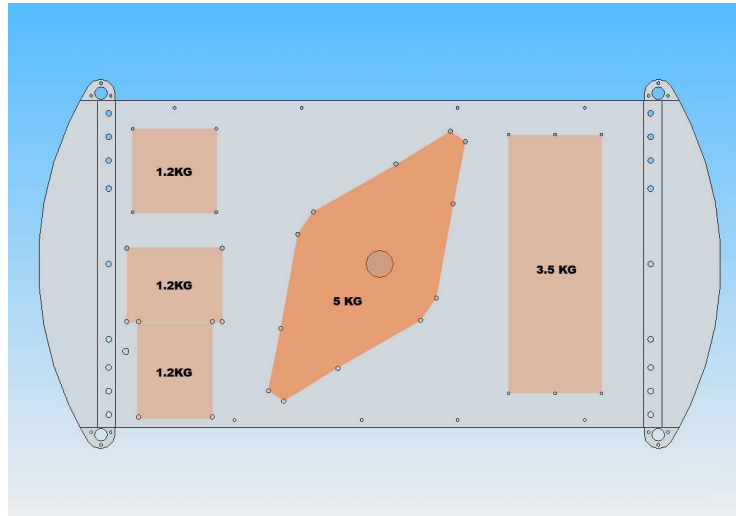


Figure 5.7: Second generation panel black box positions

In order to optimise the second generation panel rib layout a number of design and optimisation steps needed to be followed. These steps were to firstly find the position of the ribs with the use of topology optimisation. Secondly the ribs thicknesses needed to be optimised for minimum weight. The designer needs to create a basic FE model of a solid structure which can then be imported into the Genesis optimiser for the topology optimisation. The topology results will give the positioning of the required ribs to sufficiently stiffen the structure. A new FE model, containing shell element ribs, needs to be created in which the results from the topology optimisation can be implemented. This new FE model can now be imported into the Genesis optimiser where the rib thicknesses will be optimised with the use of sizing optimisation. The sizing optimisation results can now be used to update the FE model shell thicknesses to create the final FE model which can be analysed prior to manufacturing to verify the optimised structural design.

5.4.1 FE model prior to topology optimisation

In order to set up the topology optimisation model, a solid FE model consisting of the basic geometry needed to be created. A CAD model of the parts of the model that could not be optimised were created with the use of AutoDesk Inventor. This CAD model contained the aluminium semi-circular solid ends of the panel and the positioning of the black boxes bolt holes. This model can be seen in Figure 5.8. The CAD model was then imported into MSC Patran in the form of an IGES file.

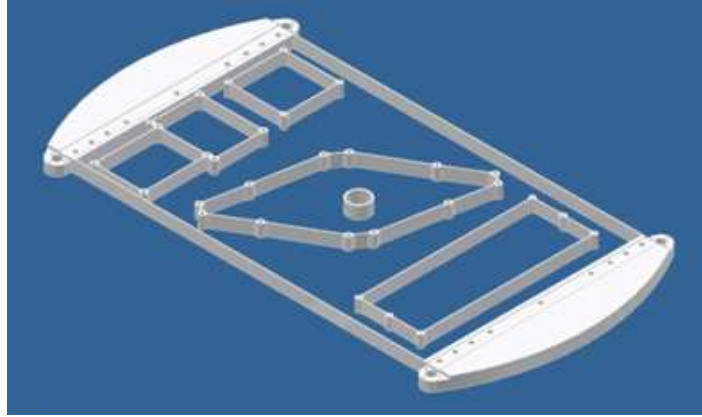


Figure 5.8: CAD model of second generation panel geometrical blackbox layout

The newly imported FE model was modified with the use of MSC Patran. Generally when ribbed and pocketed aluminium satellite structures are used, there will at least be ribs covering the outside borders of the black boxes. It was decided to use this same principle in the development of the second generation panel. These ribs were created with Quad4 shell elements, spanning between the bolt positions of each black box and covering the entire 20 mm depth of the panel with 10 elements through the depth of the panel. These shell elements were 1.5 mm thick with the properties of 6082-T6 aluminium. Quad4 elements were also used to create connections between the two semi-circular solid aluminium ends of the structure. These connection ribs were 2 mm thick aluminium with 10 elements through the depth of the structure. These ribs are shown in Figure 5.9. The mass and COG of each of the black boxes was inserted into the model with the use of mass elements. Each of these mass elements is positioned at the COG of each of the black boxes.

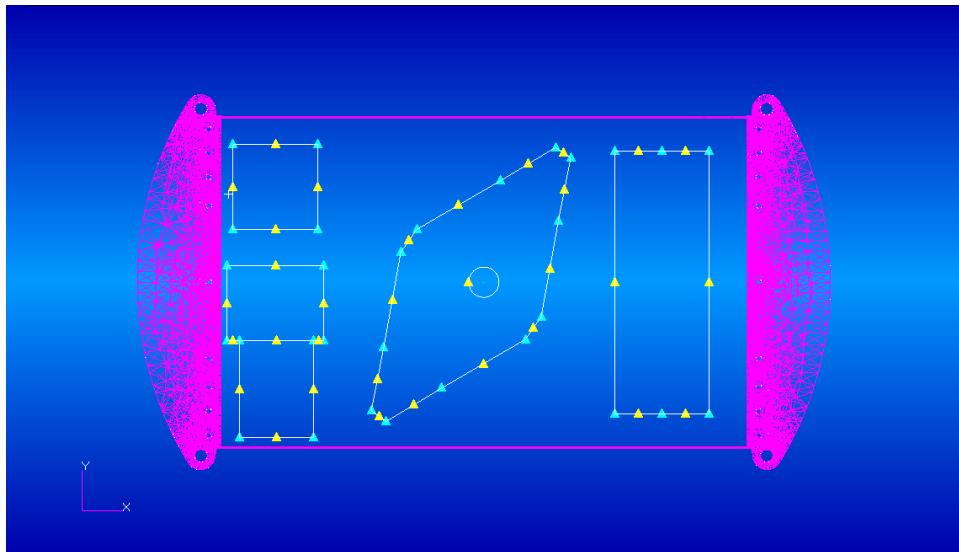


Figure 5.9: FE model of second generation panel containing ribs on the blackbox edges

Next the semi-circular solid aluminium edges were meshed with Tet3 elements. The mesh was done with auto-meshing with mesh control on the inside face of each solid

structure. This was done to ensure the nodes line up in the next step of the FE model.

Surfaces were created in the positions of the carbon fibre face sheets. These surfaces were then meshed with a large number of small Tria3 elements; this was done to set the model up for the creation of the design region that will be used in the topology optimisation. The mesh seed ensured the alignment of the nodes on the edges of the surfaces where the solid elements meet the new carbon fibre elements. The carbon fibre sheet layup consisted of 3 layers in a $[0/90/0]$ layup with the 0° angle in the longer direction of the structure. Each layer is 0.3 mm thick with the mechanical properties of the tested carbon fibre.

The carbon fibre face sheet elements were then used to extrude Wedge6 elements through the thickness of the panel. The Tria3 elements of the face sheets act as a template for the size of the wedge elements. Ten elements were extruded through the thickness of the structure. This was done to create an acceptable size ratio for the wedge elements and to align the nodes with the already created Quad4 ribs and the Tet3 solid elements. These wedge elements will act as the design region during the topology optimisation. These wedge elements were given the same aluminium properties as the rest of the aluminium parts in the model and is shown in Figure 5.10.

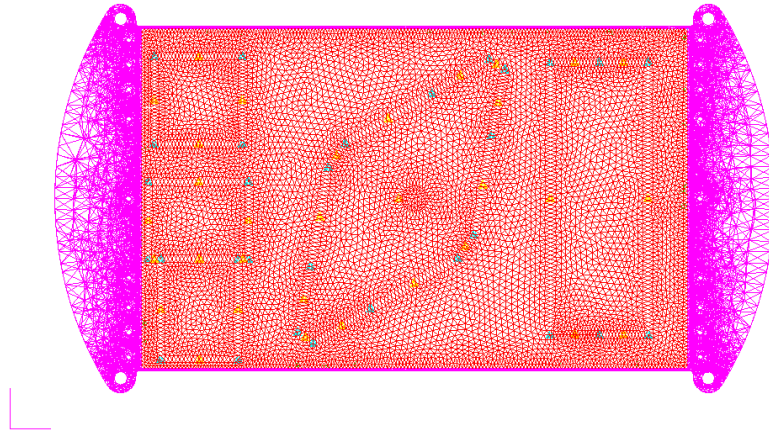


Figure 5.10: FE model of second generation panel prior to topology optimisation

The boundary conditions on the FE model were created to match that of the original SunSpace designed structure. A node was created 500 mm underneath the structure, positioned to align with the middle of the structure. From this node a set of rigid links were created to all the nodes at the four corners of the structure. These corners are designed to fit to the launch vehicle structure. The rigid links were constrained in all displacement and rotational directions as illustrated in Figure 5.10. The model was now complete and a modal analysis was done to help setting up the load case that will be used in the Genesis optimiser.

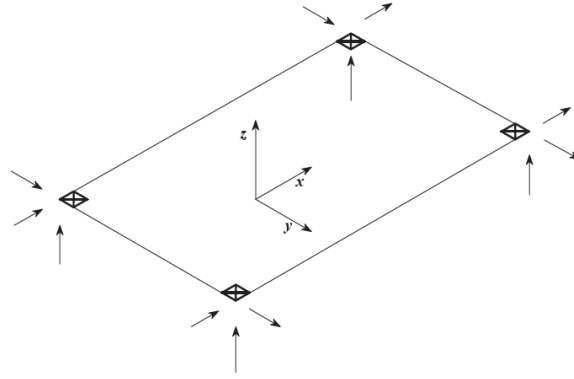


Figure 5.11: Illustration of clamped boundary condition used during the duration of the study

5.4.2 Topology optimisation of second generation panel core

The FE model created with the use of MSC Patran and analysed with MSC Nastran was imported into Genesis in the form of a .bdf (Nastran bulk data file) file. Genesis categorizes groups according to different element types and shell thicknesses, composite shell elements are categorized according to the composite layup properties of the elements. The different groups are illustrated by different colours in Genesis; the Genesis model can be seen in Figure 5.12. The imported model could now be set up for the topology optimisation.

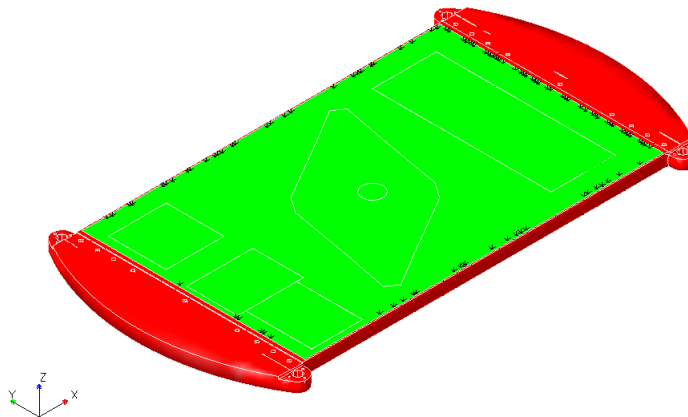


Figure 5.12: Imported model prior to Genesis topology optimisation

The first step in configuring the model prior to optimising was to define the design region and manufacturing constraints. For the design region, all the wedge elements created between the two carbon fibre face sheets were selected; the design region elements are displayed in green in Figure 5.13. The manufacturing constraints were to remove the elements through the thickness of the panel to simulate a machining process, this will also

force the optimiser to give a result that could be converted into a ribbed structure.

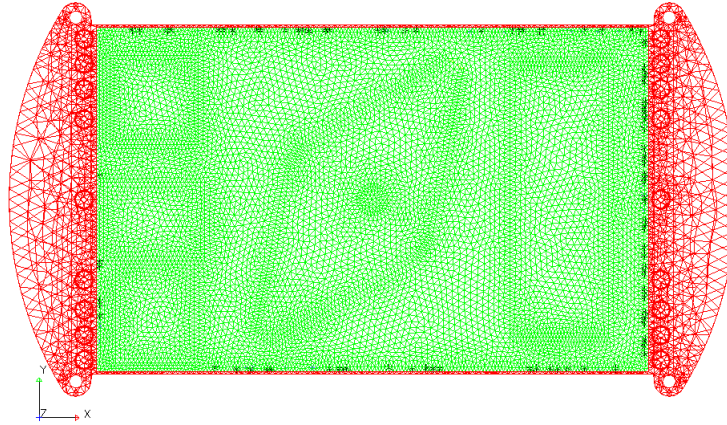


Figure 5.13: Design region for the Genesis topology optimisation

The design constraints that will be used by the Genesis optimiser were set to keep the first natural frequency higher than 130 Hz. The SunSpace designed structure has a first natural frequency of 111.5 Hz, but to optimise the present structure a lighter and stiffer structure is required as a final result. By allowing the structure to be more than 10% stiffer after the first stage of optimisation a sufficient margin will be left for the drop in stiffness during the second stage where the solid elements will be transformed into a ribbed structure.

Topology optimisation in Genesis requires the user to specify the design objectives as the maximum amount of material that Genesis are allowed to discard of during the optimisation process. For this study an iterative process was followed to find the design objective that provides the best result to use for the conversion process of solids to shells. After a number of analyses were done with different design objectives it was found that the best results were achieved with a 70% loss of material in the design region.

The Genesis optimiser used the modal analysis load case that was set up during the MSC Nastran analysis of the un-optimised structure. Genesis gives the user the option to choose between four frequency calculation methods, for this study the SMS approximation method was chosen. The SMS approximation method can be used on any size problem and the frequencies are searched according to the following table (Vanderplaats R&D, 2008a):

The lower and upper bounds are specified by V1 and V2 on the frequency range of interest. ND is the number of the desired frequencies; these frequencies include rigid body modes. The SMS approximation method requires the user to specify all of these values (Vanderplaats R&D, 2008a).

With the use of the SMS approximation method a reduced approximation of the full FE model is built. The calculated frequencies by this method are only close approx-

Table 5.1: SMS approximation frequency calculation (Vanderplaats R&D, 2008*a*)

V1	V2	ND	Modes Calculated
V1	V2	ND	At most ND modes between V1 and V2
V1	V2	Blank	All modes between V1 and V2
Blank	V2	ND	At most ND modes less than or equal to V2
Blank	V2	Blank	All modes less than or equal to V2

imations of the frequencies of the input structure. With this method a large number of frequencies can be calculated very quickly. This method is the fastest available in Genesis. The SMS approximation method calculates all the frequencies below V2 even if V1 is given. This means that the method's performance depends on the number of frequencies below V2 and not the number of frequencies between V1 and V2. The user is also given the option to switch on mode tracking; this allows the optimiser to track a certain mode shape i.e. bending or twisting modes. With mode tracking turned on the optimiser will track a mode shape even if the different mode shapes do not remain in the same order during the optimisation iterations (Vanderplaats R&D, 2008*a*). For this study mode tracking was switched off. This ensured the user that the optimiser would keep the structure stiffer than the lower boundary of 130 Hz defined in the design constraints.

The topology optimisation was done with the use of a multi-processor computer cluster from the University of Stellenbosch; six 3.2 GHz cores each with 2 Gb RAM available was used to complete the optimisation in a short time. The optimisation with the use of the computer cluster took 45 minutes to complete 8 iterations. This was 8 times faster than the laptop used to set up the model took to optimise the structure. The results of the topology optimisation can be seen in Figure 5.14 where the blue elements are the elements with a zero density and the green and red elements are the elements showing the stress paths in the design region. These elements with a density higher than zero will be replaced with Quad4 shell elements to form the ribbed structure.

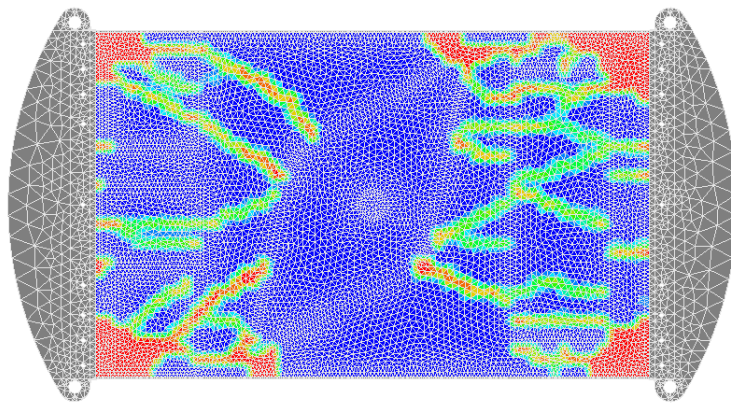


Figure 5.14: Genesis results from the topology optimisation displaying the proposed rib structure

5.4.3 FE model converting topology results into ribs

After the topology optimisation had been done a new FE model needed to be set up where the results from the topology optimisation are converted into a ribbed structure. The remaining wedge elements with a density higher than zero will be replaced by Quad4 shell elements. These new Quad4 elements can then be optimised with the use of the Genesis optimiser for the optimum shell thickness. The new FE model is created by MSC Patran by removing all the wedge elements from the first FE model created prior to the topology optimisation and inserting surfaces where the new ribs will be placed.

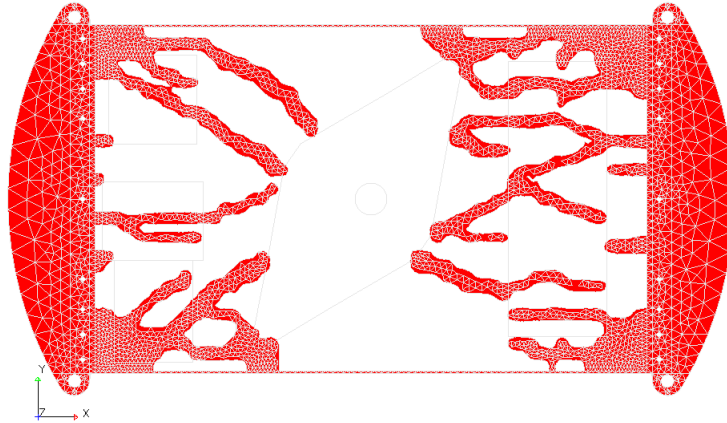


Figure 5.15: Genesis results from the topology optimisation used to position the new ribs

The mesh contained in the FE model needed to be removed before the new surfaces could be created. A new mesh could be created once the new ribs were in position. The new ribs were positioned to resemble the Genesis topology optimisation results shown in Figure 5.15. By first creating surfaces in the position of the ribs the mesh on the model could be changed, without losing the geometrical layout of the structure, until the designer is satisfied with the final mesh. The basic layout of the ribbed structure converted from the Genesis results is shown in Figure 5.16.

After closer inspection of the optimised rib layout, it was found that some of the pockets in between the ribs were too large and could cause the carbon fibre face sheets to buckle during the normal temperature fluctuations of an operational satellite. The temperatures can fluctuate between 60 °C and -20 °C. A number of ribs were added to the structure to reduce the size of the large pockets to prevent the carbon fibre face sheets from buckling. The added ribs will add weight to the structure, but the overall result will still be saving mass from the original SunSpace design. The final rib layout of the structure is shown in Figure 5.17.

This geometrical structure could then be meshed. The ribs were meshed with the use of Quad4 shell elements which will allow Genesis to optimise the thickness of the ribs. Quad4 elements are not the best elements to use for a structure under bending but the Genesis optimiser can however not analyse a structure containing Quad8 elements which can model pure bending. The solid flanges at the ends of the structure were meshed with Tet3 solid elements. The carbon fibre face sheets were meshed with the use of the paver mesh function because the mesh is not symmetrical and a combination of Quad4

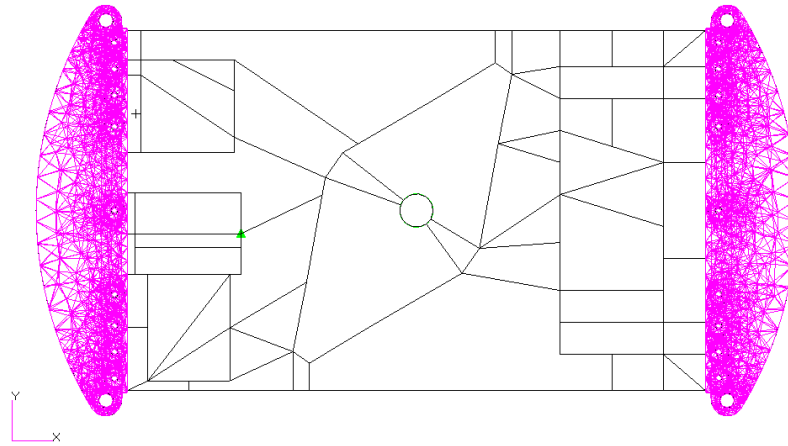


Figure 5.16: FE model displaying the layout where the Genesis results have been converted into a ribbed structure

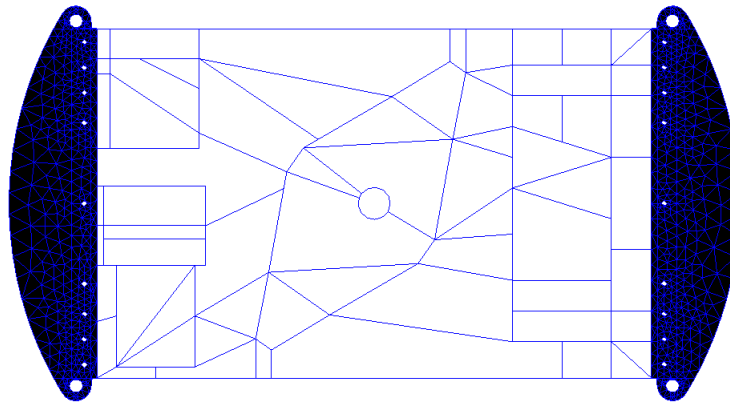


Figure 5.17: FE model displaying the rib layout where ribs have been added to make the larger pockets smaller

and Tria3 shell elements are used. In order to individually optimise the thickness of each of the ribs the FE model had to be set up in such a way that the Genesis optimiser would categorize each rib in separate groups. Since Genesis categorizes groups according to shell thickness, each of the 119 ribs was given a different thickness property. All of the ribs and the solid flanges were defined to be 6082-T6 aluminium and the carbon fibre face sheets were defined to have the layup consisting of 3 layers in a $[0/90/0]$ direction. The boundary conditions were defined to be the same as the first FE model prior to the topology optimisation. A modal analysis was done on the model to set up the load case that will be used in the sizing optimisation.

5.4.4 Sizing optimisation of second generation panel ribs

In order to find the rib thicknesses of the final second generation panel Genesis was used to optimise the thickness of each rib individually. The model was imported from the .bdf file created during the analysis of the FE model containing the optimised Quad4 element

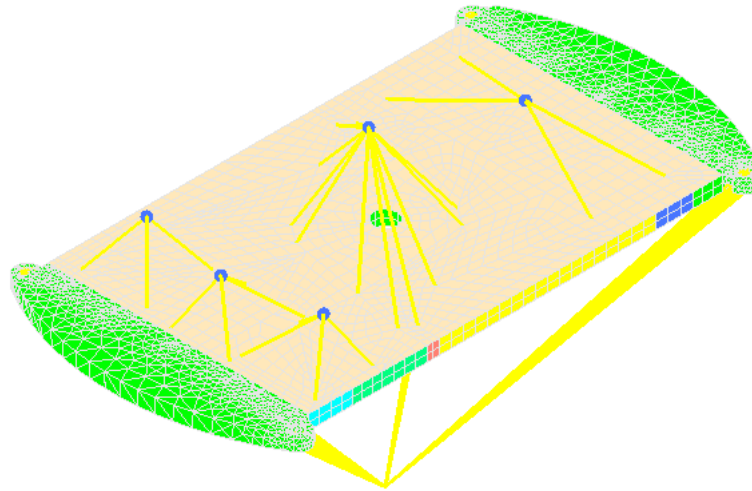


Figure 5.18: Imported ribbed model with carbon fibre face sheets and mass elements visible

rib layout developed during the topology optimisation and was defined in the previous paragraph (Figure 5.18). The model needed to be set up before the sizing optimisation could be done on the ribs. The model contained 119 different ribs which needed to be optimised. To assist the process, Genesis categorizes each rib in its own group according to shell thickness. The imported model can be seen in Figure 5.19.

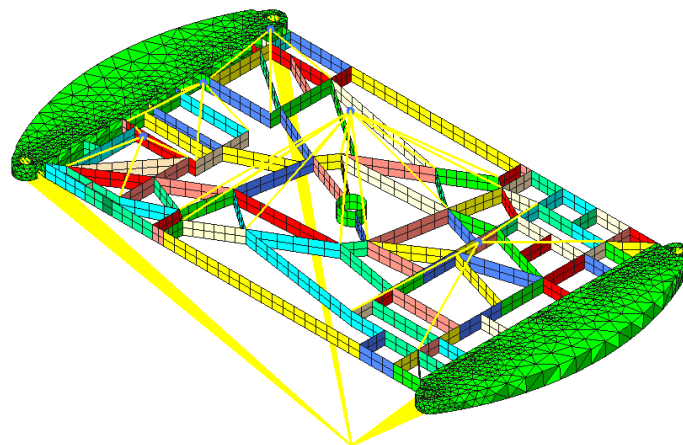


Figure 5.19: Imported Genesis ribbed model without carbon fibre face sheets visible

Sizing optimisation requires the user to specify the design variables for each region that needs to be optimised. These design variables are subjected to the manufacturability of the structure. A manufacturing study had been done to verify the thinnest ribs that could safely be manufactured. In this study 0.5 mm was successfully machined. In order to optimise each rib separately, each rib needs its own design variable. This means that the model will contain 119 different design variables. The design variables for all of the ribs on the borders of the black boxes were set to vary between a lower boundary of 1 mm and an upper boundary of 7 mm. All the ribs on the outside borders of the structure

connecting the two solid flanges were also set to vary between a lower boundary of 1 mm and an upper boundary of 7 mm. The interior ribs connecting the outer structure of the panel to the black box positions were all given each own design variable with a lower boundary of 0.5 mm and an upper boundary of 7 mm. The ring in the middle of the structure, which is the exhaust for the satellite's propulsion system, was given a lower boundary of 1 mm and an upper boundary of 7 mm.

The load case used in this stage of the structural optimisation was the same as in the topology optimisation. The modal analysis done in the FE analysis prior to the sizing optimisation was used to set up the load case. The SMS approximation was used to calculate the frequencies during the optimisation process and mode tracking were switched off. The design constraints were set to keep the first natural frequency above 115 Hz. By keeping the design constraint slightly higher than the stiffness of the SunSpace designed structure the user could be assured that the SMS approximation method would not allow the structure to be less stiff than that of the original structure.

The design objectives of the sizing optimisation were set to minimize the mass of the structure. This would ensure the optimiser to design the ribs to be as thin as possible. The sizing optimisation setup was now complete. After the optimisation process was complete the design variables all iterated to the lower boundaries. This means that the carbon fibre face sheets act as the primary stiffening agents. The first natural frequency from the sizing optimisation was 219.5 Hz. The Genesis geometrical results of the sizing optimisation were found in the Genesis output file. The frequency results from the sizing optimisation is illustrated in Appendix B.

5.4.5 FE model of optimised second generation panel

After the sizing optimisation was done the final FE model could be created in MSC Patran. The results from the sizing optimisation could now be implemented on the FE model created prior to the sizing optimisation. Since all the ribs were optimised to their respective lower boundaries the shell thicknesses of the Quad4 elements could now be changed to those lower limits. The rib thicknesses is illustrated in Figure 5.20, where the red ribs have a thickness of 1 mm and the white ribs a thickness of 0.5 mm.

This finished optimised structure now needed to be analysed with the use of MSC Nastran to verify the natural frequency results from the Genesis optimiser. A normal modes analysis was done on the structure to verify the natural frequencies with that of the optimiser. The boundary conditions for this analysis were set to be the same as for the optimisation process. The results of this analysis showed that the first natural frequency is at 141.76 Hz which means that the structure is much stiffer than the original SunSpace designed structure. The first mode of this FE analysis is shown in Figure 5.21. The modes of the frequencies higher than the first natural frequency are plotted in Appendix B.

A modal analysis was also done on the structure where the boundary conditions were slightly different. The model was set up to be free in space with only the mass elements of the black boxes attached to the structure. The clamped boundary conditions was removed from the structure; this was done to correlate the results with a modal test that was done on the manufactured structure with free boundary conditions. The first natural

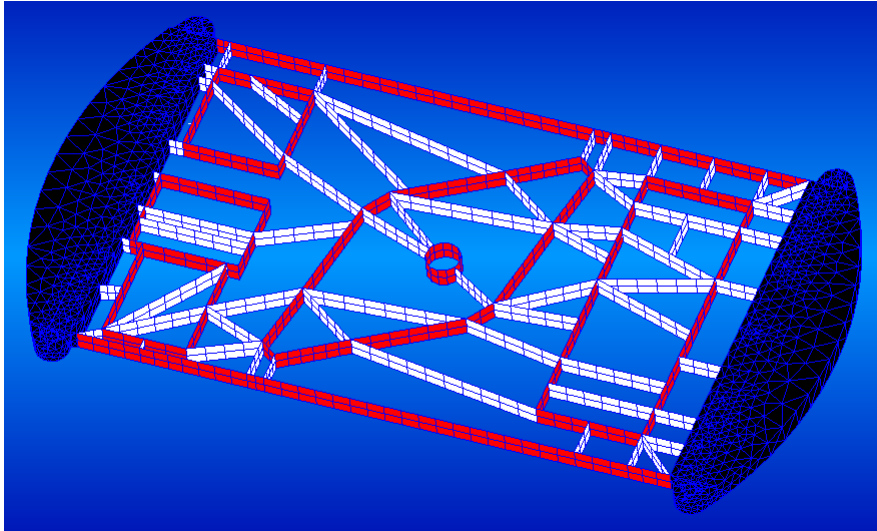


Figure 5.20: The final geometry of the structure with the rib thicknesses illustrated

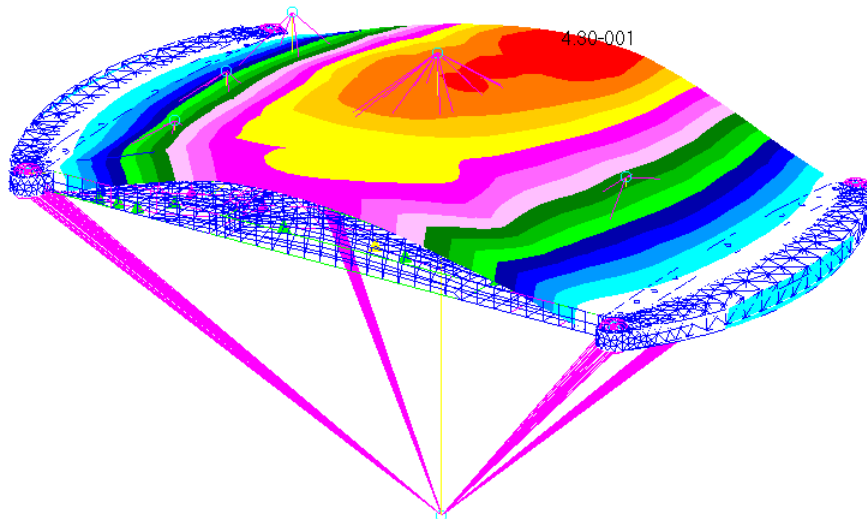


Figure 5.21: First natural frequency of FE model at 141.76 Hz with clamped boundary conditions

frequency from this FE analysis was at 145.24 Hz. The plot of this first natural mode is shown in Figure 5.22. The plots of the other natural frequencies' modes are illustrated in Appendix B.

The final FE analysis done on the structure was with the launch condition static load case. This load case is the same as the one used by SunSpace during the development of the original structure and will be known as the Quasi-Static-LoadCase. The loads represented in the load case were defined in the model with the use of an inertial load and consisted of three directional accelerations in the X, Y, and Z axis. The accelerations were defined as 102.0 m/s^2 in the negative Z direction, 38.3 m/s^2 in the Y direction and 38.3 m/s^2 in the X direction with the positive Z direction in the direction of the black boxes on the structure. These inertial forces combine into a total acceleration of 115.5 m/s^2 . A static analysis was done on the structure to determine the stresses in the ribs and thus the safety factor of the structure. The total deformation on the structure during the

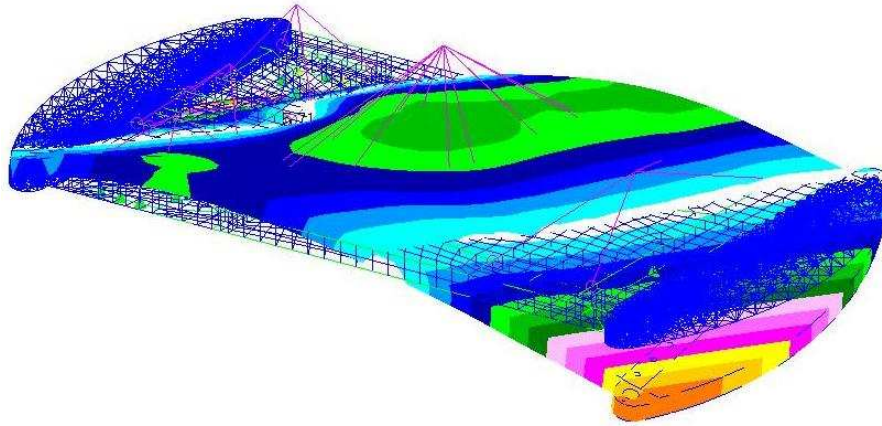


Figure 5.22: First non-rigid body mode of FE model at 145.24 Hz with free (no) boundary conditions

launch of the satellite could also be determined. The maximum stresses in the structure were calculated as 29.6 MPa in the carbon fibre sheets with a transverse maximum stress of 9.92 MPa in the 90° layer and 18.7 MPa in some of the ribs; this is illustrated in Figure 5.23 and Figure 5.24 respectively. The safety factor, calculated with maximum stress failure criteria, of the structure under the Quasi-Static-LoadCase was thus calculated as 3.5, this is in the transverse direction of the 90° layer. The tensile strength of the carbon fibre in the transverse direction is 35 MPa from literature.

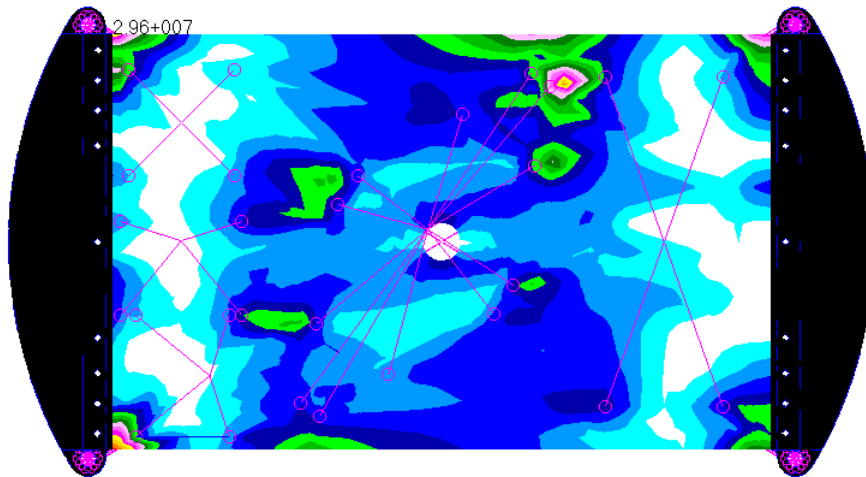


Figure 5.23: The normal stress in the fibre direction plot of the inner longitudinal carbon fibre layer (maximum fibre stress of 29.6 MPa)

The total deformation of the structure is plotted in Figure 5.25 showing the structure to deform by 0.172 mm. This is a large improvement on the original structure developed by SunSpace which deformed 0.283 mm under the same load case. This shows a large improvement on the structural stiffness.

The FE software was used to do a mass correlation on the structure. This mass correlation will however not be very accurate since the model contains a large amount of

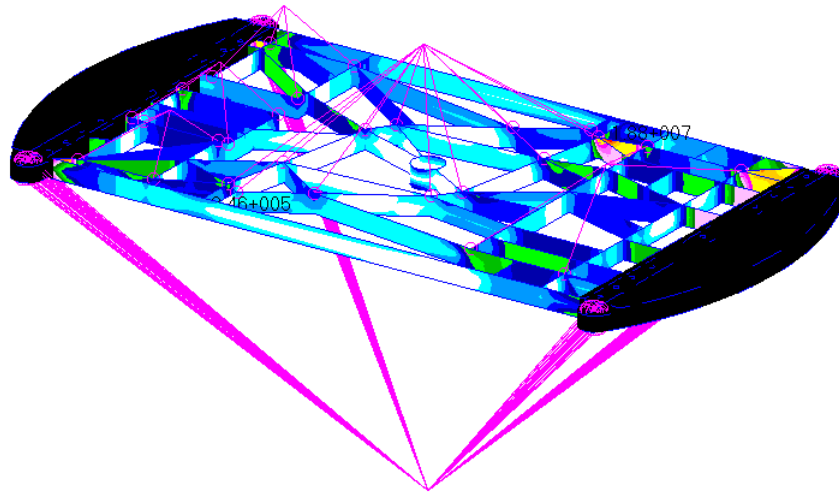


Figure 5.24: The Von Mises the stress distribution in the ribs under launch conditions (maximum rib stress of 18.7 MPa)

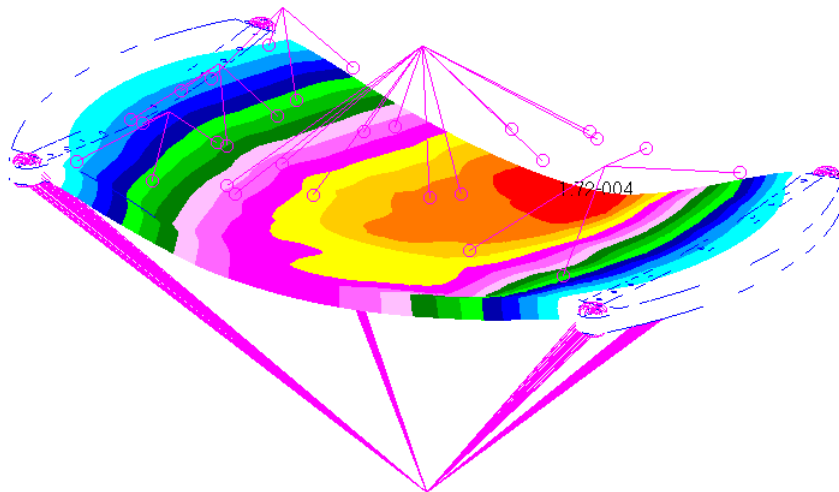


Figure 5.25: The plot illustrates the displacement of the structure under launch conditions (maximum deformation of 0.172 mm)

sharp corners which is unrealistic for the machining process. Some weight will be added to the structure when the final CAD model is developed and all the fillet radii is inserted. The mass of the FE model is 3.82 kg which is a large saving on mass from the original structure weighing 4.87 kg.

Chapter 6

Manufacturing

The finite element model showed promising results, but without a physical structure which can be manufactured and tested the value of the study would be of little significance to the aerospace industry. The model needed to be manufactured to show that the proposed rib thicknesses could be machined. The manufacturing also needs to show that the bonding problems which occurred during previous parts of the study were solved. In this chapter the manufacturing process of the entire structure will be explained in detail. The materials used during the manufacturing is covered in Chapter 4.

6.1 Ribbed reinforced aluminium core manufacturing

This section will explain the CAD modelling and manufacturing process of the ribbed aluminium core for the second generation satellite structure. The manufacturing is divided into three main sub-sections namely; aluminium core machining, carbon fibre face sheets and bonding of the face sheets to the core. Manufacturing of the aluminium core was done by Daliff Precision Engineering, which is the same company that did the manufacturing for the study done by Mr. R. Wilsenach.

6.1.1 Waterline machining

During the production of sheet metals, internal material stresses are created. This inner-material stresses can cause a structure machined from the metal sheet to deform. Machining methods have been developed to successfully manufacture thin ribbed structures. These methods eliminate the internal material stresses which allow the manufacturer to produce a flawless product. One of these methods is called waterline machining and will be explained in this section.

The first generation panel was manufactured with 1.5 mm thick ribs. With the manufacturing of the second generation panel 0.5 mm thick ribs needed to be machined. In order to do this the study done by Mr. R. Wilsenach showed that it is possible to successfully machine 0.5 mm ribs. Daliff adopted a waterline machining process to manufacture a test structure with a 0.5 mm rib. This process can be explained as follows: A CNC code is developed to incrementally remove shallow depths of material from the pockets. Typically 2.5 mm of material is removed at a time from each pocket. By doing this the pocket

depths will appear to increase in the same manner the waterline from an emptying bath recedes. The procedure ensures that the ribs are supported with a sufficient amount of material at all times, which places little stress on the ribs themselves. The manufacturing of the aluminium ribbed core was done according to the waterline machining process.

6.1.2 Conversion of FE results in to a CAD model

In order to manufacture the developed second generation panel the FE model needed to be converted into a manufacturable structure. A CAD model was created from the geometry of the FE model. The FE model was converted into an IGES file with the use of MSC Patran and imported into a new .ipt (3D modelling file) file with the use of AutoDesk Inventor. The imported model will be used purely to measure the positions of the ribs in the final CAD model. A copy of the original CAD model created before the topology optimisation was used to create the final CAD model.

With the final FE model suggesting rib thicknesses of only 0.5 mm and the bonding specifications of the adhesive that will be used requiring a bond thickness of at least 1 mm, some changes needed to be made to the structure to ensure a successful bonding process. A decision was made to manufacture the ribs in the shape of an I-beam. The top and bottom 2 mm of the ribs will be 1 mm thick to be sufficient for the adhesive to bond to, while the inner 16 mm of the ribs will be 0.5 mm thick. This will add some mass to the FE model. The I-beam or undercut in the ribs is illustrated in Figure 6.1.

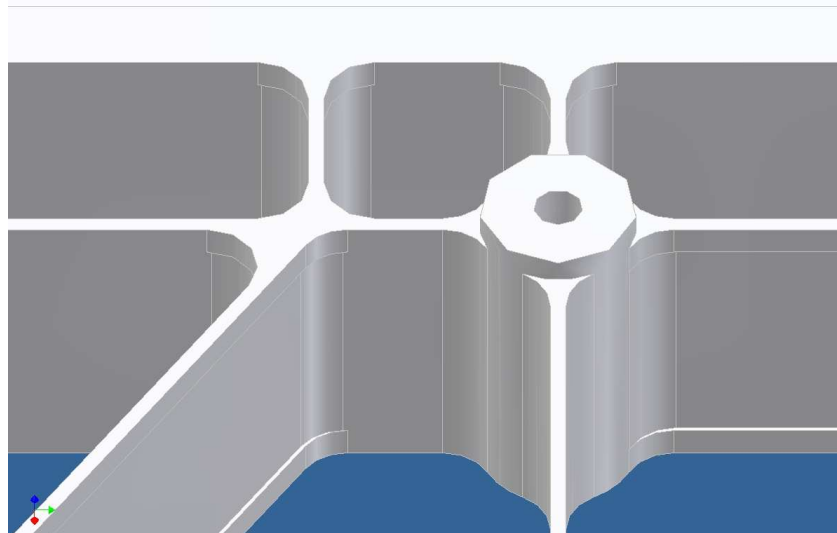


Figure 6.1: I-beam shaped ribs and bolt hole extrusion from the CAD model

On the side of the panel to which the black boxes will be mounted, small extrusions are added to the structure at the positions of the bolt holes. These extrusions will extend through the carbon fibre face sheet to ensure metal-to-metal contact between the structure and the black boxes. The metal-to-metal contact aids in the heat transfer from the black boxes to the aluminium ribbed structure.

A 6 mm diameter cutting tool will be used during the machining of the aluminium core. Fillets were added to all the corners in the CAD model which will be subjected to the 6 mm diameter of the cutting tool. The radius of these fillets was chosen to be 3.2 mm; this will allow the cutting tool to move on a continuous path without having to stop in the corners. The surface finish in the corners of the final product is of a higher quality by allowing the cutting tool to move without stopping in the corners.

The final CAD model of the second generation panel core are shown in Figure 6.2. This model was shown to the managing director of Daliff, Mr. Norbert Leicher, to confirm the manufacturability of the structure.

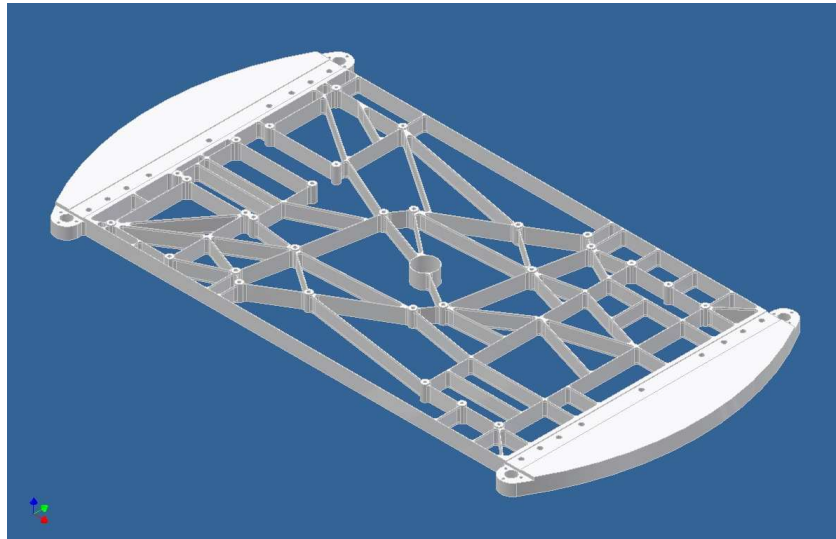


Figure 6.2: Final CAD model of the aluminium core

6.1.3 Manufacturing of the core

To manufacture the aluminium core of the second generation panel the CAD model needed to be converted into a viable CNC code. The CNC code is generated prior to manufacturing by Daliff. Daliff requested the designer to convert the CAD model into a STEP file format which could then be used to inspect the structure for any manufacturing difficulties or design flaws in terms of manufacturability. The CNC code was created to control the cutting tool to move on the outer edges of each of the pockets in the ribbed core. Waterline cutting is implemented in the machining of the structure. For structures with very thin ribs the internal material stresses are removed by allowing the structure time to relieve the stresses before the machining process is complete.

The first cut left 6 mm ribs in place with the solid lumps of material in the pockets connected to the ribs with a thin un-machined strip of material. The structure was machined from both sides which mean that it was turned over during the machining process. The strip of material that connects the solid lumps of material in the pockets to the ribs was machined to a thickness of 0.2 mm and positioned at a cutting depth of 10 mm. The structure was then left in an area where the structure was subjected to sunshine during the day and the cool night temperatures for a 1 week time. These temperature changes

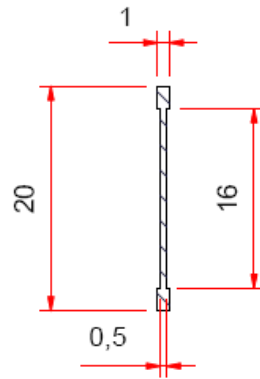


Figure 6.3: Sectional dimensions of the ribs

allowed the metal crystal structure to settle and relieve the internal stresses. When this was done the ribs could be machined to the final thickness. This was again done with the waterline process.

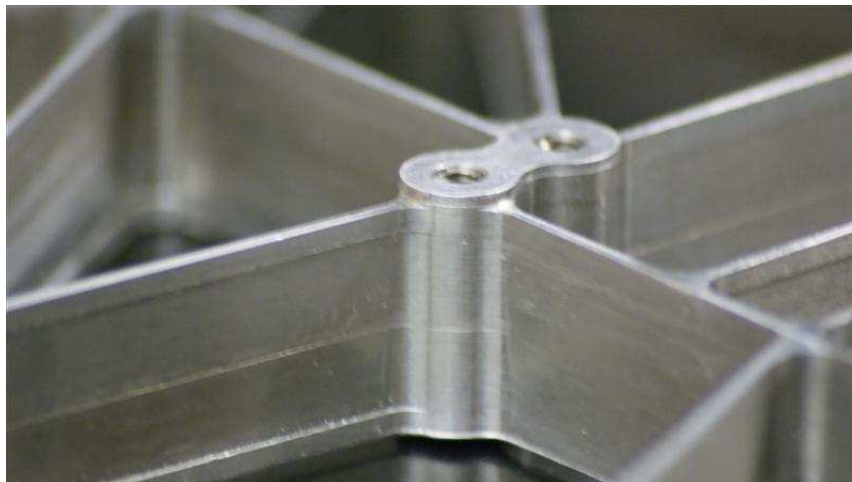


Figure 6.4: Image of the undercut in the ribbed structure

The ribs are machined to a thickness of 1 mm through a series of cuts. By using waterline cutting the ribs are thinned down to 1 mm by dropping the waterline by 2.5 mm at a time. When all of the ribs are machined to 1 mm thick all that is left is to create the undercut in the ribs and to remove the lumps of material in the pockets. In order to machine the undercut in the ribs special tooling needed to be manufactured. This special cutting tool was made from the same type of cutting tool used to machine the rest of the structure. The tool was modified to have a thinner shaft than the cutting tip as needed to machine the 0.25 mm undercut in the ribs so as to leave the 0.5 mm thick I-beam shaped rib, a section of the ribs is shown in Figure 6.3. The strip of material connecting the solid pieces of material in the pockets to the ribs is used to prevent the ribs to be forced away from the cutting tool during the machining process. After the undercut has been made on all of the ribs, the 0.2 mm thin strip is removed with the use of a Stanley knife. The core manufacturing is now complete and can be seen in Figure 6.4 and Figure 6.5. The

machined aluminium core weighed 3.32 kg, which means the final core mass is only 170 g more than the FE model core mass.

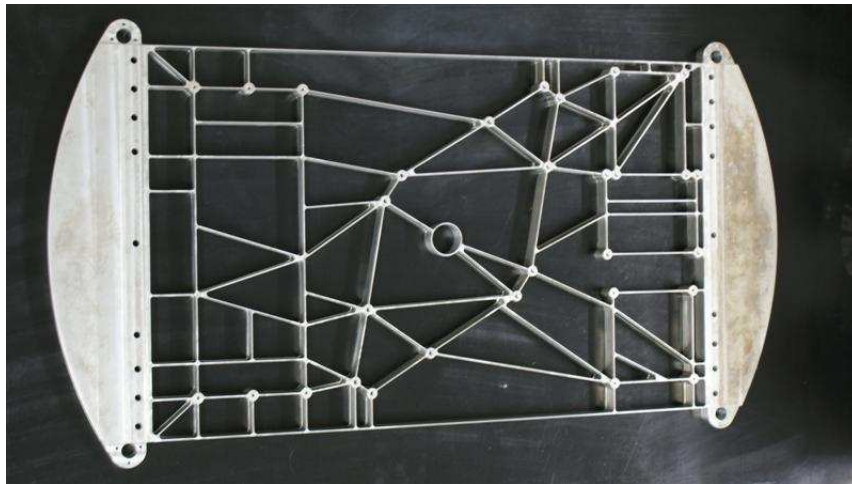


Figure 6.5: Image of the machined aluminium core

Daliff put the manufactured core through their quality control system which uses the CAD model to measure predefined points on the structure and comparing it to the manufactured structure. The structure passed the quality control and manual measurements done by the researcher confirmed the precision of the rib thicknesses, Figure 6.6.



Figure 6.6: Image of the machined aluminium core during the quality control process

6.2 Carbon fibre face sheet manufacturing

The carbon fibre face sheets were manufactured from K63712 high modulus carbon fibre manufactured by Mitsubishi Chemical. The material and its properties are covered in Section 4.1. The manufacturing technique used to manufacture the carbon fibre face sheets is simple and widely used in industry. The process is known as a wet layup and will be explained in this section.

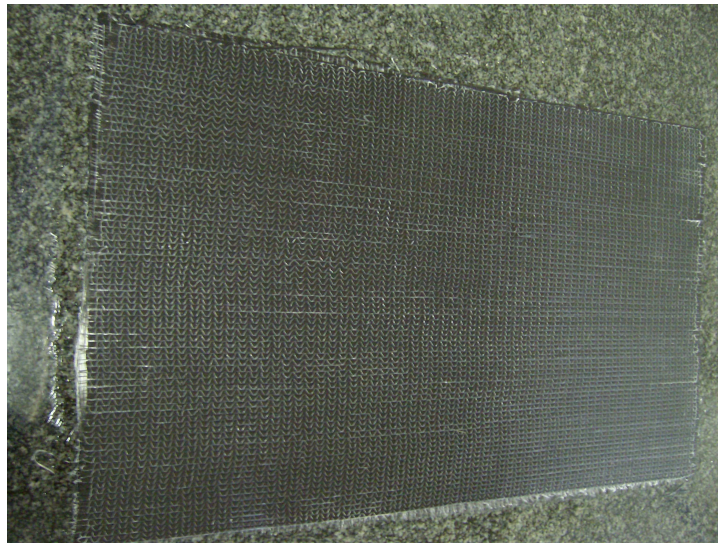


Figure 6.7: The wet carbon fibre cloth after resin application

The first step is to cut the dry carbon fibre cloth into the desired sections which will be needed for the layup required. In this study a layup of $[0/90/0]$ will be used where the 0° angle is in the longitudinal direction of the structure. The layup surface then needs to be prepared so that the resin does not stick to the surface. A flat polished granite slab is used for the layup surface and a releasing agent is applied to the surface, three thin coatings of the releasing agent is applied and left to dry. Once the releasing agent is dry the layup procedure can start.

A thin layer of resin is applied on top of the release agent with the use of a paint brush. The first layer of dry carbon fibre cloth is then laid down in position on top of the wet resin, Figure 6.7. With the use of the paint brush resin is applied to the carbon fibre cloth until the resin fully impregnated the cloth. The second layer is now placed in position, with the fibres in the desired orientation, and wetted in the same manner as the first, this process is repeated for all of the layers.

After all of the carbon fibre layers were in place and wetted with resin a sheet of peel-ply is placed on top of the wet layup. The peel-ply is removed once the curing process is complete and leaves a rough surface finish which encourages subsequent bonding to other surfaces. A single layer of perforated plastic is placed on top of the peel-ply to allow the excess resin to be drawn away from the carbon fibre layup. Breathable cotton cloth is placed on top of the plastic layer; this will absorb the excess resin which is drawn from the carbon fibre see Figure 6.8.



Figure 6.8: The complete layup of the carbon fibre before it is sealed in the vacuum bag

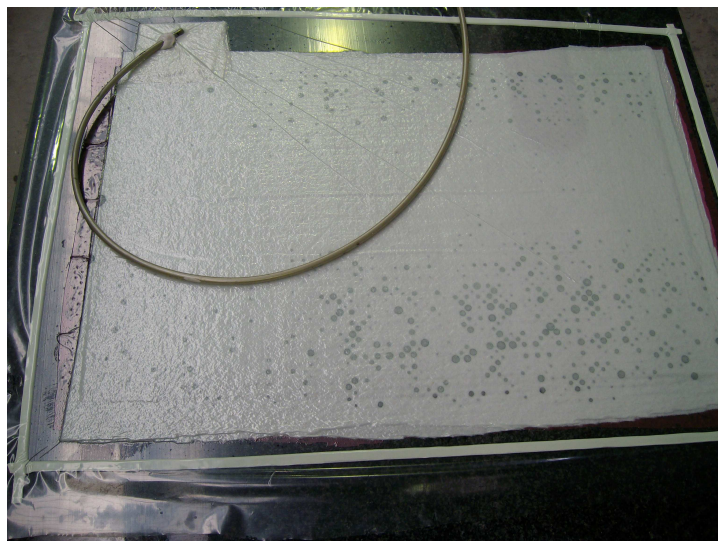


Figure 6.9: The carbon fibre layup with the vacuum drawn on the setup

The setup is covered with a vacuum bag and sealed with sticky-tape, Figure 6.9. A vacuum is drawn which will help to remove excess resin from the carbon fibre. The layup is left to cure after which it is placed in a large oven to undergo a post curing process. This post curing process took place at $120\text{ }^{\circ}\text{C}$ for a period of 12 hours. Post curing is a process in which the carbon fibre sheet is baked in an oven at temperatures higher than that at which the structure will be operating. This baking of the sheets allows the resin to cure at the elevated temperature and ensures the designer that the resin will not soften during normal operation of the structure. The structure is designed to operate at temperatures as high as $70\text{ }^{\circ}\text{C}$.

The setup is removed from the vacuum and the peel-ply is removed which in turn removes the cotton cloth and perforated plastic layer. Both of the carbon fibre face sheets were manufactured in this manner. The time to do the layup of one of the face sheets was 2 hours which includes the preparations before the layup could be started.

6.3 Carbon fibre face sheet bonding to aluminium core

Hybrid composites are manufactured by bonding a series of different materials into an unit that will act as the final product. In this case the two carbon fibre face sheets will be bonded to the ribbed aluminium core. For the bond to be strong enough the materials involved in the bonding process will be prepared to create the perfect bond. In this section the bonding process along with the material preparation prior to the bond will be explained in detail.

The carbon fibre face sheets were manufactured to be larger than the final sheet that would be bonded to the aluminium core. The sheets needed to be cut to size prior to the bonding process. A pneumatic vibrating saw was used to cut the face sheets to the correct size. The sheets were cut so that it overlaps the outside ribs of the structure by 10 mm to ensure the epoxy would have a sufficient area to bond to. This extra material will be removed once the bonding process is complete. Holes were drilled in the face sheet on the side of the panel to which the black boxes will be attached. The aluminium extrusions at the bolt hole positions will fit through these holes to allow for metal-to-metal contact and better heat transfer once the structure is complete. The top and bottom carbon fibre face sheets had a respective mass of 507 g and 520 g. This is heavier than the face sheet weight from the FE model because the FE model assumed a theoretically higher fibre volume fraction than obtained during manufacturing, see Section 7.3. After the carbon fibre sheets were prepared for the bonding process the aluminium core could be prepared.

6.3.1 Preparation of aluminium core prior to bonding

In order to ensure the adhesive attaches to the 1 mm thick aluminium ribs, the core needs to be treated chemically to improve the anti-corrosive properties and bonding surface. The treatment chosen for the aluminium core was chromic acid anodising. This treatment is not recommended by SunSpace purely for the reason that it is difficult to clean up the residue from this process. Satellites could be stored for an extensive period of time prior to a launch date; corrosion could be a problem during this time. Anodising is a suitable treatment because of its anti-corrosive, crack detection and bonding properties.

The anodising process opens up micro-celled structures, these micro-celled structures aid in the bonding process as the adhesive grips into material and ensures a good bond. To ensure a successful bond the bonding should occur within 48 hours of anodising of the aluminium core. The micro-celled structures start to close up as the anodising ages and if the bond is not made within this specified time the quality of the bond could be jeopardised. The anodising procedure is explained in detail in Appendix C.1. The anodising was done at Strand Anodising and took 4 hours to complete.

It was decided to roughen the surfaces where the adhesive would be applied. This will increase the bonding surface at a micro level. The surface was sanded with a 320 grid sand paper and cleaned by placing the structure under running water. When the anodising process was complete the aluminium ribs needed to be prepared and cleaned for



Figure 6.10: The cleaning process of the surfaces to which the adhesive will be applied

the bonding process. The surface was once again sanded and cleaned with acetone and water, see Figure 6.10. The aluminium rib final preparation prior to bonding is explained in Appendix C.2.

6.3.2 Adhesive application and bonding

Once the aluminium surfaces are prepared for the bonding process the Scotch-weld 9323 B/A adhesive can be mixed according to the weight ratio specified in the material data sheet illustrated in Appendix C. 127 g of the adhesive was mixed for the first carbon fibre face sheet. The first sheet to be bonded to the aluminium core was the face sheet on the side with the bolt hole extrusions.



Figure 6.11: The adhesive being applied on top of the ribs

A syringe with a 1.5 mm thick needle was used to apply the adhesive on top of each rib, as is illustrated in Figure 6.11. After the adhesive had been applied to all the ribs the carbon fibre face sheet is positioned so that the aluminium extrusions neatly fit in the holes drilled in the face sheet. The side of the face sheet to which the peel-ply had been applied during the manufacturing is placed on the wet adhesive. This rough surface

finish will ensure a good bond. The structure is then turned over so that the carbon fibre face sheet is positioned underneath the aluminium core. By doing this the wet adhesive will not flow away from the carbon fibre sheet and a good bond can take place. Finally an aluminium block of material is placed on top of the setup to help force the ribbed aluminium core onto the carbon fibre face sheet. The time to complete the bonding of one of the carbon fibre sheets is 2 hours 30 minutes, but the time from when the adhesive is mixed to the end of the bonding process is 1 hour. The setup is left for 7 days at room temperature in order for the adhesive to fully cure.

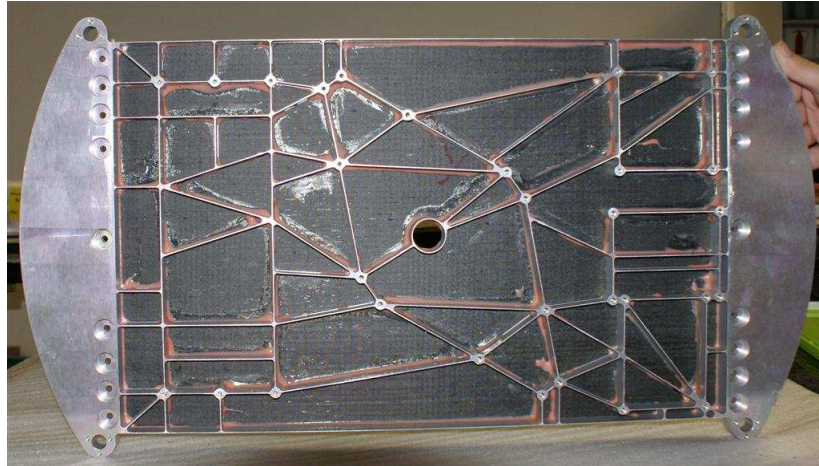


Figure 6.12: The adhesive along the ribs are illustrated after the first face sheet has been bonded

After the adhesive fully cured the second face sheet could be bonded to the ribbed core. The bond on the first face sheet is inspected and it is clear that the adhesive bonds to the ribs in the same manner as a fillet weld, Figure 6.12. Before the bonding process of the second face sheet was done, small 1 mm diameter holes were drilled in the bonded face sheet in each of the pockets between the ribs. This will allow the air on the inside of the pockets to automatically exhausts as the environmental pressure reduce during the launch of the satellite. The aluminium preparation process is repeated prior to the bonding of the second face sheet. The anodising is not repeated so the preparation starts with the cleaning and sanding of the bonding surface. When the adhesive which bonded the second face sheet to the aluminium core is fully cured all that remained was to do the final touch-ups to the structure.

6.3.3 Post bonding machining

During the bonding of the carbon fibre face sheets some of the adhesive spilled (bonded) to the solid aluminium flanges and the outside of the ribs running along the length of the structure. The adhesive on the flanges are primarily in the slots machined to fit the side panels of the satellite. The parts of the carbon fibre face sheets overlapping the outside ribs of the structure needed to be trimmed to be flush with the surface of the ribs. The excess adhesive and overlapping carbon fibre sheets is illustrated in Figure 6.13.



Figure 6.13: The access adhesive that needs to be removed during the final machining process

Removing of the access material was done by clamping the structure in a milling machine and running the cutting tool along the edges where the material needed to be removed. For future bonding it is planned to mask off surfaces where the adhesive can potentially spill.

The final second generation panel was now complete and weighed in at 4.43 kg, which is 440 g lighter than the original SunSpace designed structure that weighed in at 4.87 kg. This weight saving account for a launch cost saving of \$8 720(US) considering the cost to launch 1 kg into orbit rated at \$20 000(US).

Chapter 7

Structural Testing and Results

The FE analysis showed promising results for the design of the second generation panel. This fully manufactured second generation panel needed to be tested to compare the results from the FE analysis with the physical model. The results from the test could then be used to confirm the success of the study. In this chapter the structural tests done on the second generation panel will be explained and the results will be analysed and discussed.

7.1 Modal test of the structure

Natural frequencies of a structure are an indication of the overall stiffness of the structure. For this reason modal tests were done in order to measure the natural frequencies of the structure developed during this study. The test results will be compared to the finite element analysis of the unsupported structure.

7.1.1 Test setup for the structural modal test

In order to simulate the mass elements from the FE model, dummy masses as used by SunSpace during the development of the original structure, were bolted to the second generation panel, see Figure 7.1. These dummy masses were manufactured from mild steel plates connected to the optimised panel by threaded rods. The threaded rods allowed the designer to change the height of the COG of each of the masses. Since the masses used in this study are the same masses used by SunSpace, the stiffness correlation between the original structure and the new structure will be accurate.

Free boundary conditions are difficult to simulate in a test. The usual practise is to suspend the structure with elastic cords. The structure is however too heavy for the cords available at the test facility. An alternative was found by positioning the structure on top of an inflated inner tube from a car tire. The frequencies were measured with the use of seven accelerometers positioned in the same order as in the tests done on the original structure, see Figure 7.2. The sensors were fixed to the structure with wax which is the general practice for modal testing of small structures. The positioning of the accelerometers are illustrated in Figure 7.3. Accelerometer data as sampled by a LMS vibration spectrum analyzer. A modal hammer was used to generate the impulse necessary for the

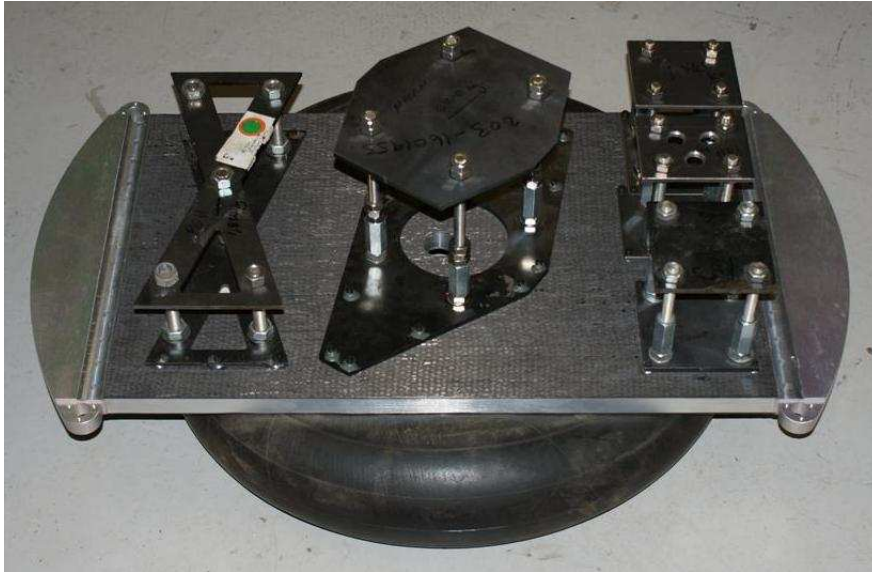


Figure 7.1: Dummy masses used to act as the black boxes during structural tests

structure to vibrate.

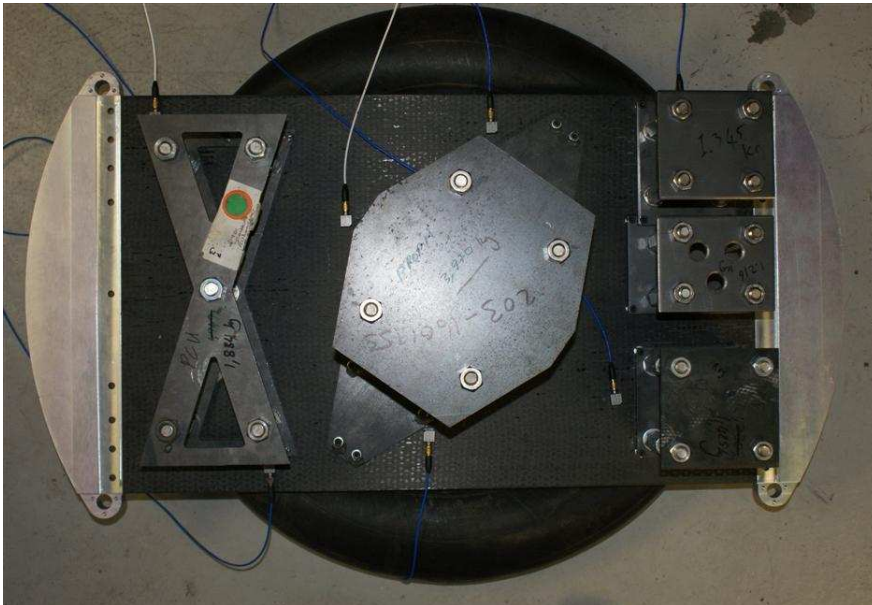


Figure 7.2: Positioning of the accelerometers during the modal test

7.1.2 Test procedure and results of the structural modal test

Once the setup was complete the test could be done on the structure. The position of each of the accelerometers was entered into the LMS software to enable the software to calculate the modes of vibration. The position of the impulse was also entered into the software. The test was done by generating an input impulse with the modal hammer on one of the corners of the structure; the LMS saves the measurement data generated by the accelerometers. The test is repeated five times to calculate the average. The hammer's

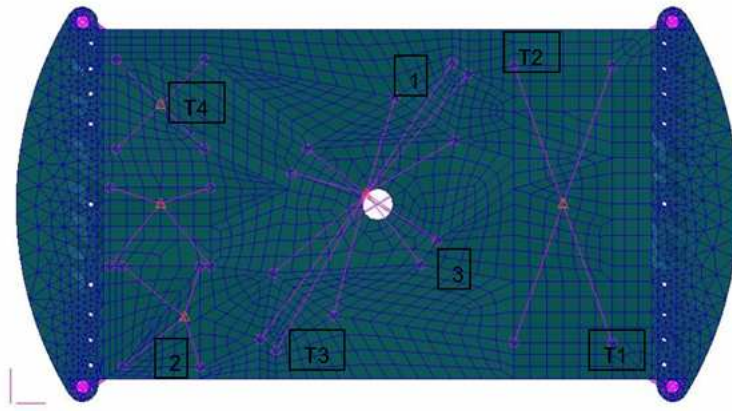


Figure 7.3: Positioning of the accelerometers during the modal vibration tests

tip includes a force transducer that measures the magnitude of the impulse and together with the accelerometer data the transfer function frequency spectrum can be calculated. The accelerometer data is stored as a complex number frequency spectrum and need to be converted into a RMS (Root Mean Square) spectrum before the frequency response plots can be presented.

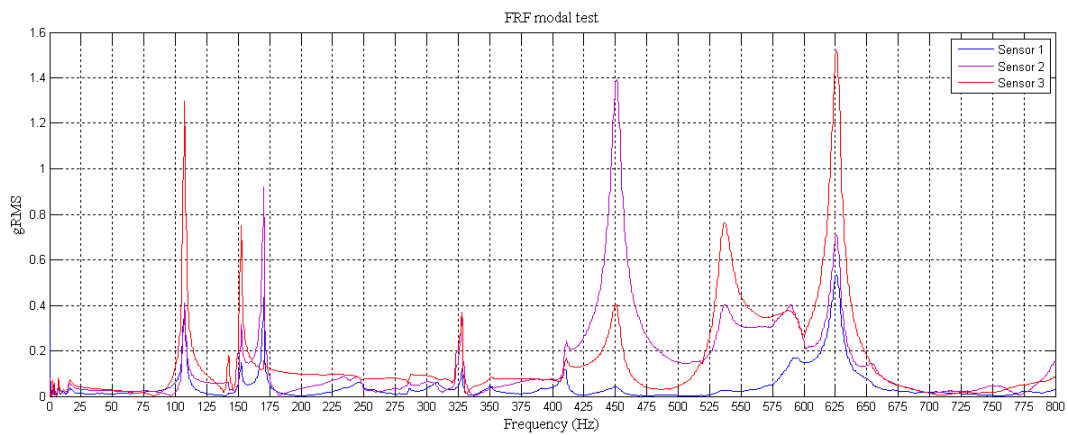


Figure 7.4: Frequency response plot sensors 1 to 3 for the modal test done on the structure

The modal test results showed a surprisingly low first natural frequency of 107 Hz, which is 38 Hz lower than that of the FE model with free boundary conditions. This frequency is however still acceptable for the structure since the original structure was manufactured to be stiffer than 90 Hz. If this is accurate, the structure would not be an improvement on the original structure regarding the stiffness of the panel. The test did show a peak at 142 Hz, 152 Hz and 170 Hz. These frequencies are very bunched together and do not correlate with the FE results at all. This can be explained in two ways, either the FE model is faulty by a large margin or the boundary conditions used in the modal test compromised the stiffness properties of the structure. During the random vibration test the natural frequencies will also be measured which will give the researcher a better indication of the validity of the modal test results. The frequency response plot for the modal results is shown in Figure 7.4.

7.2 Random vibration testing of the structure

Because the second generation panel is only a prototype, structural vibration tests need to be done. These tests will be used to test the structure under launch vibration for structural failures and natural frequencies. The tests were done at Rheinmetall Denel Munition Western Cape, which is a defence equipment testing facility situated near Macassar.



Figure 7.5: Vibration shaker used for the random vibration tests

7.2.1 Test setup for the random vibration tests

The random vibration tests done on the structure required the structure to have boundary conditions as close to launch conditions as possible on the SHTIL-2.1 launch vehicle. To achieve this, aluminium blocks, also known as a jig, used by SunSpace during the testing of the original structure, were used. The jig interfaces are designed to be rigid in accordance to the jig specifications in ECSS-E-10-03A, (Steyn, 2009). This jig consists of holes positioned in such a pattern as to allow the jig to be bolted on top of the vibrating actuator head, Figure 7.5, and to have the panel bolted on top of the jig. This is illustrated in Figure 7.6.

A torque wrench was used to fasten all the bolts holding the jig to the vibration actuator as well as the bolts holding the panel to the jig. Washers were used as spacers to ensure the structure is only supported at the four corners. For this test setup nine accelerometers were used. Seven of the sensors were positioned in the same order as the modal test as seen in Figure 7.3. The average of the two control accelerometer signals was used to control the input to the test item. The accelerometers were mounted using threaded connectors. Small amounts of Loctite QuickTite Super Glue was used to secure the accelerometer mountings. This was done because of the intensity of the vibrations required for this test. All of these sensors were connected to two SigLab vibration spectrum analyzers connected in parallel (Figure 7.7). The SigLab boxes were connected to a computer to store the measured data. Control of the actuator was done by a separate



Figure 7.6: Structure bolted to the shaker

system forming part of the test facility.



Figure 7.7: Measurement equipment of the random vibration tests

7.2.2 Test procedure and results for the random vibration tests

The random vibration tests were done to simulate the launch conditions. The first test was done by controlling the actuator to vibrate between 60 Hz and 2000 Hz in random frequency. The intensity of the first test was done at 4.6 gRMS and the test was done for a period of 4 minutes. After this test, a sine sweep was done on the structure to measure the natural frequencies of the structure. During the second part of the random vibration test the frequencies again varied between 60 Hz and 2000 Hz but was done at 12.6 gRMS, for 4 minutes. This is the highest intensity tests required for launch according to the loads specified in the SHTIL-2.1.UG. The SHTIL-2.1.UG is a user's guide that specifies the conditions and parameters of satellite integration pre-launch preparation and launch. The sine sweep was again repeated before the third part of the random vibration test was

completed. The third test was done exactly the same as the second test. The results from these tests are covered in this section.



Figure 7.8: Accelerometer connection failure during random vibration test

During the random vibration tests the data was saved after every minute of the test. This allowed the researcher to have usable data of different parts of the test, even if the sensors or the structure were to fail during one of the tests. In this section only the data from the control sensor and sensor 1 and 3 will be used in discussing the results. The data from the rest of the sensors will be illustrated in Appendix D.

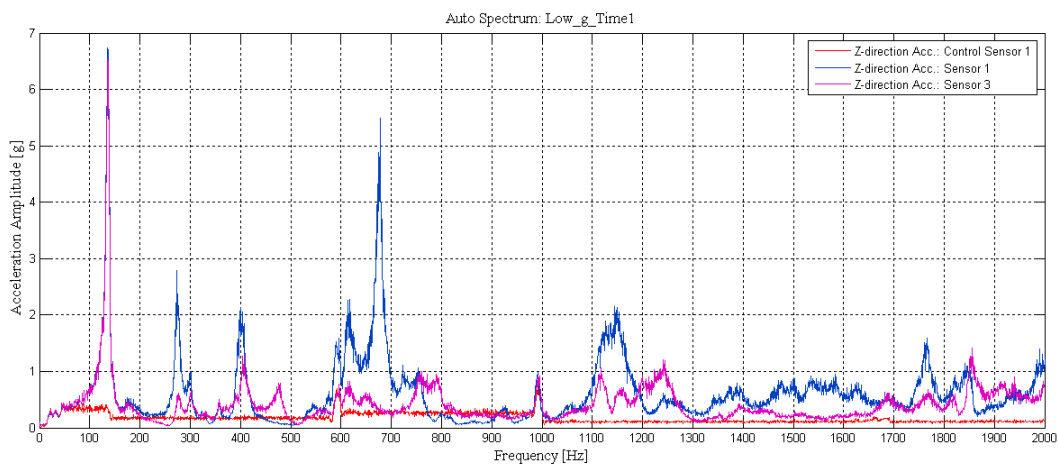


Figure 7.9: Frequency response plot of the 4.6 gRMS random vibration test

The frequency response plot illustrated in Figure 7.9 shows the data from the first minute of the first test done on the structure. During this test sensor T3 was not properly bonded to the structure and thus the data from T3 will be discarded. The positioning of sensor 1 and 3 will show the biggest deformation in the first mode of vibration. This

explains the height of the peak close to 130 Hz. The low gRMS test was completed without any structural failure. This meant that the high gRMS tests could now be done. A sine sweep was done before the first high gRMS test was done to measure the natural frequencies during each stage of the tests.

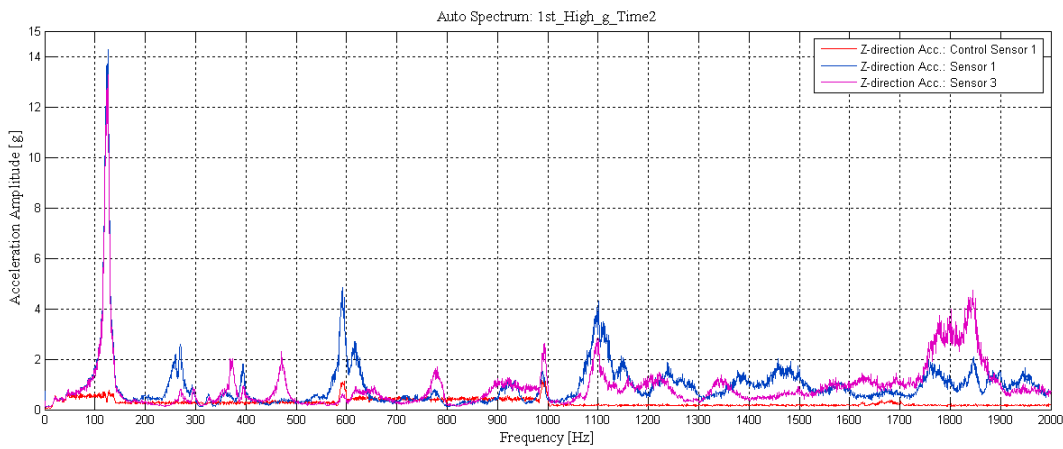


Figure 7.10: Frequency response plot of the first 12.6 gRMS random vibration test

Figure 7.10 illustrates the frequency response plot for test data from the second minute of the first high gRMS test done on the structure. During the end of this test the signals from two sensors were lost. These two sensors, T3 and 1, came off the structure and needed to be reset before the next test could be done (Figure 7.8). This first high gRMS test was completed without any structural failure which suggests that the structure will be able to endure the highest launch vibrations. After this stage of the testing process, a sine sweep was again done to measure the natural frequencies.

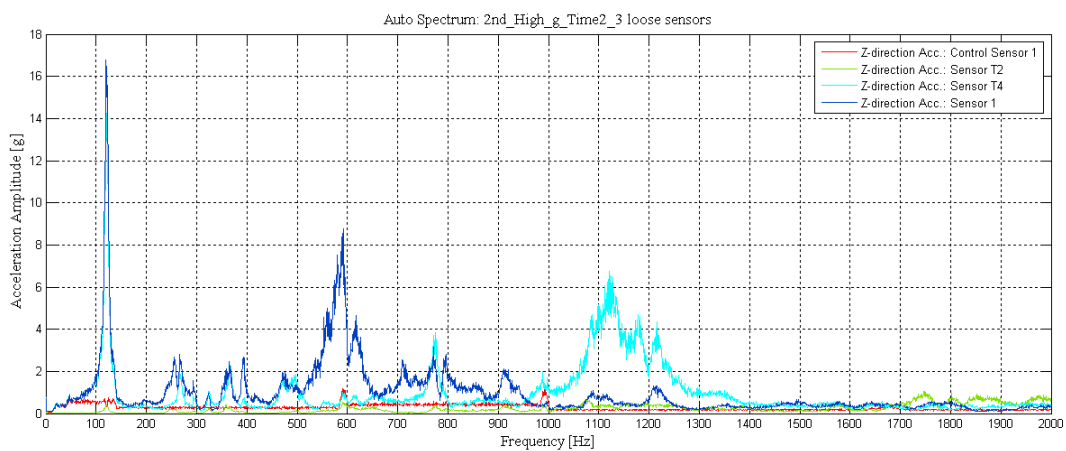


Figure 7.11: Frequency response plot of the second 12.6 gRMS random vibration test

During the final high gRMS test shown in the frequency response plot of Figure 7.11 three sensors could not be used. Sensors T3, 2 and 3 was lost due to bonding problems.

The plot is from the second minute of the final test. The structure was thoroughly inspected for any failures after this test was done. The structure was still 100% intact which suggests that the structure would have completed the journey into orbit without failure. These positive test results prove that the development of the second generation structure was successful and that the techniques used, could now be implemented in future satellite structures.

7.2.3 Testing the structure for its natural frequencies

During the random vibration test a sine sweep was done after each stage of the random vibrations. The sine sweep is done by starting the vibrating actuator at a frequency of 600 Hz and gradually lowering the frequency down to 60 Hz. During this test the accelerometers will pick up all of the natural frequency peaks in the frequency range. This section will describe the results from these tests. After the low gRMS test the sine sweep showed the first natural frequency at 127.5 Hz as illustrated in Figure 7.12.

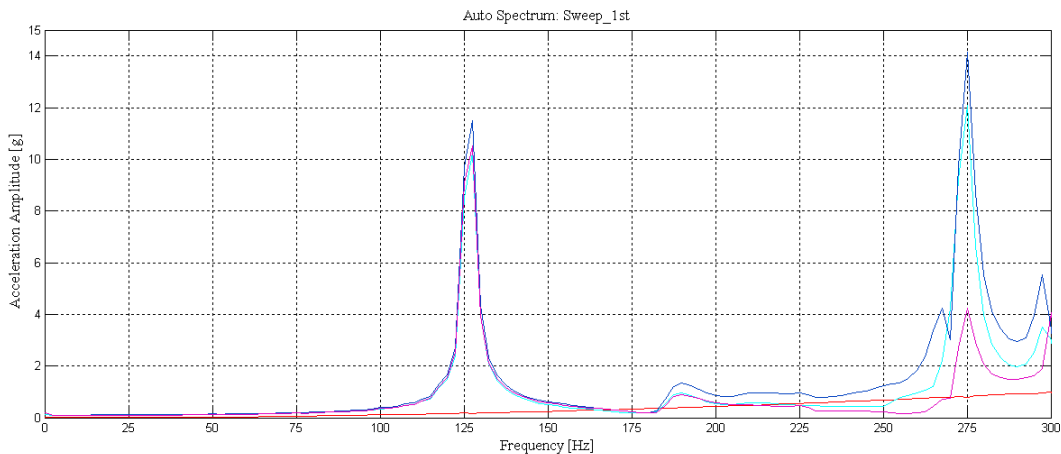


Figure 7.12: Frequency response plot of the first sine sweep

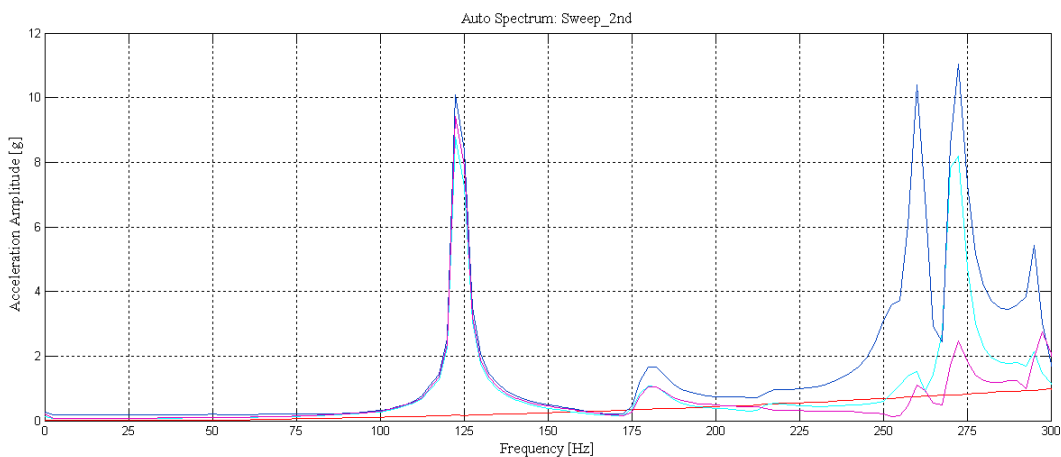


Figure 7.13: Frequency response plot of the second sine sweep

The results of the sine sweep done after the first 12.6 gRMS stage are shown in Figure 7.13. From this plot the natural frequency peaks are clearly visible with the lowest natural frequency at 125 Hz which is within 15% of the FE data. This difference is not acceptable, but since the FE model does not include the Scotch-Weld bond the stiffness of the structure might be lower than predicted by the FE model. The shear modulus of the adhesive is much lower than that of the aluminium or the carbon fibre and this can be seen as a weak point in the structure which could lower the natural frequencies. The manufactured structure is also heavier than the FE model structure. The dummy masses simulating the black boxes contributes more than 60% of the entire weight of the structure which means that the manufacturing mass addition will make a minor difference in the frequency results of the structure. This addition in weight should however lower the natural frequency of the structure.

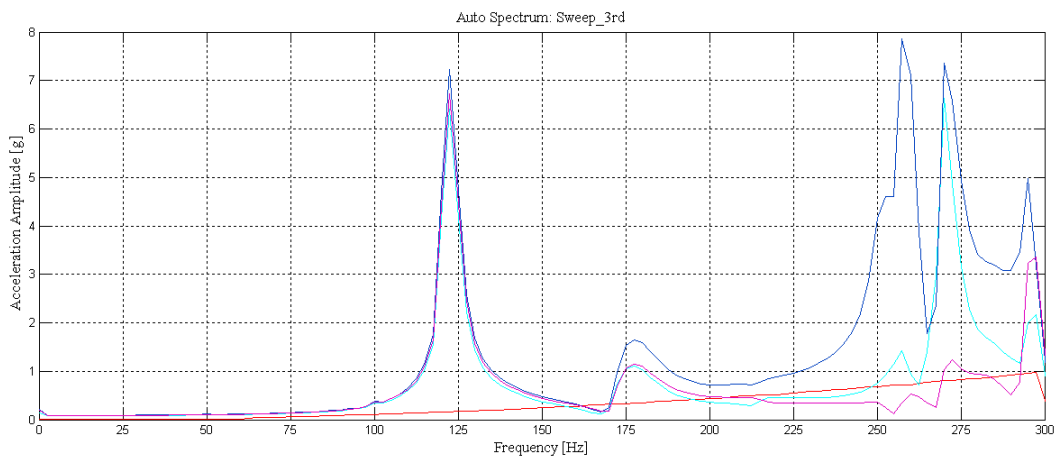


Figure 7.14: Frequency response plot of the third sine sweep

The last sine sweep done after the second 12.6 gRMS random vibration test showed a first natural frequency of 122.5 Hz as illustrated in Figure 7.14. This drop in natural frequency can be explained by settling-in of the bolt joints which connected the panel to the actuator. The test results confirm that the structure is 8.97% stiffer than the original designed structure which is a large improvement. Since the boundary conditions used for this test are the same as the conditions on the launch vehicle, this natural frequency results will be used to define the stiffness of the structure.

The higher natural frequencies are displayed in Table 7.1:

Table 7.1: Measured natural frequencies versus FE natural frequencies

Model Type	FE model	Physical model
1st natural frequency (Hz)	141.76	122.5
2nd natural frequency (Hz)	162.54	177
3rd natural frequency (Hz)	242.88	260
4th natural frequency (Hz)	394.99	270

7.3 Testing the structural stability with temperature fluctuations

For a satellite in low-earth orbit, the satellite is subjected to drastic temperature fluctuations during each orbit. During each orbit of typically 90 minutes, the satellite goes through a day and night period. During "day time" on the sunny side of the earth, temperatures can reach 60 °C. During the "night time" on the shadow side of the earth, temperatures drop down to -20 °C. The 80 °C change in temperature is seen as a qualification specification at extreme conditions. With structures manufactured from a single material this temperature changes will only affect the structure according to the thermal expansion coefficients of that material. When a hybrid composite material is used, the likelihood of the thermal expansion coefficient of the different materials to be the same are small. The difference in the thermal expansion coefficients may cause the structure to deform. This deformation can be in many different forms which include bending deformation, twisting or, with an irregular internal rib structure such as in the case of the second generation panel, non-linear deformations may be found. For this reason the structure needed to be tested to ensure the structure will be able to perform adequately under outer space conditions.



Figure 7.15: Structure in the oven during the elevated temperature test

The test was repeated three times and the measurements were taken at three different temperatures, 15 °C, 60 °C and -12 °C. The total length of the structure was measured during each stage of the test, using a 1 m long Vernier Calliper. Before the structure was heated, a series of measurements were taken to act as a base to work from. These measurements were repeated after each hot and cold cycle. The hot test was done by placing the structure in a large oven at 65 °C, Figure 7.15, for a minimum time of 2 hours to allow the entire structure to reach this elevated temperature. The measurements were taken within 5 minutes after the structure was removed from the oven to ensure the temperature of the structure will be as close to 60 °C as possible. For the cold test, the heated structure was allowed to cool down for 2 hours and then the structure was placed in a refrigerator for a time of 8 hours. The subzero structure was removed and the

measurements were taken and documented.

The tests revealed that the structure does deform under temperature changes. This deformation is dominated by the high thermal expansion coefficient of aluminium. The structure showed a definite change in length under the elevated temperatures, which was expected. The carbon fibre has a much lower CTE than aluminium. This was expected to restrain the aluminium core to deform the same amount as a structure completely manufactured from aluminium. The theoretical formula to calculate the deformation of a structure undergoing a temperature change is:

$$\Delta L = L\alpha\Delta T \quad (7.3.1)$$

Where ΔL is the change in length of the structure, L is the original length of the structure, α is the CTE of the material and ΔT is the change in temperature.

The measured changes in length are illustrated in Table 7.2:

Table 7.2: Average length changes caused by temperature changes

Structure	Hybrid structure (Measured)	Aluminium (Theoretical)
Length @ -12 °C (mm)	751.92	751.57
Length @ 15 °C (mm)	751.98	751.98
Length @ 60 °C (mm)	752.36	752.65

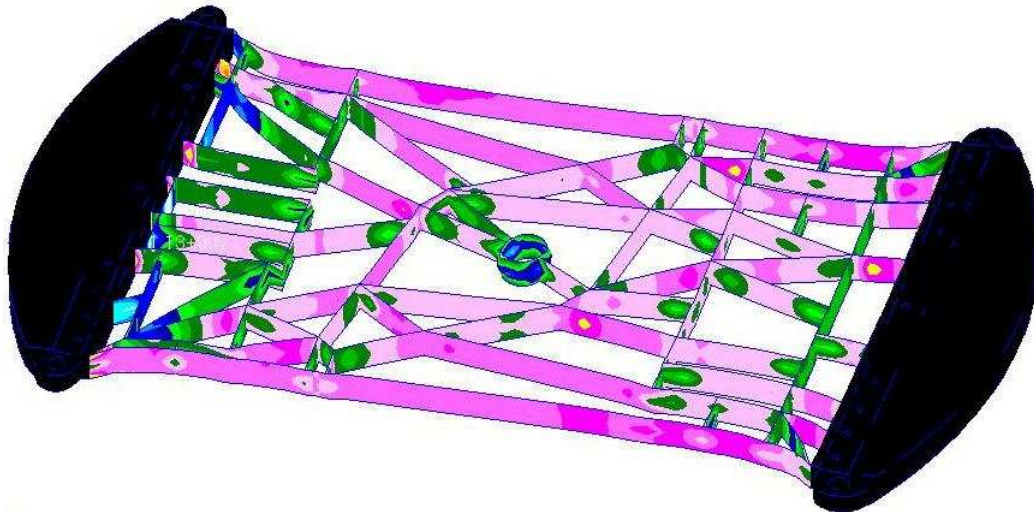


Figure 7.16: Rib stresses due to a 80 °C change in temperature

Observing Table 7.2 it is clear that the carbon fibre face sheets have a big influence on the temperature deformation of the structure. By using Equation 7.3.1 the CTE of the new hybrid structure can be calculated to be $\alpha_H = 11 \times 10^{-6} \text{C}^{-1}$. This is significantly lower than that of aluminium at $24 \times 10^{-6} \text{C}^{-1}$, but higher than that of the carbon fibre

sheets at $\alpha_{FS} = -0.76 \times 10^{-6} \text{C}^{-1}$.

To calculate the thermal expansion coefficient of the carbon fibre face sheets the fibre volume fraction needed to be calculated. This was done with the relationship:

$$\frac{E_{fm2}}{E_{fm1}} = \frac{V_{f2}}{V_{f1}} \quad (7.3.2)$$

Where $E_{fm1} = 370$ GPa is the combined modulus of elasticity of the matrix and the fibre with a fibre fraction $V_{f1} = 60\%$. The combined modulus of elasticity of the matrix and the fibre used in this study is $E_{fm2} = 286.6$ GPa as measured during the tensile test explained in Section 4.1. This leaves V_{f2} , the fibre volume fraction of the carbon fibre face sheets, as the only unknown value. It is assumed that the fibre volume fraction in the test sample and the face sheets is similar since the manufacturing method was the same. The calculation showed a fibre volume fraction of $V_{f2} = 46.5\%$, this value will be used to calculate the CTE of the face sheets.

$$\alpha_1 = \frac{1}{E_{fm2}} (\alpha_f E_f V_{f2} + \alpha_m E_m (1 - V_{f2})) \quad (7.3.3)$$

Providing $\alpha_1 = -1.17 \times 10^{-6} \text{C}^{-1}$ as the fibre direction CTE of each layer in the face sheets. $\alpha_f = -1.5 \times 10^{-6} \text{C}^{-1}$ is the CTE of the fibre in the fibre direction and the CTE of the matrix was assumed to be $\alpha_m = 60 \times 10^{-6} \text{C}^{-1}$ since it varies from $45 \times 10^{-6} \text{C}^{-1}$ to $70 \times 10^{-6} \text{C}^{-1}$ in literature. $E_f = 640$ GPa and $E_m = 3.45$ GPa are the moduli of elasticity of the fibre and the matrix respectively.

The transverse CTE is calculated from Equation 7.3.4, where $\nu_f = 0.2$ and $\nu_m = 0.35$ from literature and $\nu_{12} = 0.267$ calculated from the tensile test. The transverse CTE is calculated as $\alpha_2 = 42.8 \times 10^{-6} \text{C}^{-1}$.

$$\alpha_2 = (1 + \nu_f) \alpha_f V_{f2} + (1 + \nu_m) \alpha_m (1 - V_{f2}) - \alpha_1 \nu_{12} \quad (7.3.4)$$

$$\alpha_{FS} = \frac{1}{3E_C} (\alpha_1 E_{fm2} + \alpha_2 E_T + \alpha_1 E_{fm2}) \quad (7.3.5)$$

Now the CTE can be calculated for the entire face sheet with a [0/90/0] layup. Equation 7.3.5 is used to calculate the CTE of the face sheet to be $\alpha_{FS} = -0.76 \times 10^{-6} \text{C}^{-1}$, where the transverse modulus of elasticity is assumed from literature to be $E_T = 5.4$ GPa. The combined modulus of elasticity of the layup in the longitudinal direction of the structure is $E_C = 193$ GPa as calculated by MSC Patran.

The temperature change behaviour was further investigated by modifying the FE model to represent an aluminium ribbed and pocketed structure. A temperature load of a 80 °C was implemented in the model. This load was also added to the final FE model of the hybrid structure. The deformation changes of these two models were inspected. The second generation panel showed rib stresses of up to 160 MPa, Figure 7.16, which is very high but still much lower than the yield strength of 260 MPa. The maximum deformation of this composite structure model was 0.747 mm (Figure 7.17). The model of the ribbed and pocketed aluminium structure showed a maximum deformation of 1.44 mm, Figure 7.18, nearly double that of the hybrid structure. The maximum stress in the structure was a mere 0.76 MPa. Since the temperature range used are for extreme conditions

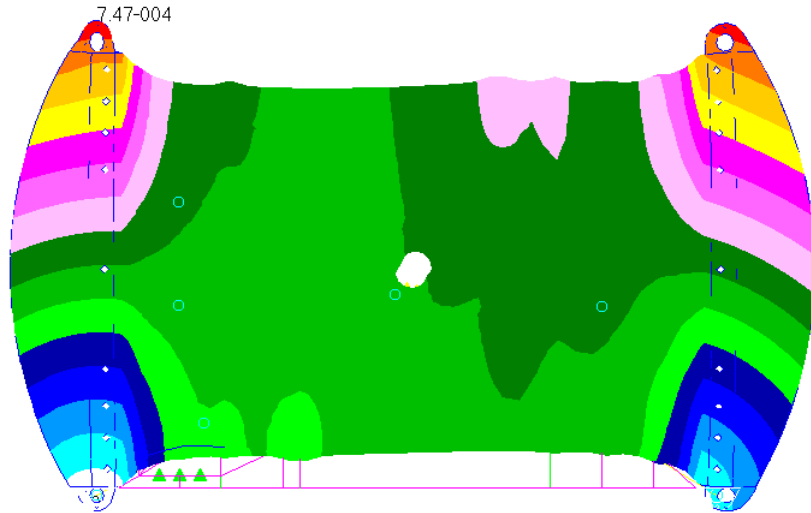


Figure 7.17: Deformation of the second generation panel due to a 80 °C change in temperature

and a average day-night temperature change of 40 °C are expected, the resulting stressed in the structure will be much lower and fatigue are not expected to have an alarming effect.

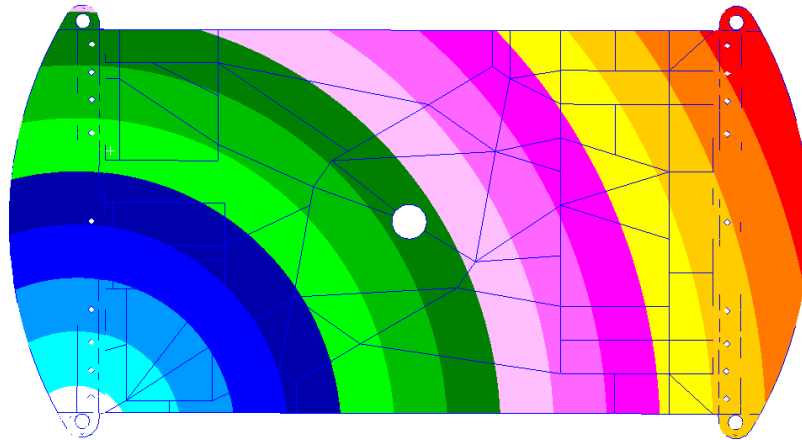


Figure 7.18: Deformation of the aluminium ribbed and pocketed panel due to a 80 °C change in temperature

These FE models showed that there are clear advantages and disadvantages to both types of structures. The choice between the two structures depend on user specifications. For an outer space environment it is however very important for the structure to be as stable as possible, providing it does not fail. The large deformations of pure aluminium structures may cause problems with imaging hardware. The hybrid composite structure is more stable and will thus be the better option to use in satellites. Honeycomb structures will be even more stable than the second generation panel but the heat transfer ability and the ability of the second generation panel to have black boxes bolted to the structure without the use of inserts, edges out honeycomb structures.

Chapter 8

Discussion and Conclusion

During the course of this study, a new generation hybrid light alloy - carbon fibre composite satellite structure panel was successfully developed. The development of this structure was to improve the stiffness to weight properties of conventional aluminium ribbed and pocketed structures. This newly developed structure will also surpass the heat removal ability of aluminium honeycomb sandwich structures, and have the luxury of specifically positioned bolt holes for black box attachments without the use of inserts. The sandwich structure core was developed and optimised with computer software, Genesis, and the basic black box layout was taken from the base plate of the Sumbandila satellite designed by SunSpace and Information Systems.

In order to get a better understanding of recent studies done on sandwich structure core designs a literature study was conducted in Chapter 2. Reasons are given why these existing core structures were not used for the development of the sandwich structure core for this study. This chapter gives a brief overview of a trial study done in 2007 on a ribbed aluminium core sandwich structure and the problems that occurred during that study.

In Chapter 3 the mathematics behind the calculation of stresses and strains for the elements used in the FE (Patran/Nastran and Genesis) models are explained.

A manufacturing study was done by Mr. R. Wilsenach to inspect the machinability of 6082-T6 aluminium and the effect of high modulus carbon fibre vs. low modulus carbon fibre on the stiffness of the structures. The materials used for the manufacturing and modelling of the structure were explained in Chapter 4. In this chapter all the material tests done on the selected materials are explained. A tensile test was done to verify the mechanical properties of the K63712 carbon fibre used to manufacture the face sheets of the structure. The tests revealed a high modulus of elasticity in the fibre direction of 286.6 GPa and a Poisson's ratio of 0.267. Compression tests were done on the room temperature curable 3M Scotch-weld 9323 B/A adhesive to determine the shear modulus of the adhesive. The test results showed a modulus of elasticity of 2.79 GPa and a shear modulus of 0.997 GPa, which makes this a high strength epoxy. An outgassing test was done on the 3M Scotch-weld 9323 B/A adhesive to determine whether the adhesive will be able to perform according to the ASTM standards for adhesives used in a space environment. The test results were compared to an adhesive, 3M Scotch-weld 2216 B/A Gray, used by Mr. R. Wilsenach in his BEng final year project. The adhesive used by Mr. R. Wilsenach is listed as a space grade adhesive and has thus satisfied the ASTM outgassing specifications. A TML of 0.37% during vacuum at an elevated tem-

perature of 60 °C and a CVCM of 0.099% were found which is lower than the allowed 1% for TML and 0.1% for CVCM. This test results confirm that the 3M Scotch-weld 9323 B/A adhesive qualifies as a space grade bonding agent. This chapter also gives a brief overview of the properties of magnesium since it might be used in the next stage of the development of hybrid light alloy - carbon fibre composite satellite structure panels.

In Chapter 5 the effect of high modulus carbon fibre on the stiffness of the first generation panel core was investigated. The first generation core was optimised to investigate the abilities of the Genesis optimiser and to lighten the structure. The implementation of high modulus carbon fibre drastically improved the stiffness of the structure by 97.9% and the optimiser reduced the weight of the structure by 33%. These results motivated the researcher to use the Genesis optimiser along with MSC Patran FE modelling to develop the second generation panel core. A CAD model containing the basic layout of the structure and the positioning of the black boxes was developed. After importing the model into MSC Patran, the model was modified with the addition of wedge elements in the space where the final ribbed structure would be, the carbon fibre face sheets were also added to the model in the form of shell elements. The boundary conditions and mass elements to represent the black boxes were also added to the model. This model was then imported into the Genesis optimiser to be setup for the topology optimisation which would ultimately reveal the final rib positions. The design constraints were to design the structure to have a first natural frequency higher than 130 Hz, all the wedge elements created in the space of the final ribs were selected to be the design region. The design objectives were to remove 70% of the material in the design region and to remove the material through the thickness of the panel, this enables the structure to be manufactured with the use of a milling machine.

The results from the topology optimisation were used to create a FE model with an optimised rib layout. This new model could now be used to find the optimum rib thickness of each of the ribs. To do this Genesis sizing optimisation was used. A design variable was created for each of the ribs with its desired thickness as the lower boundary of the design variable. The design objective was to design the structure to be as light as possible and the design constraint to keep the first natural frequency higher than 115 Hz. The results from this sizing optimisation were then used to create the final optimised ribbed FE model which could be analysed. The final FE model has a first natural frequency of 141.76 Hz, which means that the structure is much stiffer than the original SunSpace designed structure. The model was then subjected to launch acceleration conditions of a representative Russian launch vehicle and analysed to find the safety factor of the structure. The analysis showed a safety factor of 3.52 with a maximum transverse stress of 9.92 MPa in the carbon fibre face sheets. The FE model results of the second generation hybrid panel performed much better than the FE model of the SunSpace designed structure with deformations of 0.172 mm and 0.283 mm respectively under the launch acceleration of 115.46 m/s². The FE model predicted a weight saving of 1.05 kg without taking the cutting tool radius and weight of the adhesive into consideration.

In Chapter 6 the manufacturing process of the composite sandwich structure is explained. A CAD model of the final design of the second generation panel was created to make the structure fully manufacturable. This model added 1 mm flanges to the 0.5 mm thick ribs to improve the bonding area. Bolt holes were also added to the structure with 1.25 mm high extrusions of aluminium added to the bolt positions. These extrusions will

extend through the carbon fibre face sheet to form a metal to metal connection with the black boxes. The CAD model was converted into a STEP file and sent to Daliff Precision Engineering to manufacture the aluminium core. The manufactured aluminium core weighed 3.32 kg. Carbon fibre face sheets were manufactured from three layers K63712 high modulus carbon fibre orientated in [0/90/0] with the 0° in the longitudinal direction of the panel. The face sheets were cut to size and holes were drilled in the top face sheet, the face sheets had a combined weight of 1.027 kg before bonding. 3M Scotch-weld 9323 B/A were used to bond the carbon fibre face sheets to the aluminium core. Only one face sheet could be bonded at a time because the adhesive curing time is 7 days at 25 °C. After both of the face sheets have been bonded the access adhesive was removed with a milling machine to finish the manufacturing of the second generation panel. The total weight of the second generation panel is 4.43 kg.

The development of the second generation panel resulted in an overall weight saving of 0.44 kg. This can be seen as an approximate \$8 800(US) saving in launch cost alone, but there are other factors that need to be considered. The manufacturing cost of the SunSpace designed structure was R10 000(ZAR) where the manufacturing cost of the second generation panel core alone was R14 902.65(ZAR). The material cost of the carbon fibre face sheets was R2 000(ZAR) that includes the carbon fibre cloth and resin for both sheets, with its labour cost R1 500(ZAR) for 6 manhours of manufacturing and post bonding machining. The cost of the adhesive used to bond the carbon fibre to the aluminium was R1 170(ZAR) with a labour cost of R1 250 for 5 manhours rated at R250(ZAR) per hour. By assuming a Rand/Dollar exchange rate of R7.50(ZAR) the launch cost saving calculates to R66 000(ZAR), if calculated purely on mass saving. The difference in manufacturing cost of the SunSpace designed structure and the second generation panel designed in this study is R10 822.65(ZAR). This concludes that the overall saving to the satellite owner for launching this panel into orbit can be R55 177.35(ZAR). If an entire satellite can be manufactured from similar structures the saving can be considerable.

Chapter 7 covers the physical tests done on the structure which include modal, random vibration and temperature tests. The modal tests were done on a free structure only supported by an inflated motor vehicle tire inner tube; dummy masses were bolted to the structure to simulate the weight of the black boxes. Accelerometers were used to measure the frequency peaks. The test results did not correlate with the FE results with a first natural frequency of 107 Hz, the second natural frequency were measured to be at 142 Hz which is much closer to the FE model first natural frequency. The FE model does not contain the adhesive bonding the carbon fibre face sheets to the aluminium core. This will effectively make the FE model stiffer than the physical structure. The difference between the results are however too large, the only explanation is that the boundary conditions used to support the structure had a negative impact on the test results. Sine sweeps done during the random vibration tests were used to measure the natural frequency of the structure. The boundary conditions of these tests were fixed which will result in more accurate results. The final sine sweep measured a first natural frequency of 122.5 Hz. This is still lower than the FE results, but with only a 13.5% difference in results. The FE results will be closer to the measured value when the model contains the bonding layer. The sine sweep results confirm that the structure is 8.97% stiffer than the SunSpace designed structure.

Random vibration test were done to test the durability of the structure when sub-

jected to launch vibrations. The tests were done at two intensity levels, 4.6 gRMS and 12.6 gRMS. The low intensity test was done for a period of 4 minutes and the high intensity tests were done in two stages of 4 minute tests each. After the tests were done the data were analysed and the structure inspected for any failures. The structure did not fail in any way, thus the structure will be able to successfully launch into orbit after which no external forces will be subjected on the structure.

Temperature fluctuation tests were done on the structure to inspect the stability of the structure when subjected to outer space environmental conditions. The test results proved that the structure deforms less than a structure manufactured from only aluminium. This is due to the negative coefficient of thermal expansion of the carbon fibre which restricts the aluminium to expand as normally. On imaging satellites this could be a big advantage purely because of the stability of the materials used to manufacture the panel.

During the course of this study an optimised hybrid aluminium ribbed core was successfully developed with the use of Genesis software. The study proved that the concept of individually designed ribbed core sandwich structures is stiffer and lighter than aluminium ribbed and pocketed structures. This can lead to large savings on overall satellite costs

Some tests still need to be done on the structure. The heat removal ability of the structure need to be tested and compared to honeycomb and aluminium ribbed and pocketed structures. Alternative materials, such as magnesium, for the core must be looked at. The use of magnesium can save at least 1 kg, especially at prescribed solid regions of the core material (e.g. semi-circular flanges and rib intersections), on the current structure design which could lead to large savings considering an unofficial rated cost of \$20 000(US) for every kilogram to be launched into orbit. The sizing optimisation should be repeated to ensure the structure does not fail structurally. If magnesium was to be used, the bonding of carbon fibre sheets onto a magnesium structure should be inspected. The machinability of magnesium should be tested to find the minimum rib thickness for a magnesium core. Future studies could also look into the damping properties of ribbed metal core sandwich structures and the effect of different core materials and bonding agents.

The second generation structure design process will be used to develop the structure panels for the next generation satellite developed by SunSpace and Information Systems. This technology may also be used on other aerospace structures for improved stiffness to weight properties.

Appendices

Appendix A

Material Properties



K63712
COAL TAR PITCH-BASED CARBON FIBERS

TYPICAL PROPERTIES

<i>Tensile Strength</i>	<i>380 Ksi</i>
<i>Tensile Modulus</i>	<i>92 Msi</i>
<i>Ult Elongation</i>	<i>.4 %</i>
<i>Yield</i>	<i>250 yard/Lb</i>
<i>Density</i>	<i>2.12 g/cm³</i>
<i>Electrical Resistivity</i>	<i>6.6 x 10⁶ohmm</i>
<i>Thermal Conductivity</i>	<i>140 W/m²K</i>
<i>Sizing Amount (Epoxy Type)</i>	<i>2 %</i>
<i>Number of Filaments</i>	<i>1 2 K</i>
<i>Filament Diameter</i>	<i>11 u</i>
<i>Twist</i>	<i>0 untwisted type</i>
<i>Carbon Content</i>	<i>over 99 %</i>

Standard Package Size:
3 lb Spool Size, 16 Spools per Case
5.5 lb Spool Size, 9 Spools Per Case

This information we believe to be useful for consideration and evaluation. However it should not be taken as a warranty or representation for which we undertake any legal responsibility, or as recommendation or permission to carry out any patented invention commercially.



Mitsubishi Chemical America ● 401 Volvo Parkway Chesapeake VA 23320 ● Phone: 757-382-5750
 Fax: 757-312-8259 ● Website: www.mitsubishichemical.com

Figure A.1: High modulus carbon fibre manufacturers data sheet

i COMPOSITES.COM									
High Modulus Carbon/Graphite Fibers									
Fiber Properties (Typical)									
Type	Name	Mfg	Tensile Modulus (msi)	Tensile Strength (ksi)	Thermal Conductivity (W/m° K)	Density (g/cc)	Tow Size (K)	Fiber Elongation (%)	0° Laminate Compression Strength (ksi)
Pan	M40J	Toray	54	640	<100	1.77	6,12	1.2	>175
Pan	M46J	Toray	63	610	<100	1.84	3,6,12	1	>140
Pitch	K63303,306	Mitsubishi	63	493	--	2.04	3,6	--	--
Pitch	K63312	Mitsubishi	63	377	--	2.04	12	--	--
Pitch	YSH-40A	NGF	59	570	124	2.05	0.4	0.8	--
Pan	UHM	Hexcel	64	500	<100	1.88	3,6	0.8	110
Pitch	XN-50A	NGF	75	560	180	2.14	0.5,1,2	0.7	60
Pitch	YSH-50A	NGF	75	560	120	2.10	3,6	0.7	80
Pitch	P75S	BP-Amoco	75	325	200	2.00	0.5,1,2	0.4	65
Pitch	P75SP	BP-Amoco	75	500	--	2.15	0.5,1,2	0.7	75
Pitch	K1351L	Mitsubishi	90	522	--	2.12	1	0.6	
Pitch	K1352U,1U	Mitsubishi	75	530	140	2.12	1,2	0.6	65
Pan	M55J	Toray	78	585	<100	1.91	6	0.8	125
Pan	M60J	Toray	85	569	<100	1.94	3,6	0.7	110
Pitch	K63712	Mitsubishi	92	500	220	2.12	12	--	--
Pitch	K13710	Mitsubishi	92	500	220	2.12	10	--	55
Pitch	YSH-60A	NGF	92						
Pitch	P100	BP-Amoco	110	350	--	2.14	2	0.3	45
Pitch	P100HT	BP-Amoco	110	525	--	2.15	2	0.5	50
Pitch	XN-70A	NGF	105	530	320	2.16	0.5,1,2	0.5	55
Pitch	YSH-70A	NGF	105	530	250	2.16	3	0.5	65
Pitch	K1392U,1U	Mitsubishi	110	540	210	2.15	1,2	0.5	58
Pitch	XN-80A	NGF	114	530	--	2.17	1,2	0.5	50
Pitch	YS-80A	NGF	114	530	320	2.15	1,3,6	0.5	--
Pitch	K13A10	Mitsubishi	115	377	--	2.14	10	--	--
Pitch	K13A11	Mitsubishi	115	537	--	2.16	1	0.5	--
Pitch	P120	BP-Amoco	120	325	600	2.16	2	0.3	45
Pitch	K13B2U	Mitsubishi	120	550	260	2.16	2	0.4	50
Pitch	K63b12	Mitsubishi	125	377	--	2.15	12	--	--
Pitch	XN-85A	NGF	120	530	430	2.17	1,2	0.4	54
Pitch	K13C2U,1I	Mitsubishi	130	550	620	2.20	1,2	0.4	57
Pitch	K13D2U	Mitsubishi	136	537	800	2.2	2	--	--
Pitch	K800	BP-Amoco	130		800				
Pitch	YS-90A	NGF	130	530	430	2.19	1.5,3,6	0.3	50

Figure A.2: Data sheet comparing high modulus carbon fibres from icomposites.com (iComposites, 2009)



Technical Data Sheet

CeTePox[®] AM 3502 A/B

Characteristics Germanischer Lloyd (GL) approved epoxy system for hand lay up with adjustable pot life in combination with CeTePox AM 3504 B

Properties and Fields of Application CeTePox AM 3502 A/B is an epoxy system for hand lay up techniques with low exothermic heat, outstanding wetting and adhesion properties. This epoxy system is suitable for the production of high performance laminates or in combination with honeycomb for lightweight construction elements for boat building and wind mill rotor blades. The system offers an excellent cost-performance ratio. By combination of hardeners CeTePox AM 3502 B and 3504 B, which are miscible in any ratio, the reactivity of the system can be adjusted while mixing ratio of resin and hardener will remain constant at 100:30 pbw.

	Property	Unit	Comp A	Comp B
Typical Data	Viscosity @ 25°C	Pas	1,3-1,9	0,01-0,02
	EEW	g/equiv.	180-200	-
	Amine equivalent	g/equiv.	-	53-57
	Density @ 23°C	g/cm ³	1.12-1.14	0,93-0,95

Mixing Ratio	Parts by Weight	pbw	100	30
---------------------	-----------------	-----	-----	----

System Properties	Viscosity of Mixture @ 25°C	Pas	0,25 - 0,31	
	Pot life (100g) @ 23°C	h	10	
	Pot life (100ml) 23°C to 40°C	min	155-215	
	Curing Time @ 25°C	h	12	
	Post Curing Time	h	5h @ 70°C and 5h @ 80°C	

Properties of cured resin	7 ply roving fabric GW323-280 H1, glass content 58,7%, 12 h @ 25°C and 10 h @ 80 °C			
	Flexural Strength	N/mm ²	832	
	E-Modulus (flex)	N/mm ²	20 730	
	Flexural Strength (2h boiling)	N/mm ²	792	
	E-Modulus (flex) (2h boiling)	N/mm ²	20 080	
	Tensile Strength	N/mm ²	743	
	E-Modulus (tensile)	N/mm ²	35 630	
	Tg (DSC)	°C	85	

Shelf Life & Storage Store this material in a clean, dry environment in its tightly closed original container. These products are not considered especially temperature or moisture sensitive, but should ideally be stored at temperatures between 18-25°C and kept from moisture contamination. Storage at lower temperatures could lead to crystallization and may require the application of heat to reverse. If the product appears crystalline or is thicker than normal when opened, heat for 4-6 hours at 65°C to re-liquefy prior to use. If the recommended storage conditions are observed the products will have a minimum shelf-life of 6 months from the date of shipment.

Remarks with Regard to Occupational Safety Mandatory and recommended industrial hygiene procedures should be followed whenever these products are being handled and processed. For additional information please consult the corresponding material safety data sheets and/or the recommendation of APME.

IMPORTANT: The following supercedes Buyer's documents. **SELLER / MANUFACTURER MAKES NO REPRESENTATION OR WARRANTY, EXPRESS OR IMPLIED, INCLUDING OF MERCHANTABILITY OR FITNESS FOR A PARTICULAR PURPOSE.** No statements herein are to be construed as inducements to infringe any relevant patent. Under no circumstances shall Seller / Manufacturer be liable for incidental, consequential or indirect damages for alleged negligence, breach of warranty, strict liability, tort or contract arising in with the product(s). Buyer's sole remedy and Seller's sole liability for any claims shall be Buyer's purchase price. Data and results presented are based on controlled or laboratory work and must be confirmed by Buyer by testing for its intended conditions of use. The product(s) has not been tested for, and is therefore not recommended for, uses for which prolonged contact with mucous membranes, abraded skin, or blood is intended; or for uses for which implantation within the human body is intended.

AM TI 3502 /E 03-05/V 06

CTP Advanced Materials GmbH – Stahlstrasse 62 – D-65428 Rüsselsheim

Figure A.3: CeTePox 3502 manufacturers data sheet

3M**Scotch-Weld™****9323 B/A Structural Adhesive****Product Data Sheet**

Updated : March 1996
Supersedes : July 1995

Product Description	9323 B/A is a two part room temperature curing adhesive offering the following advantages:	Toughened Epoxy system with good elevated temperature resistance.	Mixed adhesive is thixotropic for ease of application.
	Extremely high strength.	High environmental resistance.	Available in 3M premetered applicator. High impact resistance.

Physical Properties
Not for specification purposes

	BASE	ACCELERATOR
	Toughened Epoxy	Modified Amine
Specific Gravity	1.15	1.10
Mix Ratio By Weight By Volume	100 100	27 29
Consistency	Thixotropic paste	Red paste
Solids Content	100%	100%
Colour	Off White	Orangy Purple
Work Life	50g mixed material 2 hours 30 minutes 127g mixed material 2 hours 158g mixed material 1 hour	
Shelf Life	6 months from date of despatch by 3M when stored in the original carton at 21°C (70°F) & 50 % Relative Humidity	

Performance Characteristics
Not for specification purposes

Service Temperature Range	-55°C to 82°C (-67°F to 180°F)	In low load bearing applications the adhesive bonds in temperatures up to 150°C.
Water Resistance	Good	
Weathering Resistance	Good	
Fuel and Oil Resistance	Excellent	

Figure A.4: 3M Scotch-Weld 9323 B/A manufacturers data sheet

Date : March 1996
9323 B/A Structural Adhesive

Performance Characteristics (Cont...)
Not for specification purposes

Overlap Shear Strength on FPL etched 1.6mm thick 2024 T3 clad aluminium.

Test Conditions	15 Days at RT		24 Hours at RT + 1 hour at 80°C		2 hours at 65°C	
	N/mm ²	psi	N/mm ²	psi	N/mm ²	psi
-55°C	38.1	5525	29.0	4200	23.7	3535
23°C	36.2	5250	40.8	5915	39.6	5740
60°C	29.0	4200	32.0	4640	Not Tested	
82°C	22.1	3200	23.4	3390	25.4	3680
120°C	4.0	580	3.5	505	Not Tested	
150°C	2.6	380	2.5	360	Not Tested	

T-Peel Strength on FPL etched 0.8mm thick 2024 T3 clad aluminium.

In order to ensure optimum peel properties with this product, it is recommended that joints be assembled within 20 minutes of applying the adhesive to the surfaces. Prior to application the above work lives remain valid.

Test Conditions	24 hours at RT + 1 hour at 80°C		2 hours at 65°C	
	N/cm	piw	N/cm	piw
-55°C	10.3	6	11.6	6.5
+23°C	52.2	30	58.5	33
+82°C	43.3	25	54.3	31

Durability on etched aluminium.

Values refer to overlap shear strength on 1.6mm thick 2024 T3 clad aluminium.

Test Conditions	15 Days at room temperature		2 hours at room temperature + 60 minutes at 80°C	
	N/mm ²	psi	N/mm ²	psi
Control				
30 Days Immersion	38.2	5540	41.6	6030
Water at RT	34.3	4970	38.9	5640
Gasoline at RT	36.6	5300	38.0	5510
M.15 at RT	30.2	4380	32.0	4640
JP4 at RT	35.8	5190	39.3	5700
Engine Oil at RT (20W40)	36.4	5280	40.9	5885
Hydraulic Oil at RT (Skydroll 500B)	37.3	5410	36.8	5335
5% Salt Spray at 35°C	33.9	4870	35.1	5090
120°C Dry Heat	34.9	5060	33.1	4800
70°C, 95% RH	32.8	4755	35.3	5120
50°C, 95% RH	37.0	5365	36.0	5220

Figure A.4: Continued

Date : March 1996
9323 B/A Structural Adhesive

Impact Strength

The following data show typical data obtained with bonds made and tested using an IZOD pendulum impact device according to AFNOR 76-115 test method.

Substrates:
Upper 25mm x 25mm x 8mm.
Lower 35mm x 25mm x 8mm.
2024T3 etched aluminium.
Glue line thickness: 0.125mm
Unit : kJ/m²

	15 Days at RT	1 hour at 80°C	2 hours at 56°C
Impact Value	17.4 ± 4.4	28.7 ± 3.3	32.2 ± 3.2

Suggested Cleaning Procedure for Aluminium:

Vapour Degrease - Hang skins in condensing vapours of perchloroethylene for 5 minutes.

Alkaline Degrease - Immerse in Oakite No. 164 solution (9-11 oz/gallon water) at 82°C to 93°C (180°F to 200°F) for 10 - 20 minutes. Rinse in generous quantities of clear running water.

Acid Etch - Place in either of the following solutions for 10 minutes at 66°C ± 4°C (150°F ± 5°F).

Rinse - Rinse face sheet in clear running water.

Dry - Air dry 15 minutes, force dry 10 minutes with parts at 66°C ± 4°C.

If primer is to be used, priming should be done within 4 hours of surface preparation.

	A (FPL Etch)	B
Distilled Water	30 parts by wt	30 parts by wt
Sulphuric Acid	10 parts by wt	10 parts by wt
Sodium Dichromate	1 part by wt	4 parts by wt

Cure Cycle:

In general the curing of 9323 B/A to a thermoset condition is a time-temperature relationship. The only pressure requirements are that the parts must be held in contact and alignment during the cure cycle.

To effect a useful cure in a reasonable length of time, a minimum temperature of 24°C (75°F) is required. The following cure cycle is suggested to obtain dense glue lines which give the standards reported.

Figure A.4: Continued

Date : March 1996
9323 B/A Structural Adhesive

Standard Room Temperature Cure: Prepare overlap shear bonds in the manner described and allow to cure as follows:

Apply 2 psi bonding pressure uniformly to the bond line using dead weights.

Allow Panels to cure undisturbed at a temperature of 24°C (75°F) for 24 to 48 hours.

In addition to standard room temperature cure, the following times and temperatures will give a minimum of 2,000 psi tensile shear at 24°C (75°F) on acid etched aluminium.

Temperature	Time
5°C (40°F)	7 days
66°C (150°F)	120 minutes
121°C (250°F)	5 minutes
177°C (350°F)	2 minutes

Additional Product Information **Work Life:** The work life of mixed 9323 B/A is approximately 2 hours 30 minutes in a mass of 50grams at an ambient temperature of 23°C.

The work life of the mixed adhesive will be lengthened by reducing the temperature or amount of adhesive and will be shortened by higher temperature or larger amounts of adhesive. **Caution:** Heat is generated during cure.

Directions for Use Proper adhesive application is as important as proper joint design, surface preparation and adhesive choice to obtain maximum joint properties. Poor adhesive application techniques can result in partial or complete failure of an assembly.

9323 B/A performance data was developed using the following suggested procedures. Variation from these procedures should be fully evaluated by the user to ensure bond properties sufficient to meet the requirements of any particular assembly.

Surface Preparation: A thoroughly cleaned, dry, grease-free surface is essential for maximum performance. Cleaning methods, which will produce a break free water film on a metal surface are generally satisfactory.

Adhesive Mixing: Mix only those amounts of adhesive which can be used within the work life of the mixture. To achieve optimum physical properties of the adhesive, mixing of the base and accelerator must be very thorough. Care should be taken not to incorporate excessive air into the adhesive during mixing and application as entrapped air will tend to give a porous and weakened bond. When weighing the components, be sure that containers are free of wax or oil. When thoroughly mixed the adhesive should be a uniform colour. As a final check to ensure that the components are adequately mixed, spread a thin film on white paper and examine closely for streaks of base or accelerator. Temperature of the adhesive should not exceed 27°C (80°F) during mixing.

Equipment Suggestions: Application can be carried out with a spatula, trowel or flow equipment. Suitable two part metering and mixing equipment is available. Contact your 3M Representative for assistance in selecting application equipment to suit your specific needs.

Bond Line Thickness: Optimum performance is obtained with a 0.002" to 0.005" (0.05 - 0.125mm) cured bond line. For maximum peel strength allow 0.010" (0.25mm) glue line thickness. Coverage 4m²/litre (at 0.010" thickness).

Clean Up: Excess adhesive can be cleaned prior to curing with Scotch-grip Solvent No. 2. **NOTE:** Solvent No. 2 is flammable. When using solvents for clean up it is essential that proper safety precautions are observed.

Figure A.4: Continued

5

Date : March 1996
9323 B/A Structural Adhesive

Applications	Bonds metal, glass, ceramics, plastics, composites and rigid rubbers.	Particularly suited to applications requiring resistance to harsh environments. e.g. oil, gasoline, anti-freeze, dry heat.
Health and Safety Information	<p>PART A contains: 2,4,6 - Tris (Dimethylaminomethyl) phenol, polymeric diamine.</p> <p>PART B contains: Epoxy Resin.</p> <p>Precautions: Irritating to skin. Risk of serious damage to eyes. May cause sensitisation by skin contact. May be harmful if swallowed. Avoid contact with skin and eyes. Wear suitable gloves and eye/face protection.</p>	<p>First Aid:</p> <p>Eye Contact: Immediately flush eyes with copious amounts of water for at least 15 minutes, holding eyes open. Call a physician.</p> <p>Skin Contact: Wash immediately with plenty of soap and water.</p> <p>Ingestion: Drink two glasses of water and call a physician immediately. Do not induce vomiting.</p>
Specifications	May be released to AFS 1899 and DTD 900/1622.	Water Research Council Approval.

3M and Scotch-Weld are trademarks of the 3M Company.

Values presented have been determined by standard test methods and are average values not to be used for specification purposes. Our recommendations on the use of our products are based on tests believed to be reliable but we would ask that you conduct your own tests to determine their suitability for your applications. This is because 3M cannot accept any responsibility or liability direct or consequential for loss or damage caused as a result of our recommendations.

**Specialty Tapes & Adhesives**

© 3M United Kingdom PLC 1996

3M United Kingdom PLC
3M House,
28 Great Jackson Street,
Manchester,
M15 4PA

Customer Service :
Tel 0161 236 8500
Fax 0161 237 1105

3M Ireland
3M House, Adelphi Centre,
Upper Georges Street,
Dun Laoghaire, Co. Dublin,
Ireland

Customer Service :
Tel (01) 280 3555
Fax (01) 280 3509

Figure A.4: Continued



DALIFF
PRECISION ENGINEERING (PTY) LTD

VAT No. 492 0161 546 Reg. No. 1996/010962/07
 17 MILAN STREET AIRPORT INDUSTRIA CAPE TOWN SOUTH AFRICA
 P O BOX 292 EPPINGDUST 7475 EMAIL norbert@daliff.co.za
Tel: +27 (0) 21 386 1851 Fax: +27 (0) 21 386 2520

**QUOTATION
4504**

To : UNIVERSITY OF STELLENBOSCH Fax : Contact: Philip Roets	From : NORBERT LEICHER Reference : Date : 24/04/2009
--	---

We are pleased to quote as follows

Page 1

#	Qty	Description	Drawing No	Unit Price	Total Excl
1	1	Philip Roets Paneel		R 13 072.50	R 13 072.50

	Sub Total	R 13 072.50
	VAT	R 1 830.15
	Total	R 14 902.65

Conditions of sale:

- Prices : Exclude VAT
- : Subject to revision if quantity ordered differs from quantity requested for quotation.
- Terms : Strictly 30 Days (If credit approved). Interest will be charged at prime + 2% on all overdue accounts.
- Delivery: : 14 Days from receipt of your order. (Please confirm this when placing an order).
- Quote Valid : 30 Days. Unless otherwise specified.
- Ownership : Remains vested in Daliff until full payment is received.

Trusting the above meets your approval

Yours faithfully

NORBERT LEICHER

DIRECTORS: N. LEICHER (Managing) R. CHUTE (Chairman)

Figure A.5: Quotation for the manufacturing of the aluminium core structure

AirCRAFTMaterialsUK.com Ltd

Unit C5, Regent Park, Princes Estate, Princes Risborough, Bucks, HP27 9LE, UK

Tel. 44 (0) 1844 275560 Fax. 44 (0) 1844 346892

PRO-FORMA INVOICE

THIS IS NOT A TAX INVOICE

Invoice Address CAMPBELL SCIENTIFIC AFRICA MESON STREET TECHNOPARK STELLENBOSCH SOUTH AFRICA		Attention HERMAN MALAN		22393
		Quotation Date		Customers Reference
		Valid Until	Customer Fax Number 27 21 880 0240 Customer Tel. Number 27 21 880 0885	

Quantity	Description	Unit Price GBP	Value GBP
3	PCES MAGNESIUM ALLOY AZ31B-H24 (AMS 4377) 25.4MM X 160MM X 460MM	438.77	1,316.31
1	PCE MAGNESIUM ALLOY AZ31B-H24 (AMS 4377) 25.4MM X 420MM X 800MM	1,914.66	1,914.66
1	CARRIAGE CHARGE (LOCAL TAXES / DUTIES NOT INCLUDED)	210.00	210.00
***** EX-STOCK, SUBJECT TO PRIOR SALE LEAD TIME: 7-10 DAYS PAYMENT: IN ADVANCE (BANK TRANSFER)			
AircraftmaterialsUK.com Ltd. IS NOT RESPONSIBLE FOR WIRE TRANSFER FEES THEY MUST BE INCLUDED IN YOUR PAYMENT		Sub Total:	3,440.97
Barclays Bank PLC. Business Banking, PO Box 23, Hamilton Road, Slough, Berks, SL1 4NX Swift Code: BARCGB22, Sort Code. 20-40-71		VAT:	0.00
GBP Account No. 20285021 IBAN GB 18 BARC 2040 7120 2850 21 USD Dollar Account No. 64609900 IBAN GB26 BARC 2040 7164 6099 00 EUR Euro Account No. 46064499 IBAN GB19 BARC 2040 7146 0644 99		Total:	3,440.97
		Currency	GBP
Quote Notes:			
Your contact is: Chris Justice Tel. 44 (0) 1844 275560		Payment Terms Proforma	

Conditions of sale available on request or at :<http://www.aircraftmaterialsuk.com/terms>

Page: 1/1

Figure A.6: Quotation for magnesium to be used to manufacture the optimised core structure

SAERTEX SOUTH AFRICA (PTY) LTD.

REG. NO 1997/021106/07

**SUPPLIERS OF NON-CRIMP WOVEN & NON-WOVEN FIBREGLASS & OTHER TECHNICAL MATERIALS**

TELEPHONE: +27(0)21 862 7790/1
 FACSIMILE: +27(0)21 862 7846
 E-MAIL ADDRESS: saertexsa@global.co.za
 VAT REG. NO. 4530170705

25 BOLAND STREET
 DALJOSAFAT, PAARL 7646
 SOUTH AFRICA
 P.O. BOX 671
 S-PAARL 7624

QUOTATION

TO: GRP Tubing
 ATT: Albert Verburg
 FAX: 021 - 853 4080
 E-MAIL: blokkies@grptubing.co.za

DATE: 13/08/2008
 PAGES: 1
 REF: Ronald at U.S.

STYLE	DESCRIPTION	QTY	UNIT	R/UNIT
11348/01	V100055-00420-01270-000000 Description: 419g/m ² Uni-directional Carbon Fabric Dimensions: 127cm x 16lin/m Carbon Fibre in Construction: Mitsubishi K63712	20.32	m ²	R 819.70
FREIGHT				
Option 1	Seafreight, lead time approx. 5 weeks			R 500.00
Option 2	Airfreight, lead time 1 - 2 weeks			R 2000.00

Please Note:

The quoted price excludes VAT and is subject to prior sale. The freight charges are estimates. We will only have the exact freight costs once the material has arrived in SA. GRP Tubing will then be invoiced accordingly

Should our quotation meet your approval, please inform us which freight option you wish to use and place an official order for the quoted fabric.

If you have any questions please do not hesitate to contact us.

Kind regards,
 Nicolaas van Wyk

DIRECTORS: E. JACOBS* (MANAGING) B.H. LAMMERS*
 *GERMAN

Figure A.7: Quotation for importing Mitsubishi K63712 high modulus carbon fibre

Appendix B

Design and Optimisation Plots

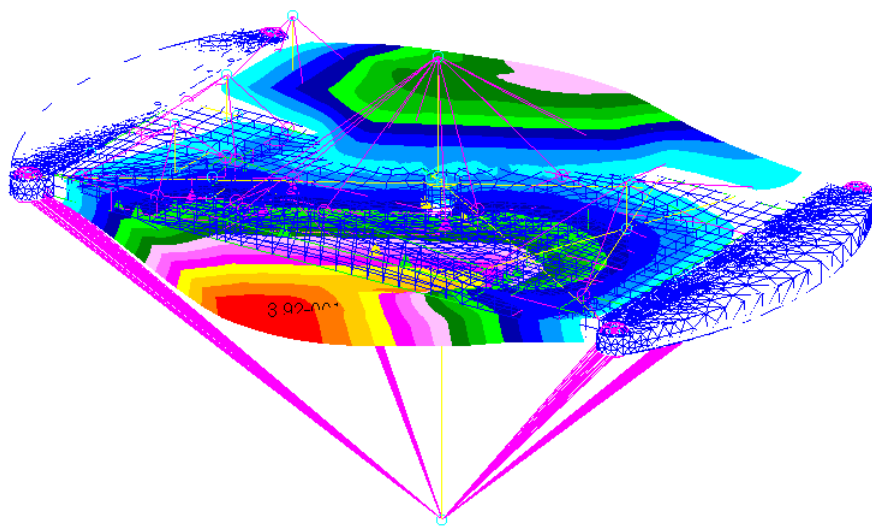


Figure B.1: Second natural frequency of the structure with clamped boundary conditions at 162 Hz

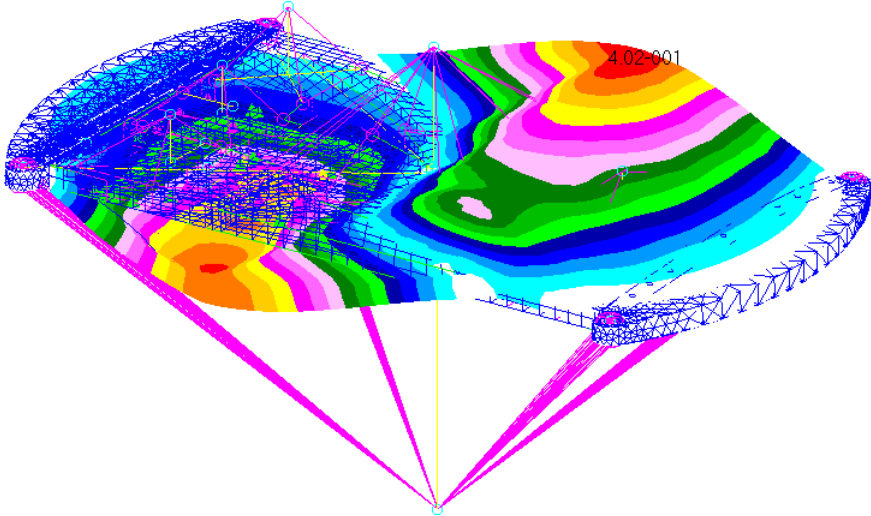


Figure B.2: Third natural frequency of the structure with clamped boundary conditions at 242 Hz

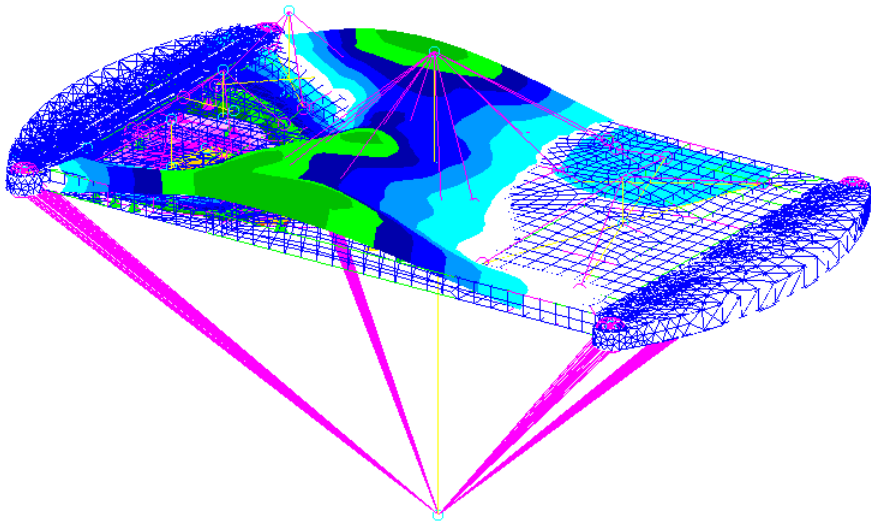


Figure B.3: Fourth natural frequency of the structure with clamped boundary conditions at 394 Hz

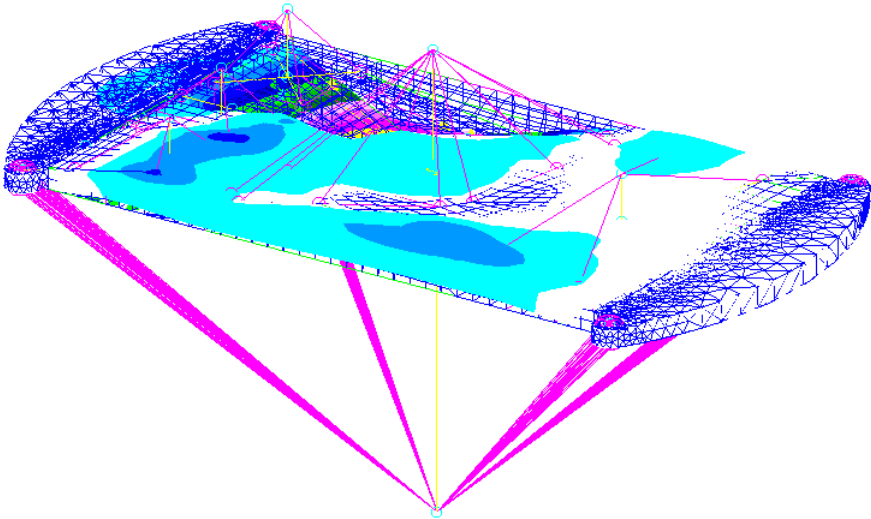


Figure B.4: Fifth natural frequency of the structure with clamped boundary conditions at 441 Hz

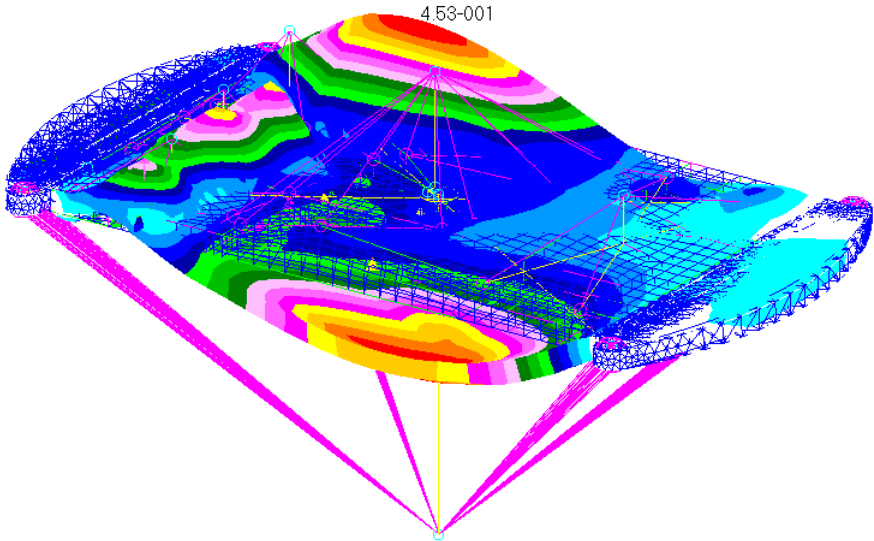


Figure B.5: Sixth natural frequency of the structure with clamped boundary conditions at 471 Hz

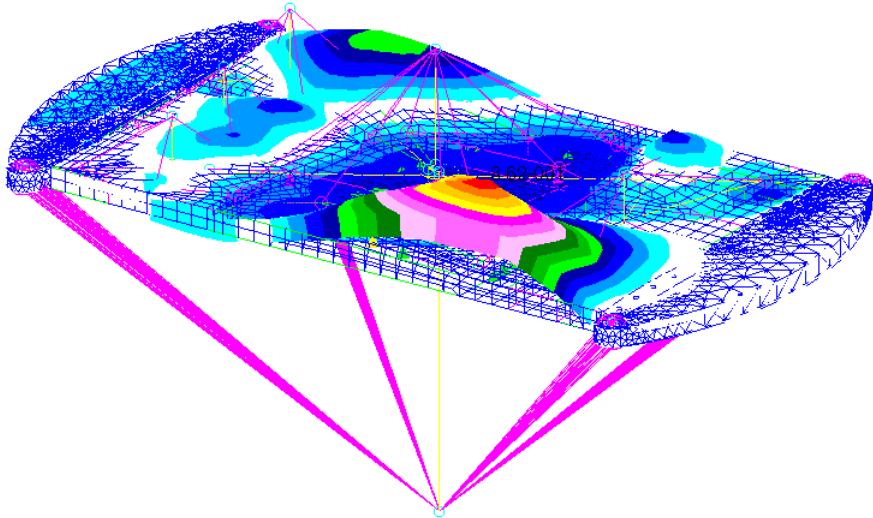


Figure B.6: Seventh natural frequency of the structure with clamped boundary conditions at 514 Hz

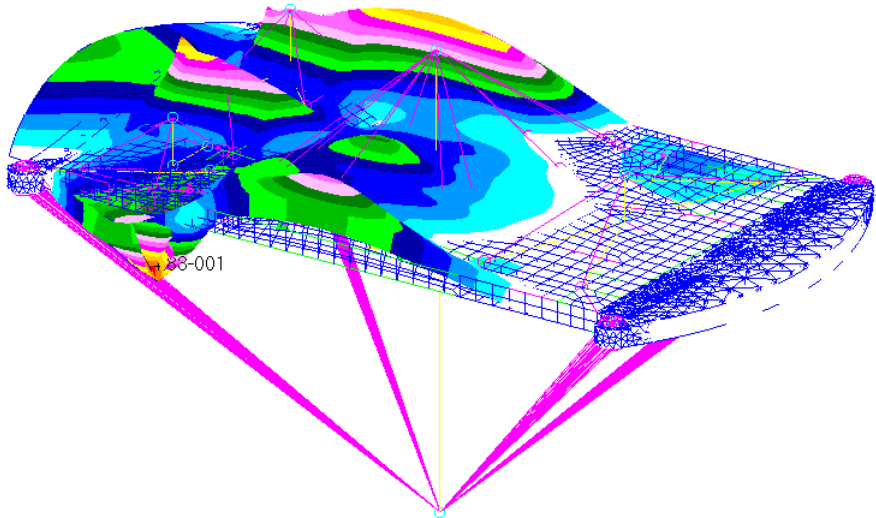


Figure B.7: Eighth natural frequency of the structure with clamped boundary conditions at 578 Hz

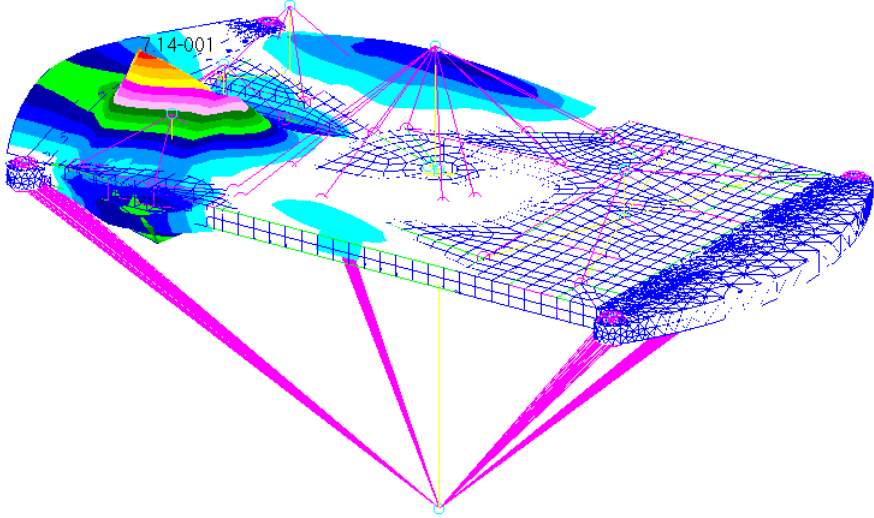


Figure B.8: Ninth natural frequency of the structure with clamped boundary conditions at 614 Hz

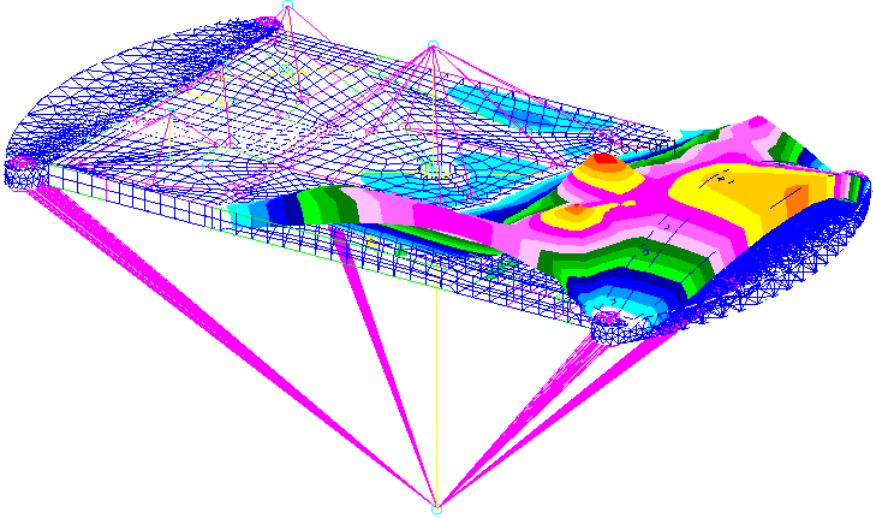


Figure B.9: Tenth natural frequency of the structure with clamped boundary conditions at 646 Hz

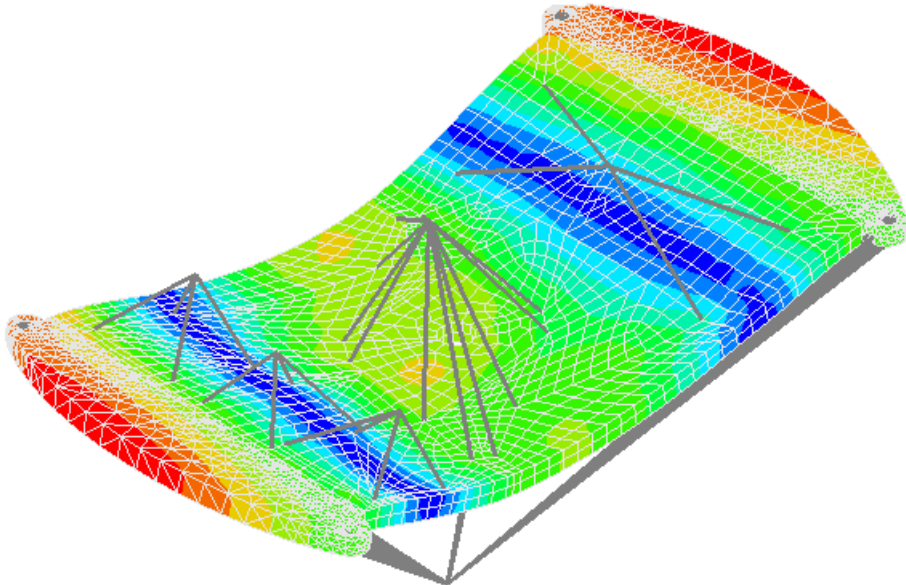


Figure B.10: First natural frequency of the structure after Genesis sizing optimisation at 219 Hz

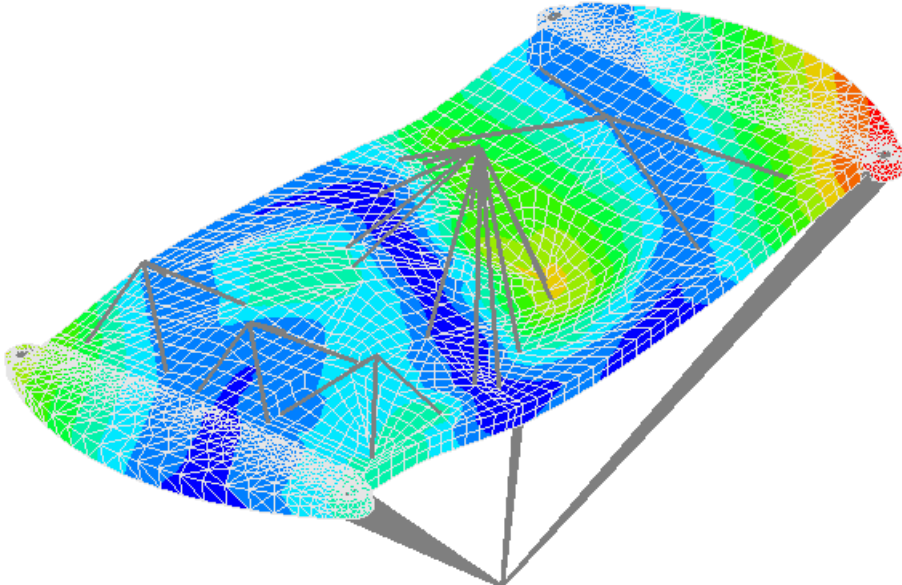


Figure B.11: Second natural frequency of the structure after Genesis sizing optimisation at 245 Hz

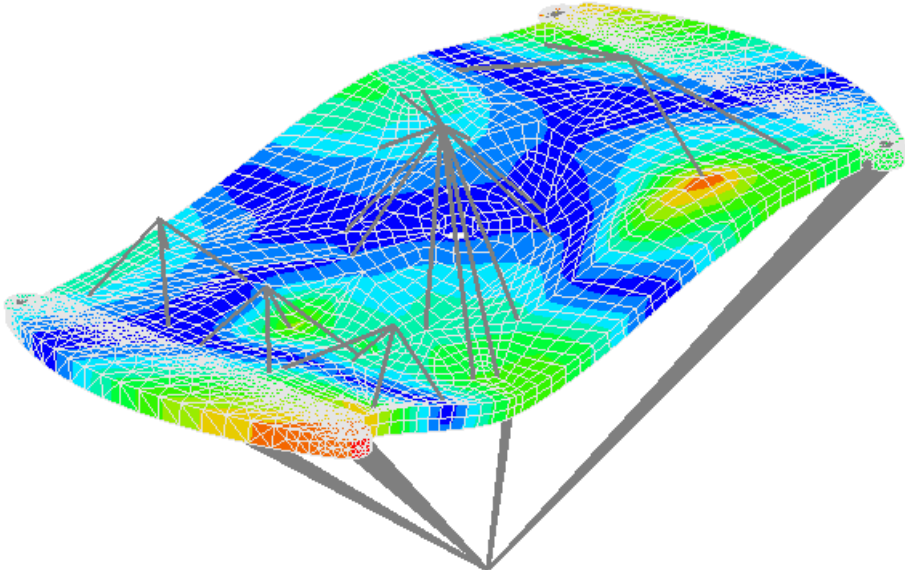


Figure B.12: Third natural frequency of the structure after Genesis sizing optimisation at 322 Hz

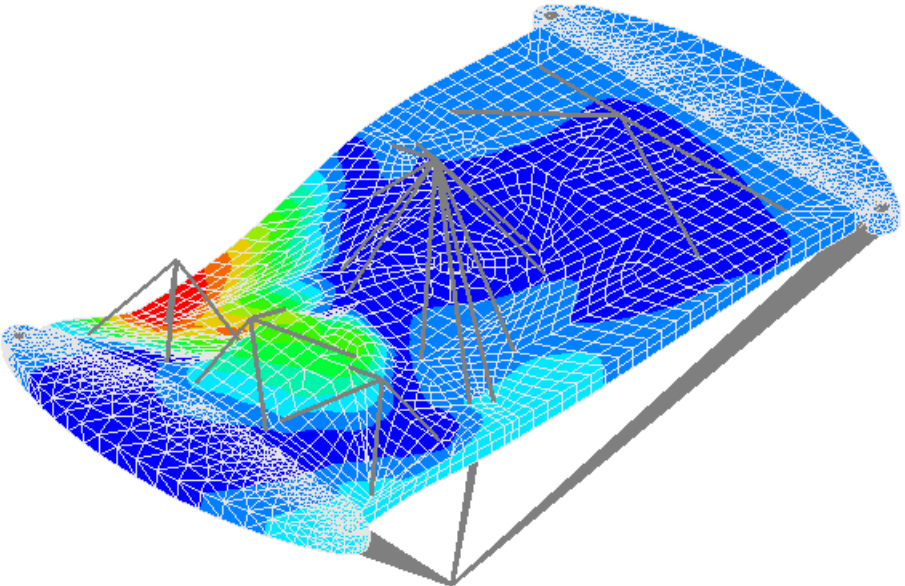


Figure B.13: Fourth natural frequency of the structure after Genesis sizing optimisation at 468 Hz

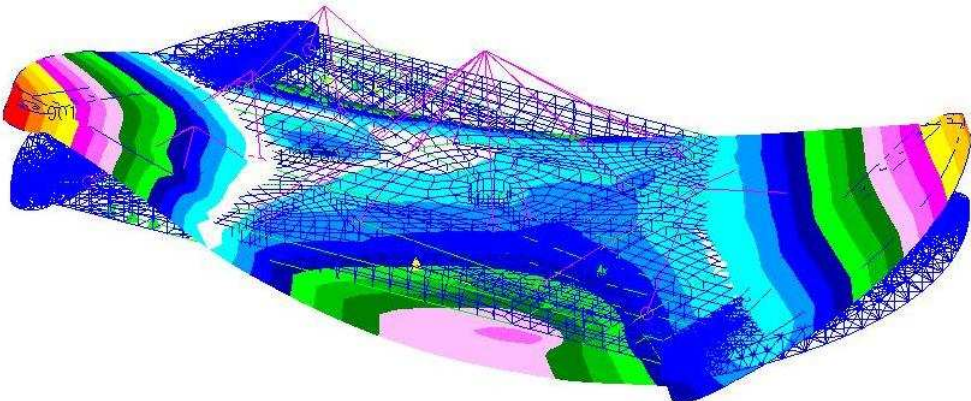


Figure B.14: Second natural frequency of the structure with free boundary conditions at 199 Hz

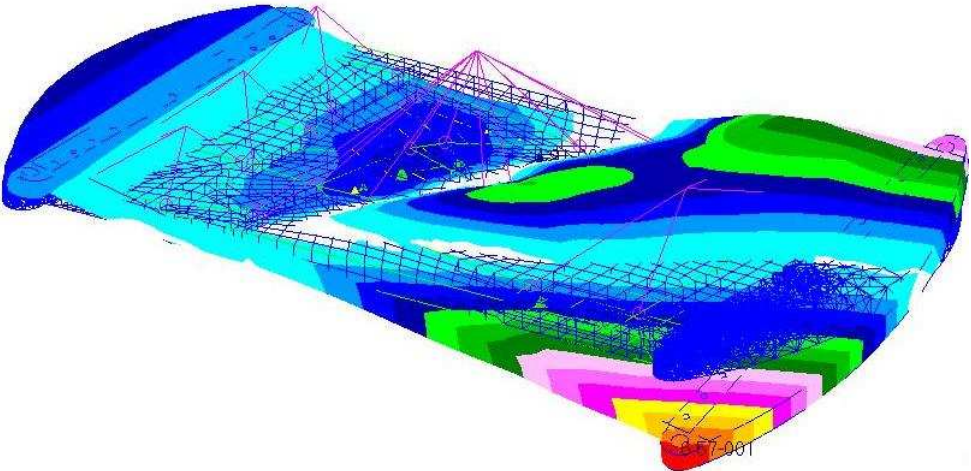


Figure B.15: Third natural frequency of the structure with free boundary conditions at 236 Hz

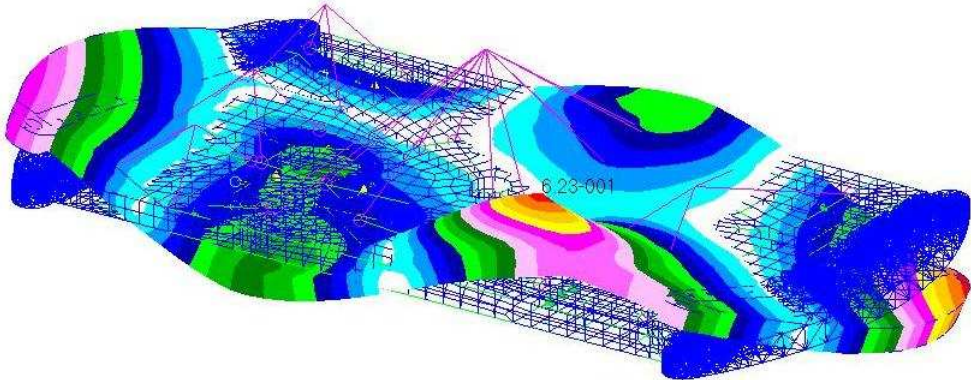


Figure B.16: Fourth natural frequency of the structure with free boundary conditions at 295 Hz

Appendix C

Manufacturing Techniques

C.1 Chromic acid anodising

The following procedure is certified as per Defence Standard 03-24/1 (Wilsenach, 2008).

1. Attach parts to be anodised to titanium jigs and ensure good electrical contact.
2. Etch the parts in a strong solution of caustic soda and water for ± 3 minutes at room temperature.
3. Rinse in clean water.
4. Rinse in a nitric-acid/water solution (ratio 1:1) to remove sludge and neutralise any residual caustic.
5. Rinse in de-ionised water.
6. Place parts in a chromic acid (CrO_3) solution (10% weight ratio of chromic acid in de-ionised water). Parts attached to the titanium jigs act as the anode.
7. Place a stainless steel (SS) rod in the chromic acid solution. The SS rod acts as the cathode.
8. A direct current of ± 18 Volt is passed through the anode.
9. Anodising takes place and build-up of an anodised film is detected.
10. Remove parts after 1 hour and rinse in clean tap water.
11. Allow to dry in room temperature.

C.2 Aluminium rib preparation before the bonding

1. Wear gloves and safety goggles.
2. Wash all parts with soap and rinse under running water.
3. Degrease all parts with acetone and lint-free medical towels.
4. Sand surfaces with 320 grit water paper.
5. Rinse under running water.
6. Rinse with distilled water.
7. Do chromic acid anodising.
8. Sand surfaces with 320 grit water paper.
9. Rinse under running water.
10. Dry with lint-free medical towels.
11. Rinse with distilled water (use a clean paint brush if necessary).
12. Oven dry parts at 100 °C for at least 30 minutes.
13. Leave to cool for at least 10 minutes.
14. Degrease all parts with acetone and lint-free medical towels.
15. Oven dry parts at 100 °C for at least 10 minutes.
16. Apply adhesives for bonding.

Appendix D

Test Results

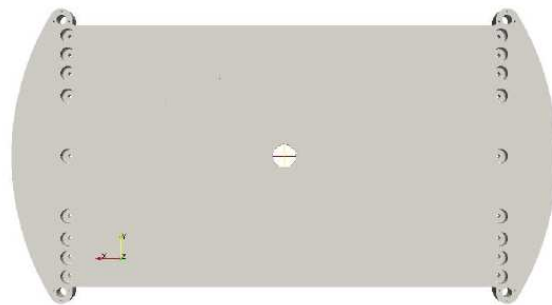


Figure D.1: Side view of the structure to be mounted to the shaker table



Figure D.2: Setup for random vibration test

D.1 Random vibration test results

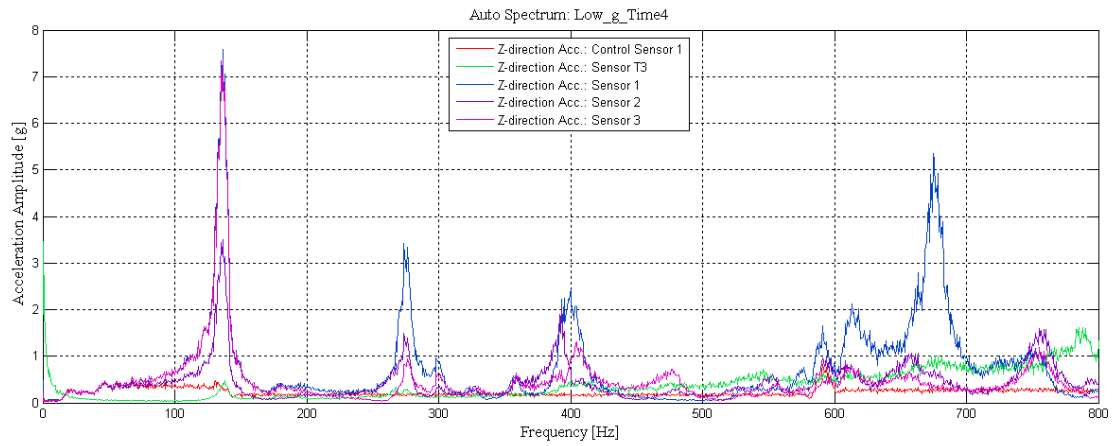


Figure D.3: Frequency response plot of the low intensity random vibration test with sensor T3 failing

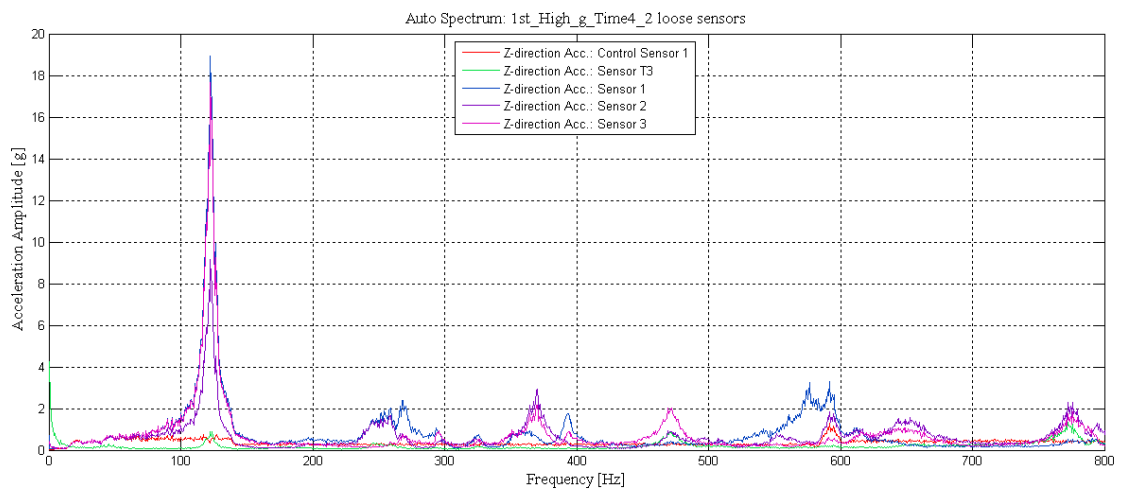


Figure D.4: Frequency response plot of the 1st high intensity random vibration test with sensors T3 and 1 failing

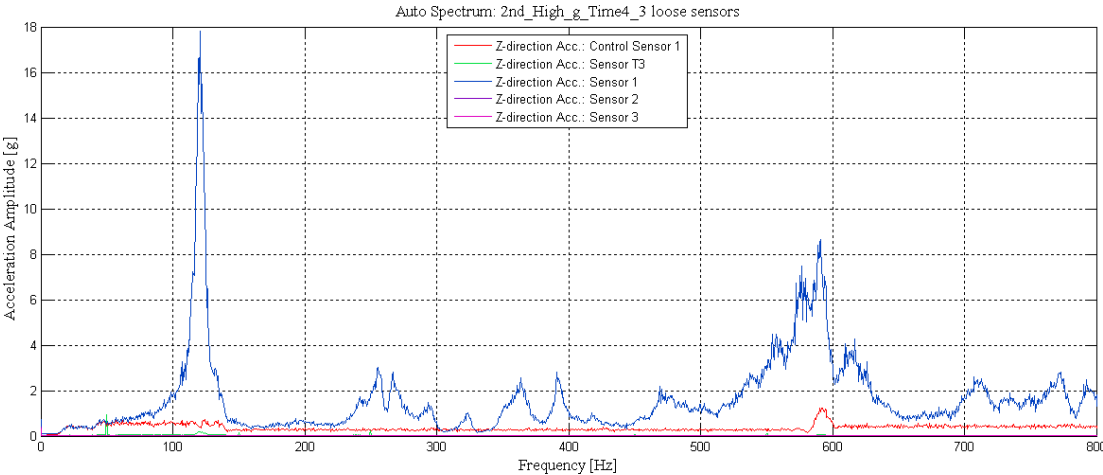


Figure D.5: Frequency response plot of the 2nd high intensity random vibration test with sensors T3, 2 and 3 failing

Bibliography

- ASTM (1999). *Standard Test Method for Total Mass Loss and Collected Volatile Condensable Materials from Outgassing in a Vacuum Environment*. American Society for Testing and Materials, e595-93 edn.
- AZOM (2009). 6082-t6 material properties.
Available at: <http://www.azom.com/Details.asp?ArticleID=2813>
- Callister Jr, W.D. (2003). *Materials Science and Engineering an Introduction*. John Wiley & Sons, Inc. New York.
- Cook, R. (1994). *Finite element modeling for stress analysis*. John Wiley & Sons, Inc. New York, NY, USA.
- ECSS (2002). *Space product assurance - Thermal vacuum outgassing test for the screening of space materials*. European Cooperation for Space Standardization, ecss-q-70-02 edn.
- Fan, H., Meng, F. and Yang, W. (2007). Sandwich panels with Kagome lattice cores reinforced by carbon fibers. *Composite Structures*, vol. 81, no. 4, pp. 533–539.
- Hosur, M., Abdullah, M. and Jeelani, S. (2004). Manufacturing and low-velocity impact characterization of hollow integrated core sandwich composites with hybrid face sheets. *Composite Structures*, vol. 65, no. 1, pp. 103–115.
- iComposites (2009). High modulus carbon fibre.
Available at: <http://www.icomposites.com/CARBONTR.htm>
- Kaw, A.K. (1997). *Mechanics of Composite Materials*. RCR Press, New York.
- Kim, B. and Lee, D. (2008). Characteristics of joining inserts for composite sandwich panels. *Composite Structures*, vol. 86, no. 1-3, pp. 55–60.
- Kim, B. and Lee, D. (2009). Development of a satellite structure with the sandwich T-joint. *Composite Structures*.
- Lim, C., Jeon, I. and Kang, K. (2008). A new type of sandwich panel with periodic cellular metal cores and its mechanical performances. *Materials and Design*.
- MatWeb (2009). 7075-t6 material properties.
Available at: <http://www.matweb.com/folders/Compare.aspx?FolderID=4159056>
- Roets, P. (2007 October). Design a hybrid aluminium/carbon fibre satellite structure panel. Tech. Rep., Department of Mechanical and Mechatronic Engineering, University of Stellenbosch.

- Steyn, H. (2009). Vibration test procedure: Philiproets meesters aluminium. Tech. Rep., SunSpace and Information Systems.
- Styles, M., Compston, P. and Kalyanasundaram, S. (2007). The effect of core thickness on the flexural behaviour of aluminium foam sandwich structures. *Composite Structures*, vol. 80, no. 4, pp. 532–538.
- Vanderplaats R&D, I. (2008 Decembera). *Genesis Analysis Manual*. Vanderplaats Research & Development, INC., 1767 South 8th Street, Suite 200, Colorado Springs, CO 80905, version 10.1 edn.
- Vanderplaats R&D, I. (2008 Decemberb). *Genesis Design Manual*. Vanderplaats Research & Development, INC., 1767 South 8th Street, Suite 200, Colorado Springs, CO 80905, version 10.1 edn.
- Wang, K., Kelly, D. and Dutton, S. (2002). Multi-objective optimisation of composite aerospace structures. *Composite Structures*, vol. 57, pp. 141–148.
- Wilsenach, R. (2008). Design of a hybrid aluminium/carbon fibre aerospace satellite structural panel (ssp). Tech. Rep., Department of Mechanical and Mechatronic Engineering, University of Stellenbosch.